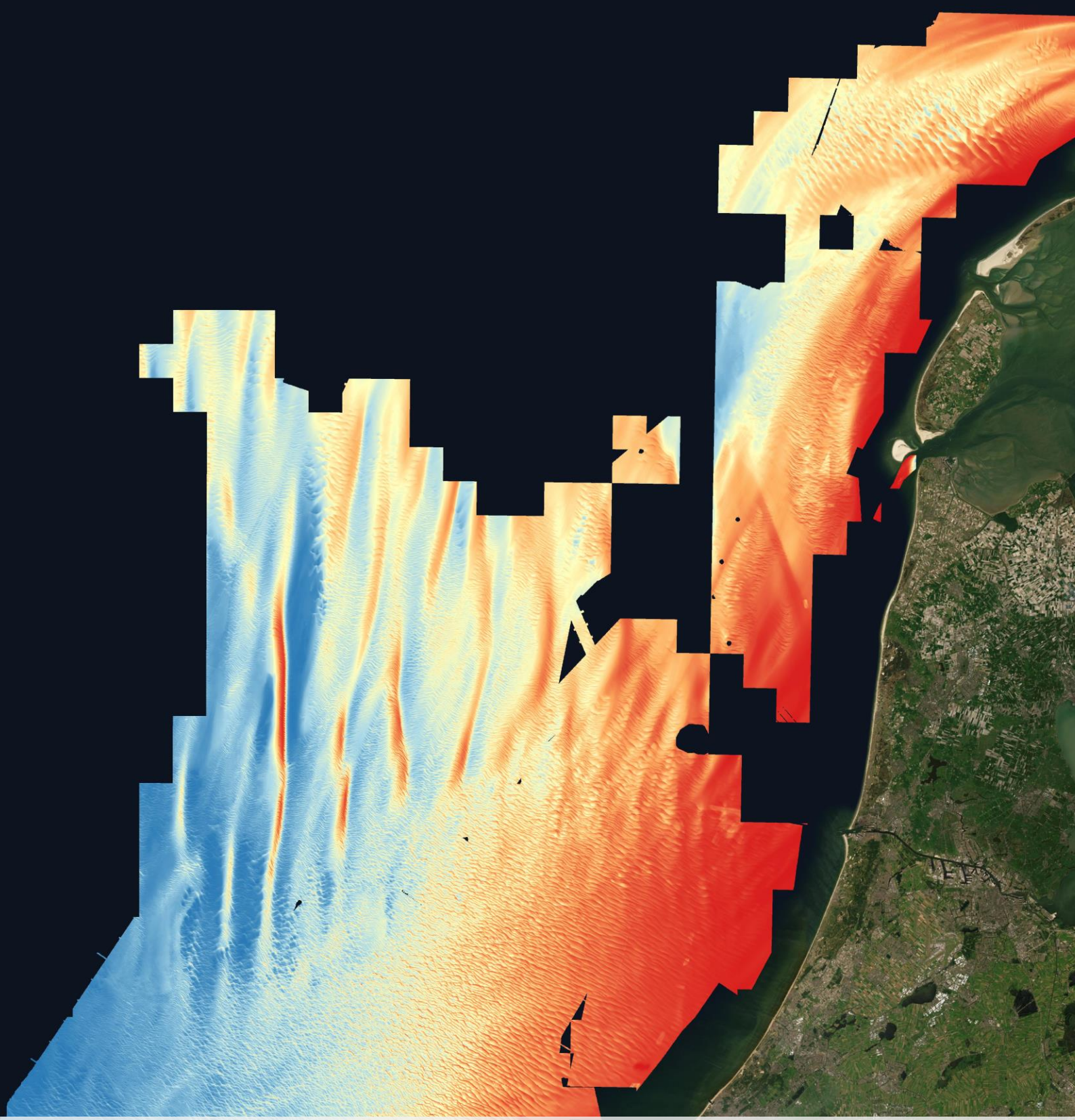

Shifting Sands

Developing new measurement methodologies in GIS to analyse the spatial variability of tidal sand wave migration on the Netherlands Continental Shelf

Master's Thesis

Rens van der Meijden

November 2021

UNIVERSITY OF TWENTE.

Ministerie van Defensie

Colophon

Title:	Shifting Sands
Subtitle:	Developing new measurement methodologies in GIS to analyse the spatial variability of tidal sand wave migration on the Netherlands Continental Shelf
Document type:	Master's Thesis
Status:	Final
Date:	10-11-2021

Author:	Rens van der Meijden
Student number:	S2205475

Educational institution:	University of Twente
	Drienerlolaan 5
	7522 NB, Enschede
	Faculty of Engineering Technology
	Department of Water Engineering and Management
Graduation committee:	
Head of committee:	Dr. ir. P.C. Roos (Pieter) and Dr. ir. J.J. van der Werf (Jebbe)
Daily supervisor:	Dr. ir. J.H. Damveld (Johan)
Daily supervisor:	Ir. D. Ecclestone (David)

Preface

Writing this preface marks the end of my Master's Thesis on tidal sand wave migration, which is completed within the context of the Master Civil Engineering and Management with a specialization in River and Coastal Engineering. The research is conducted from March to November 2021 and is a joint initiative between the University of Twente and the Dutch Ministry of Defence.

Even though the project is fully done during the Corona pandemic, which meant working from home for most of the time, I really enjoyed my time working on it. One main thing about research that I enjoy is the possibility of adding to the existing knowledge base by tackling previously unsolved problems. Of course, it helps to stay motivated when the practical relevance of the research topic is high.

First, I would like to thank Johan Damveld (University of Twente) and David Ecclestone (Dutch Ministry of Defence), who closely supervised me during the project. The light-hearted atmosphere during our weekly meetings was just what I needed in such a serious time. Special thanks to David as well for preparing the artificial bathymetric datasets that were used as a complement to the vast amount of available field data. I am looking forward to our continuing collaboration in the coming weeks, in which a scientific publication will be written.

Furthermore, I would like to thank Pieter Roos and Jebbe van der Werf for their shared role as head of the graduation committee. The constructive feedback I received from you really helped to improve the quality of the content.

Finally, thanks to my family and friends, who provided the greatly appreciated distraction during the past months of hard work.

I hope you enjoy reading this Msc Thesis.

Rens van der Meijden

Enschede, 10 November 2021

Summary

Tidal sand waves are large-scale bed features that occur in sandy, relatively shallow coastal seas, such as the Netherlands Continental Shelf (NCS) and the South China Sea. They have typical heights and wavelengths of 1-10 m and 100-1,000 m, respectively. Furthermore, they migrate with typical speeds of 0-5 m/year. It is mainly the combination of their significant dimensions and dynamic behaviour which makes sand waves highly relevant to a variety of offshore activities. For the NCS, there is an abundance of observational studies that quantifies sand wave migration. However, these mostly consider a limited number of sand waves at small-scale survey sites. This way, areally averaged estimates for migration rate and direction are less robust and large-scale spatial patterns are not revealed. Moreover, commonly applied measurement methodologies only capture migration perpendicular to the sand wave orientation.

The aim of this research is to gain insight in the spatial variability of tidal sand wave migration on the NCS. This is done by developing an efficient migration detection method in a Geographic Information Systems (GIS), which quantifies migration rate and direction from bathymetric timeseries (a combination of two unique bathymetric surveys in time) in two horizontal directions.

Two potentially suitable methods were implemented in QGIS: Pairs of Source and Target Points (PSTP) and Spatial Cross Correlation (SCC). PSTP quantifies migration rate and direction by measuring the displacement of vectorised crest and trough lines, which are extracted from consecutive bathymetric datasets in time. SCC locates the two most correlated points in different bathymetric datasets and quantifies migration rate and direction by measuring the distance and angle between these points.

To validate the output of PSTP and SCC, artificial bathymetric datasets were prepared for which migration distance and direction was pre-defined. When the migration distance is between the raster resolution (25 m) and half the wavelength, migration is measured in the correct direction and with sufficient accuracy. It was found that, when analysing field data, the accuracy of both methods is limited for migration distances that are small relative to the raster resolution. To account for this, the time in between two surveys was taken sufficiently long. The performance of PSTP and SCC was tested at four field sites: an offshore site, a site with multiple large sandbanks, and moderately dynamic coastal site and a highly dynamic coastal site. These sites were selected to cover a variety of different morphodynamics and underlying topographies. The obtained spatial and frequency distributions of migration rate and direction were qualitatively comparable for all locations. Quantitative differences mainly occur because the measurements of PSTP are restricted to integer grid cell positions whereas SCC can provide measurements in between these grid cell positions. Furthermore, using a single set of input parameters for SCC is not optimal at locations where the sand wave morphodynamics strongly vary. PSTP was selected as the most suitable method for a large-scale analysis of sand wave migration at the NCS. Its preferability is mainly based on the fact that, compared to SCC, the optimal input parameters are quickly found and need less changing in between different analyses. In addition, sources of errors and anomalies can be readily identified.

Subsequently, PSTP was used to analyse over 300 bathymetric timeseries. The analysed timeseries cover virtually all sand wave fields on the NCS. To gain insight in the spatial variability of migration rate and direction, the resulting 1,900,000 data points were aggregated to an average value per square kilometre.

Regarding the migration direction, three distinct patterns were revealed. First, the sand waves north of Rotterdam migrate in a northern and north-eastern direction. Migration directions are deflected

from north to east on the seaward flanks of the Brown Ridge and the Breeveertien banks, which are sandbanks located roughly between 40-100 km offshore of Noord-Holland. Furthermore, clockwise bilateral migration was observed on the flanks of the Brown Ridge. On the flanks of the Zeeland Banks, a notable observation was that the sand waves migrate in a clockwise as well as an anti-clockwise direction. Finally, the sand waves in the south-western corner of the NCS migrate to the north-east and south-west on a scale smaller than one square kilometre.

Migration rates show significant spatial variability over the NCS. Average migration rates at the main field, located between IJmuiden and Zeeland, typically range between 0-3 m/year, although migration rates of up to 12 m/year are observed at the Zeeland Banks. The fields at the Wadden Island are more dynamic, with average migration rates typically ranging between 2-8 m/year. The highest average migration rates of 10-21 m/year occur near the coast of Texel and Vlieland. Three spatial patterns were revealed. First, migration rates increase non-linearly from the North Hinder bank in the south-western corner of the NCS in north-eastern direction towards the Wadden Islands. Furthermore, migration rates decrease rapidly from the coast in offshore direction, which is especially clear at the Wadden Islands, IJmuiden and the Maasvlakte. Finally, migration rates are higher where sand waves are located on top of a shoreface connected ridge or a sandbank, as was seen at the Zeeland Banks, the Brown Ridge and the Breeveertien Banks. For the latter, the sand waves on the seaward flank migrate faster than the sand waves on the landward flank.

The obtained results are scientifically and practically relevant in multiple ways. First, this research has shown that GIS are highly applicable for analysing the spatial variability of tidal sand wave migration in shelf seas. Present-day GIS packages come with a vast amount of data manipulation and visualisation tools, which gives them an edge over programming packages such as Python or MATLAB. Even more so because GIS packages such as QGIS and ArcGIS have an integrated Python environment in which processing tools can be automated. With PSTP and SCC, two methods have been developed that have shown great potential for future analyses on sand wave migration at different spatial scales.

Furthermore, a great amount of migration data has been produced which can be the starting point for new research. Insight in the contribution of processes and parameters governing sand wave migration can be obtained by correlating the aggregated migration rates to environmental data. In addition, the migration data can be used for the verification and validation of future process-based models. Finally, the NCS-wide analysis provides insight in the spatial variability of sand wave migration rate and direction at an unprecedented coverage. These insights can be valuable for offshore infrastructure planning, optimising hydrographic re-survey policies, dredging and mine hunting strategies.

Key terms and abbreviations

GIS:	Geographic Information System
LAT:	Lowest Astronomical Tide
MBES:	Multibeam echo sounder
NCS:	Netherlands Continental Shelf
NLHO:	Netherlands Hydrographic Office
PSTP:	Pairs of Source and Target Points
SBES:	Single beam echo sounder
SCC:	Spatial Cross Correlation
TSS:	Traffic Separation Scheme

The terms below, which are written in *italics* for the remains of this document, are included here because they are not explicitly defined in the text. Note that these are the definitions which are used for the purpose of this research.

Buffering:	A buffer is a zone that is drawn around any feature (point, line, or polygon) which encompasses all the area within a specified distance from that feature. This zone is drawn in the form of a new polygon.
Clipping:	With vector data: The boundaries of a polygon layer are imposed on a vector layer. Only the parts of the features in the input layer that fall within the polygons of the overlay layer are added to the resulting layer. With raster data: The boundaries of a pre-defined rectangle are imposed on a raster layer. Only the grid cells that fall within pre-defined boundaries are added to the resulting layer.
Compound sand waves:	Sand waves with superimposed megaripples.
Critical water depth:	Definition of the NLHO: sum of the draught of a ship (m), Under Keel Clearance (m, 20% of the draught) and a 2 m safety margin.
Lee:	The distance from the sand wave crest to the nearest trough. Regarding terrestrial dunes, it refers to the side that is sheltered from the dominant wind direction. The second largest type of marine bedforms, which can be classified in between sandbanks and tidal sand waves. They have typical wavelengths of 1,500 m, heights of several metres and are oriented approximately 60° clockwise with respect to the main tidal current direction. On the NCS, they occur north of Vlieland, among others.
Lowest Astronomical Tide:	The lowest tide level which can be predicted to occur under average meteorological conditions and under any combination of astronomical conditions.

Morphometry:	Refers to the quantitative analysis of form, a concept that encompasses size and shape.
Raster data:	Raster data is stored as a grid of values which are rendered on a map as pixels. Each pixel is associated with a specific geographical location on the Earth's surface.
Separation zone:	A zone separating the traffic lanes in which vessels are proceeding in opposite or nearly opposite directions; or separating a traffic lane from the adjacent sea area; or separating traffic lanes designated for particular classes of vessels proceeding in the same direction.
Stoss:	The distance from the sand wave crest to the furthest trough.
Traffic separation scheme:	A routing measure aimed at the separation of opposing streams of traffic by appropriate means and by the establishment of traffic lanes.
Vector data:	A coordinate-based data structure that represents geographic features as points, lines, and polygons. Each point feature is represented as a single coordinate pair, while line and polygon features are represented as ordered lists of vertices. Attributes are associated with each vector feature, as opposed to a raster data model, which associates attributes with grid cells.

Contents

1. Introduction

1.1. Background and motive

1.1.1. Tidal sand waves: definitions, characteristics, and practical relevance

Tidal sand waves are large-scale, sinusoidal-like, 2-D or 3-D bed features that occur in sandy, relatively shallow coastal seas, such as the Netherlands Continental Shelf (NCS), the South China Sea, and Monterey Canyon, California (Van der Veen et al., 2006; Zhang et al., 2016; Zhou et al., 2018). In shallow water, the strength of the tidal motion is sufficient to generate the bed shear stress that induces sediment transport (Van Dijk & Kleinhans, 2005; Passchier & Kleinhans, 2005; Hulscher & Dohmen-Janssen, 2005).

Table 1 contains the properties of the marine bedforms that commonly occur in shelf seas (Morelissen et al., 2003; Dorst, 2009; Van Dijk et al., 2011). Sand wave dimensions are characterised by typical heights of 2-5 m, although they can grow up to 10 m, and typical wavelengths of 100-1000 m (Ashly, 1990). In addition, the crest-orientation is approximately perpendicular to the mean tidal current direction and their morphological timescale is of the order of years to decades (Hulscher, 1996). Hence, tidal sand waves are significantly larger than other dynamic bedforms, such as megaripples, and significantly more dynamic than other large-scale bedforms, such as tidal sandbanks.

Table 1 Marine bedform classification

Bedform type	Wavelength (m)	Height (m)	Timescale	Crest orientation (° tidal current)	Migration rate (m/year)
Megaripples	7 - 40	< 1	Hours	90	100
Tidal sand waves	100 – 1,000	1 - 10	Years – decades	90	0 - 20
Long bed waves	1,000 – 2,000	1 – 10	Centuries	60	Unknown
Offshore sandbanks (tidal ridges)	1,000 – 10,000	5 - 50	Centuries	0 - 30	0 – 1

The large horizontal scale of tidal sand waves is revealed in Figure 1, which contains the bathymetry near the coast of IJmuiden. As can be seen, the sand waves are oriented perpendicular to the coast.

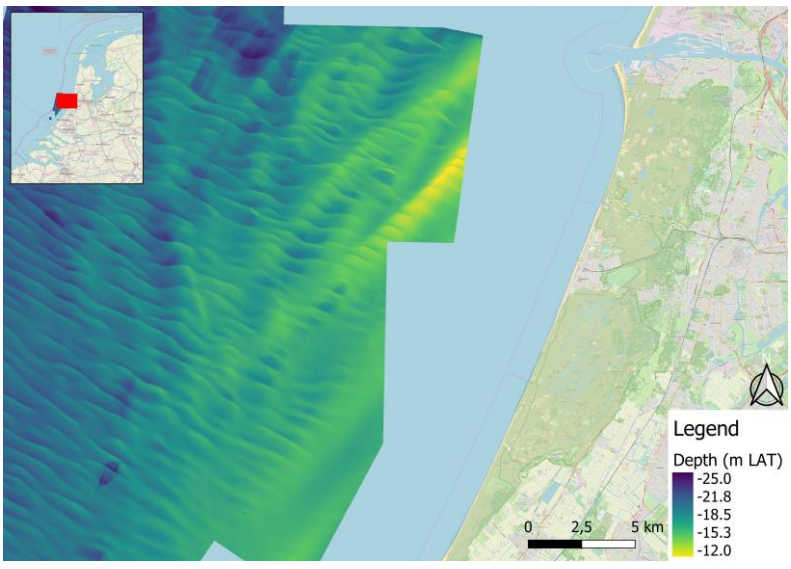

Figure 1 Bathymetry near the coast of IJmuiden

Tidal asymmetry[1], wind-driven flow and the alteration of the tidal flow by sandbanks can result in a residual current, and hence residual sediment transport, which induces sand wave migration. The migration magnitude is, among others, influenced by surface waves, grain size and water depth (Van Dijk & Kleinhans, 2005; Sterlini, 2009; Campmans, 2018). Typical migration rates range between 0-5 m/year but can exceed 10 m/year (Van Dijk et al., 2011).

The combination of their significant dimensions and dynamics makes sand waves highly relevant to a variety of offshore activities. For instance, with pipeline and cable routing, large sand wave fields are avoided as migrating sand waves can lead to exposure, free spanning and overheating (Whitehouse et al., 2000; Németh & Hulscher, 2003; Deltares, 2017a), see Figure 2.

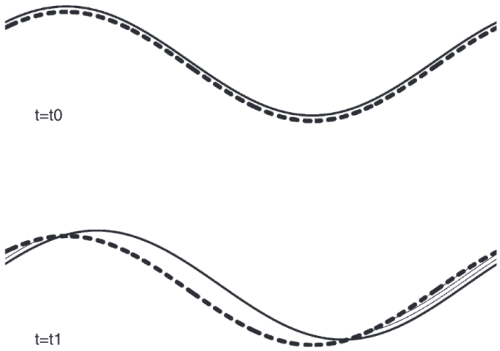

Figure 2 Pipeline (dotted) exposure due to sand wave migration (Morelissen et al., 2003)

Furthermore, for the wind warm and oil and gas industry, long term predictions of sand wave mobility and possible seabed levels are required to design their vertical structures (Bolle et al., 2013; Games & Gordon, 2015). Finally, knowledge of sand wave morphology and dynamics is relevant for optimising hydrographic re-survey policies, dredging and mine hunting strategies (Németh & Hulscher, 2003; Dorst, 2009; REASeuro, 2019). A side-scan sonar image of a mine (in the centre) on a rippled seafloor is given in Figure 3. When bedform dynamics are high, these mines become buried and exposed over time. Prior to the execution of offshore construction projects, knowledge on sand wave migration rates is required to asses to potential burial depth of these mines (REASeuro, 2019).

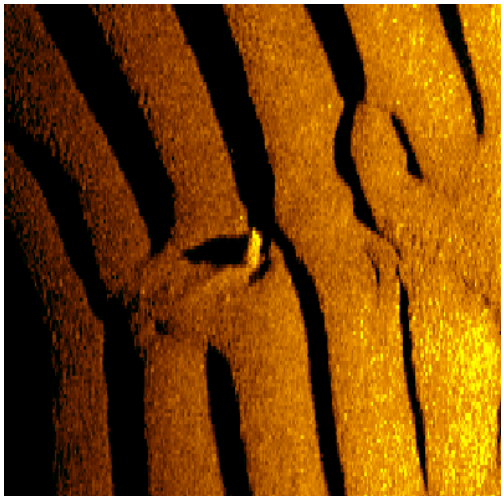

Figure 3 Side-scan sonar image of a mine on the seabed (Ministry of Defence, 2021)

[1] Relevant types of tidal asymmetry are those that induce residual sediment transport. These are, among others, differences in flow velocity and in the duration of slack water between flood and ebb (Wang et al., 1999).

Due to their practical relevance, sand wave morphodynamics has been the subject of many studies in the past. Applied methods commonly regard process-based modelling and (bathymetric) data analysis.

1.1.2. Process-based modelling of sand wave morphodynamics

The term process-based modelling covers both idealised models and complex numerical models. The former represents a strongly idealised situation and is therefore mainly suitable for studying specific properties or behaviour or the influence of certain environmental parameters. The model equations are often linearised with respect to the amplitude of the bed features, hence the term linear models. The linearisation of the model equations means these models are only valid for small-amplitude bed waves during the initial stages of formation.

By including various processes in a sophisticated way, complex numerical are better able to simulate the properties and dynamics of equilibrium sand waves. Their complexity, combined with the fact that they are solved numerically, results in relatively high computational requirements. Although they can be applied in an idealised way to isolate certain processes, they are mainly suitable for site-specific problems and engineering applications (Damveld , 2020).

A drawback of process-based modelling in general is the fact that it requires (various) simplifications and assumptions, which reduces the reliability of quantitative output. Even with a minimum number of simplifications, it has proved a challenging task to model the stochasticity of environmental processes and sand wave morphodynamics that is observed in the field. Although present-day models are increasingly able to simulate the properties of equilibrium sand waves in a realistic way, they are not yet suited to make accurate predictions. This especially applies to migration, which is governed by a large variety of interacting physical processes. In most studies, model performance is still only assessed by comparing the general order, the average value, and the standard deviation of the modelled migration rates to those observed in field data (Besio et al., 2003; Borsje et al., 2013; Campmans et al., 2018; Van Gerwen et al., 2018).

1.1.3. Data-driven analyses on sand wave morphodynamics

The fact that present-day models are not yet capable of providing sufficiently accurate results is the main reason why observational studies are preferred for quantifying migration. Stochasticity can be observed in the field and although quantitative dynamics still contain uncertainties, they are usually more accurate than those obtained with a model. Furthermore, for future process-based models to be calibrated and validated, accurate field data are required.

Whereas morphological characteristics can be quantified using a single bathymetric survey in time, migration can only be measured when a timeseries is available. These comprise at least two bathymetric surveys, which are collected at different times.

In literature, there is an abundance of observational studies concerning small sites and local environmental conditions (Van Dijk et al., 2011). In quantifying sand wave migration from bathymetric timeseries, it is common practice to measure the displacement of crest and trough points which are extracted from crest-perpendicular transects. For the NCS, such work was done by Knaapen (2005), who quantified migration at 12 sites and used his findings to calibrate a migration predictor. The study by Van Dijk & Kleinhans (2005) investigated the dynamics of *compound sand waves* and the relation to environmental mechanisms at a coastal as well as an offshore site. In a similar fashion, Deltares (2015), analysed sand wave dynamics at the Borssele Wind Farm Zone by drawing multiple transects in the dominant migration directions. Outside the NCS, similar methods are applied by Li et al. (2011), Lin et

al. (2009) and Zhang et al. (2019), who studied sand waves superimposed on a sandbank and on the shelf break of the South China Sea, respectively.

The 1DH-approach described above has the advantage that it is straight forward and robust. However, a downside is the fact that lateral migration is not detected. Several 2DH-methods were developed that are capable of quantifying migration in two horizontal directions. Dorst (2009) applied deformation analysis at several study sites on the NCS and Duffy & Hughes-Clarke (2005) used a spatial cross correlation technique in the Bay of Fundy. The latter, or adaptations from it, was also tested in the Marsdiep tidal inlet (Buijsman & Ridderinkhof, 2008), the Monterey Submarine Canion in California (Zhang et al., 2016) and at the Taiwan Banks in the South China Sea (Zhou et al., 2018). Whereas Buijsman & Ridderinkhof (2008) and Zhang et al. (2016) both considered a single study area, Zhou et al. (2018) included multiple sites along two transects covering the entire width of the Taiwan Banks. Therefore, some limited insight was obtained in the spatial variability of migration rates and directions.

For the NCS, the first study that focussed on the large-scale spatial variability of seabed and bedform dynamics was performed by Van Dijk et al. (2011). Their focus was on vertical seabed dynamics. In addition, dimensions and migration rates of individual sand waves were extracted from crest-perpendicular transects at a dozen sites. Several years later, Damen et al. (2018) analysed the spatial variability of observed sand wave morphology on the NCS and its relation to environmental mechanisms. Aggregating the quantitative data per square kilometre revealed distinct spatial differences in height, length, and asymmetry between sand wave fields. However, sand wave migration was not considered.

It is evident that observational studies analysing the large-scale spatial variability of sand wave migration are sparse. Hence, there is a need for a large-scale data-driven approach on quantified sand wave migration. To facilitate such an analysis, developing a 2DH-measurement methodology which detects crest-perpendicular and lateral migration from bathymetric timeseries is required.

1.2. Knowledge gap

There is an abundance of attempts to quantify tidal sand wave migration in shelf seas worldwide. However, most of these focus on small-scale sites with specific environmental conditions and do not provide insight into large-scale spatial differences.

Furthermore, in the past, migration was predominantly quantified by measuring the crest and/or trough displacement along crest-perpendicular transects. Quantitative results of migration rate and direction can show significant variability when only a small number of transects is drawn. A 2DH-analysis with a large number of data points improves overall accuracy and provides better insight into the areally averaged sand wave dynamics. Such methods are described in literature, but they were never tested on a large spatial scale.

Hence, there is a need for a shelf sea-wide analysis of sand wave migration using a fast and efficient 2DH-measurement methodology. Obtained insights are valuable for, but not limited to, offshore infrastructure projects, bathymetric survey planning, dredging and mine hunting strategies. The field data to be obtained can be used for verification and validation of process-based models. In addition, by correlating the migration data to environmental parameters, insight in the contribution of processes and parameters governing tidal sand wave migration can be obtained.

1.3. Aim of the research

The knowledge gap forms the basis for the research aim. For this research, the NCS is used as the study site. Obtained results can form a steppingstone for large-scale analyses in other shelf seas. The aim of the research is as follows:

To gain insight in the spatial variability of tidal sand wave migration rate and direction on the Netherlands Continental Shelf, by developing a 2DH-measurement methodology for analysing timeseries of bathymetric data.

1.4. Research questions

Based on the research aim, two research questions are formulated.

Q1: Which methods can be used, and which method is favourable to quantify sand wave migration based on timeseries of bathymetric data on a large spatial scale?

Q2: What is the spatial variability of sand wave migration rate and direction on the Netherlands Continental Shelf?

1.5. Document outline

The theoretical framework can be found in Chapter 2. Then, the methodology and applied data are addressed in Chapter 3. The developed migration detection methods are described in Chapter 4. These methods are validated with artificial bathymetric data in Chapter 5 and tested with field data in Chapter 6. An evaluation of the tests with artificial and field data and the selection of a preferred method for the large-scale analysis on the NCS can be found in Chapter 7. The results from the large-scale analysis are given in Chapter 8. Finally, the discussion, conclusions and recommendations can be found in Chapter 9, 10 and 11, respectively.

2. Theoretical framework

2.1. Mapping the seabed of the Netherlands Continental Shelf

2.2.1. Bathymetric data collection

Bathymetric data is in essence information about the water depth and underwater topography of oceans, seas, lakes, and rivers (Hell et al., 2012). It is widely used for, but not limited to, the compilation of nautical charts, studying marine life, hydrodynamic modelling and the investigation of changing coastline features and seabed morphodynamics (Van Dijk et al., 2011; National Ocean Service, 2020).

Bathymetric survey data of the NCS is collected and managed by the Netherlands Hydrographic Office (NLHO). The data is stored in the digital Bathymetric Archive System (BAS). These comprise single beam echo soundings (SBES) and multibeam echo soundings (MBES) (Van Dijk et al., 2011).

Single Beam Echo Sounders (SBES). The first SBES were developed in the beginning of the 20th century. The water depth below the acoustic transducer is determined by measuring the travel time of a sound wave that is sent towards and reflected by the seabed. As can be seen in Figure 4 (left), the spatial coverage is rather low as no measurements are taken in the across-ship direction. To cover a significant portion of the seabed, the vessel must traverse back and forth several times (Mayer, 2006).

Multibeam Echo Sounders (MBES). The development of MBES in the 1970's was a significant improvement over SBES. The working principle relies on the intersection of a transmit beam that is wide (120 – 150 degrees) in the across-ship direction and multiple (100-240) receive beam that are wide in the along-ship direction, see Figure 5. As can be seen in Figure 4 (right), this technique results in many simultaneous depth measurements across a wide swath (up to 7.5 times the water depth) of the seabed with each measurement having a high horizontal (small percentage of water depth) and vertical (<1% of the water depth) resolution (Mayer, 2006). This way, larger portions of seafloor can be covered in a shorter time when compared to SBES.

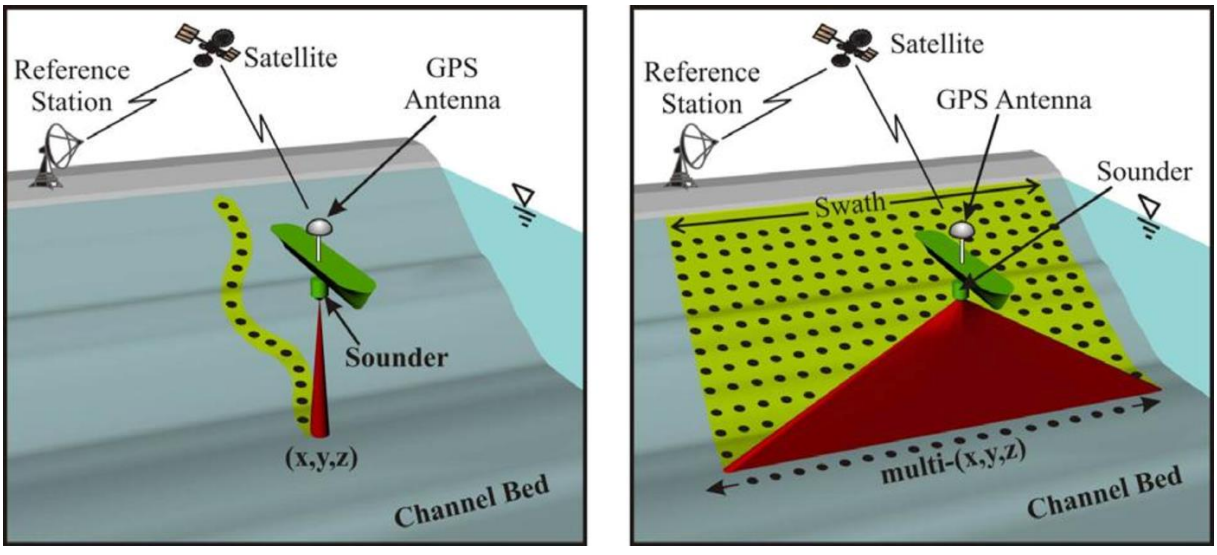

Figure 4 Point data obtained with single beam (left) and multibeam echo sounder (right) (Neary & Gunawan, 2011)

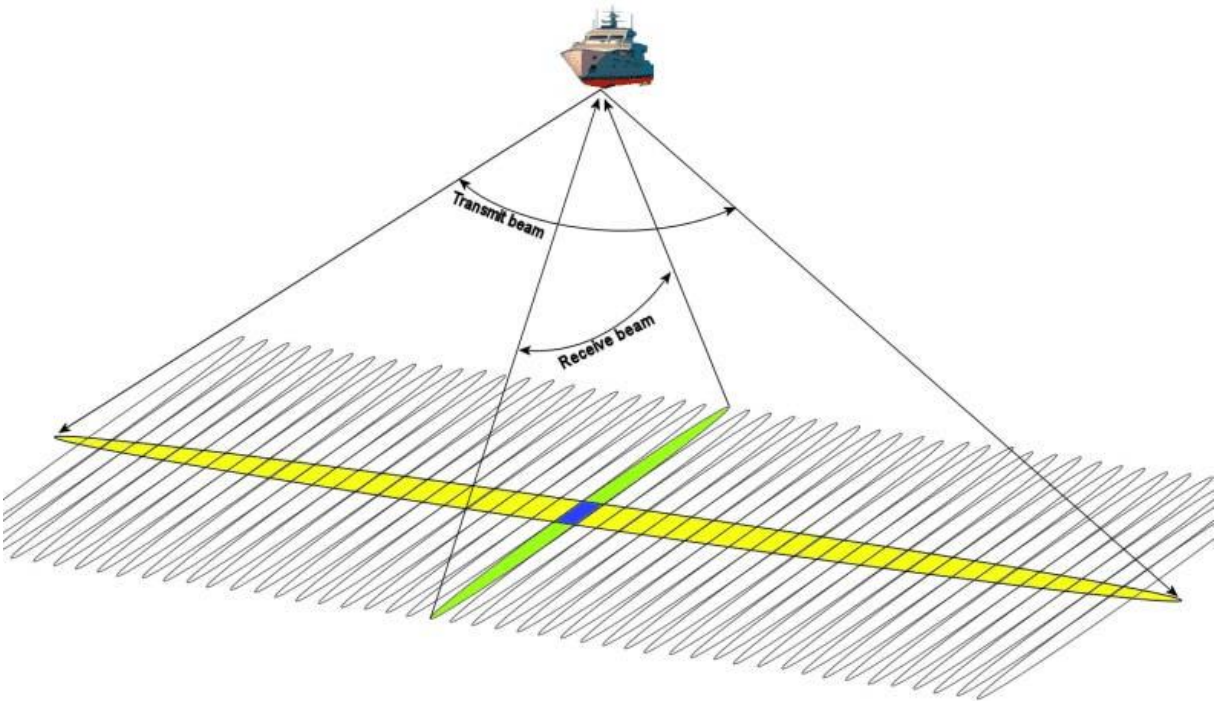

Figure 5 Intersection of a transmit beam and many receive beams gives many depth measurements across a wide stroke (Zwolak, 2015)

2.2.2. Ocean mapping systems and data uncertainty

Besides echo sounding technology, ocean mapping systems comprise GPS systems to determine the positioning of the depth measurements. The horizontal positioning error of these systems has improved from approximately 10 metre in the 1990s, to 1-2 metre in the 2000s, to several centimetres today (Knaapen, 2004; Van Dijk & Kleinhans, 2005; Mayer, 2006). In addition, positioning of the echo measurements is often hampered by ship movement. During post-processing, MBES data is corrected for ship movement while SBES data is not (Van Dijk et al., 2011).

Vertical accuracy is reduced by, among others, tidal water level fluctuations and inaccurate knowledge of the sound speed through the water column. Tidal reduction has long been applied to correct for the former. However, the methods of tidal reduction have changed over time. In the past, this was done using tide gauges or permanent tidal control stations (Van Dijk & Kleinhans, 2005; Van Dijk et al., 2011). Nowadays, tidal reduction is taking place with the use of PREMO, which stands for Prediction Module, a digital database containing water levels for the entire NCS (Van Dijk et al., 2011; Hounjet et al., 2012).

Finally, echo sounding data is corrected for changes in the speed of sound underwater by measuring variables such as temperature, salinity, and pressure with CTD (Conductivity, Temperature and Depth) sensors or direct measurement by means of Sound Velocity Profilers (SVP). Although these devices become better over time, in environments where the spatial and temporal variability of the sound speed structure of the water column is large, changes in the speed of sound introduce significant noise in the echo sounding data (Knaapen, 2004; Mayer, 2006). Regarding MBES measurements, inaccurate knowledge about the sound speed results in an erroneous bathymetry where adjacent survey tracks overlap (Simons et al., 2010; Van Dijk et al., 2011). Figure 6 (A) shows the geometry of a typical MBES survey, consisting of a series of tracks sailed parallel to each other. Figure 6 (B) shows the measured bathymetry for each swath in case erroneous sound speeds are used. It is evident that significant differences can occur for overlapping surveys. Approaches to eliminate these errors aim at collecting

additional sound speed measurements or at optimising the results from overlapping MBES swathes itself (Simons et al., 2010).

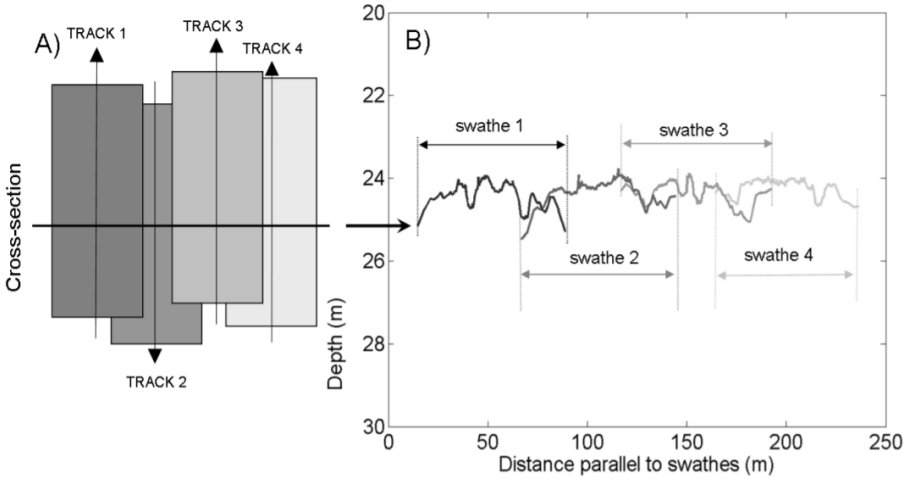

Figure 6 Adjacent tracks (A) and measured bathymetry for each track (B) (Simons, 2009)

2.2.3. Bathymetric survey data of the Netherlands Continental Shelf

Bathymetric survey data of the Netherlands Continental Shelf is acquired using SBES or MBES technology according to the S44 Order 1 standards for hydrographic surveys of the International Hydrographic Organization (IHO) (Van Dijk et al., 2011). In the early 1990s, the NLHO developed a digital Bathymetric Archive System (BAS) in which survey data, binned in cell sizes of 5 metre by 3 metre, is stored. Due to constrains of the system, only the minimum water depth per bin is stored and values that describe the quality of an echo sounding (Total Propagated Uncertainty, standard deviation, mean and maximum depth) are removed (Righolt et al., 2010). Prior to the introduction of the BAS-database, SBES data was written or plotted on *fair sheets*. These were digitized by the NLHO in 2011.

The bathymetric data at the NLHO can thus be divided in three categories: SBES data from digitised fair sheets, SBES data from the BAS database and MBES data from the BAS database. Importantly, since new standards were published by the IHO over the years and the methods of pre-processing, correcting for ship movement and tides have changed and improved over time, one must be careful when comparing different data sources. Survey tracks for both SBES data and MBES are predominantly sailed parallel with the tidal current direction (northeast-southwest) or north-south, such that marine bedforms of sand wave scale are crossed normal to their crest (Van Dijk et al., 2011).

The data properties for each data source are given below.

SBES data from digitised fair sheets (< 1990s). These written fair sheets comprise historical SBES data, acquired prior to the late 1980s, early 1990s. An important difference of these sheets compared to the digital datasets from the BAS is that the data density is much lower as only a small number of depth values can be written on fair sheets. Here, one value represents many SBES data points. Since only the shallowest echo soundings are selected, the water depth in these fair sheets is significantly underestimated (Van Dijk et al., 2011).

SBES data from the BAS-database. SBES data is not corrected for ship movement because the beam width is considered sufficiently wide to compensate for ship movement. Furthermore, vertical precision is in the order of decimetres (< 0.5 m) and the horizontal precision is even lower. Especially the older SBES data was often collected using less accurate horizontal positioning systems. Another

characteristic of the SBES data is its shoal-biased nature, which is a result of the beam width and the fact only the first return of the echo sounding is measured. Mainly in the case of small-scale bed features such as megaripples, the troughs are underestimated whereas the crests are correctly measured. Prior to the year 2000, tidal reduction was done using water level estimates from tidal gauges. The mean reduction level (MRL) was estimated based on water level measurements over several months. Finally, the distance between data points along a track line can vary between 3-35 m and the distance between track lines can be 50 m up to 1000 m (Van Dijk et al., 2011).

MBES from the BAS-database. In contrast to the SBES data, the MBES data in the BAS database is corrected for ship movement. Furthermore, the precision of the vertical soundings is comparable to the SBES data. However, as explained in the previous section, inaccurate knowledge about the speed of sound underwater reduces the precision of the outer beams, which results in an erroneous bathymetry where adjacent survey tracks overlap. Although these errors are partly resolved when processing the data, some residual artifacts may remain. The data density of the MBES data is much higher compared to the SBES data, as it often contains one data point every 5 by 3 m. After the year 2000, a different method of tidal reduction was applied as from then on, the echo soundings were reduced to mean sea level (MSL) (Righolt et al., 2010; Van Dijk et al., 2011).

2.2. Tidal sand waves: definitions and properties

2.2.1. Definition and classification

Tidal sand waves are generally described as large-scale, sinusoidal-like, 2-D or 3-D bed features that occur in sandy, relatively shallow coastal seas (Hulscher & Dohmen-Janssen, 2005; Van Dijk & Kleinhans, 2005; Passchier & Kleinhans, 2005). In these shallow waters, the strength of the tidal motion is sufficient to generate the shear stress at the seabed that induces sediment transport. Large-scale bed features differ from small-scale bed features, such as megaripples, in the sense that their wavelengths are generally much larger than the water depth. The geoscientific classification in 2-D or 3-D bed features is based on the fact for 2-D features, the distance between two crests is much shorter than the crest length itself (Hulscher & Dohmen-Janssen, 2005). The crest shape of 3-D bed features is much more irregular, which is illustrated in Figure 7. As can be seen, the crestline changes from straight and continuous (2-D bed features) to irregular and incontinuous (3-D bed features).

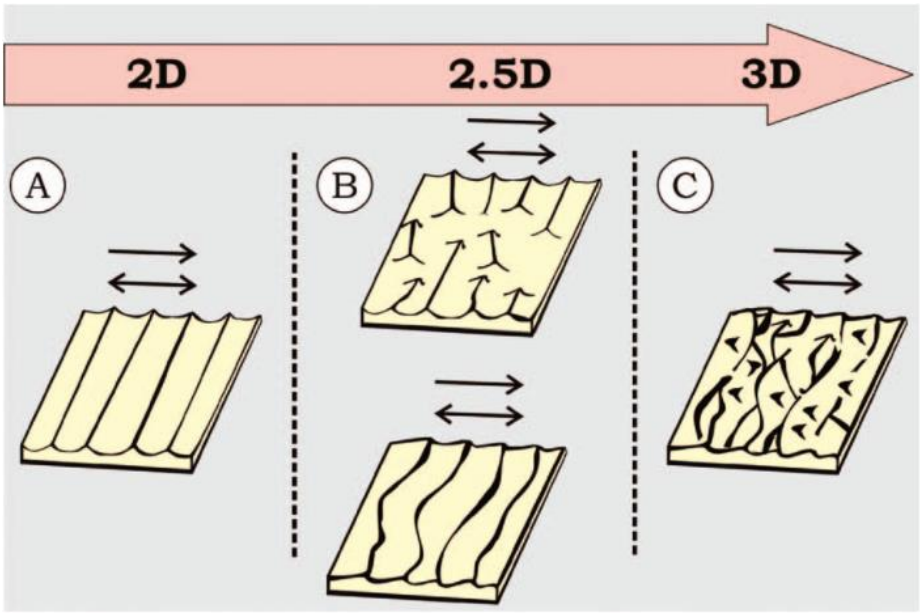

Figure 7 Classification of 2-D, 2.5-D and 3-D bed features based on the crestline (Perillo et al., 2014)

According to a first-order classification of large-scale subaqueous bedforms proposed by Ashly (1990), tidal sand waves can also be referred to as large or very large, 2-D subaqueous dunes.

2.2.2. Morphological properties

Characteristics that are useful to classify large-scale bed features are among others length, height, asymmetry, steepness, and crest orientation (Ashly, 1990; Hulscher, 1996; Knaapen, 2005).

First of all, length (L in Figure 8) is defined as the distance between the trough positions on opposite sides of the crest (Knaapen, 2005). For sand waves, typical wavelengths vary between 100-1,000 m (Ashly, 1990; Hulscher, 1996). However, in some studies, much longer bed features are classified as sand waves as well (Zhang et al., 2014). Given their typical length scale of order hundreds of metres, sand waves fall in between smaller megaripples and larger *long bed waves* and sandbanks, see Table 1 (Morelissen et al., 2003; Van Dijk et al., 2011).

The height (H in Figure 8) is defined as the difference between the crest level and the baseline of the two trough levels on either side of the crest (Knaapen, 2005). Sand wave height is of the order of several metres, although they can be much higher as well (Ashly, 1990; Hulscher, 1996). These high-amplitude sand waves, with heights of up to 10 m and even larger, are sometimes referred to as giant sand waves (Zhou et al., 2018; Zhou, et al., 2020). Based on their typical height, sand waves can be classified in between megaripples and tidal sand banks, see Table 1 (Morelissen et al., 2003; Van Dijk et al., 2011).

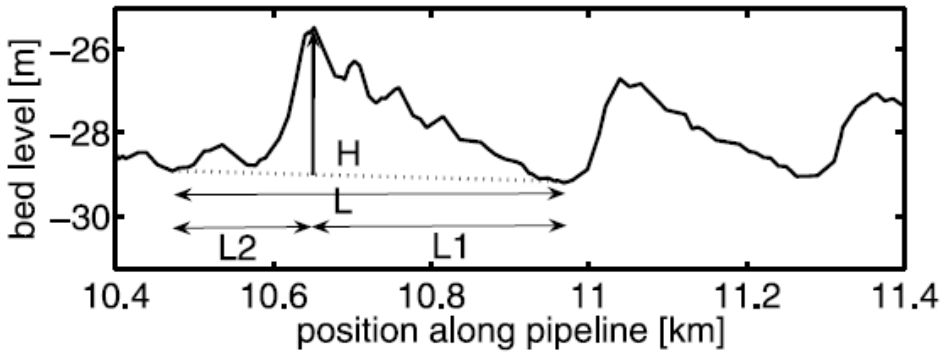

Figure 8 Sand wave characteristics length (L) and height (H) (Knaapen, 2005)

By subtracting the length of the *lee* side (L_2 in Figure 8) from the length of the *stoss* side (L_1 in Figure 8), and dividing by the length, one can determine the dimensionless asymmetry parameter A, see Equation (1) (Damen et al., 2018; Cheng et al., 2020). According to this definition, the asymmetry parameter is a measure of how far the crest leans towards the nearest trough. A is 0 for fully symmetric sand waves and A is 1 for fully asymmetric sand waves.

$$A = \frac{L_1 - L_2}{L} \tag{1}$$

The steepness is defined as the ratio between sand wave height and length (Damen et al., 2018). According to the classification from Ashly (1990), sand wave steepness typically varies between 1:30 and 1:100 and greater.

In general, the crest orientation of sand waves is approximately perpendicular to the mean tidal current (Hulscher, 1996; Hulscher & Dohmen-Janssen, 2005). As can be seen in Figure 9, the orientation of sand waves is distinctly different from other tidal bed features, such as sand banks and tide-parallel ridges, which are oriented obliquely or parallel with respect to the tidal current.

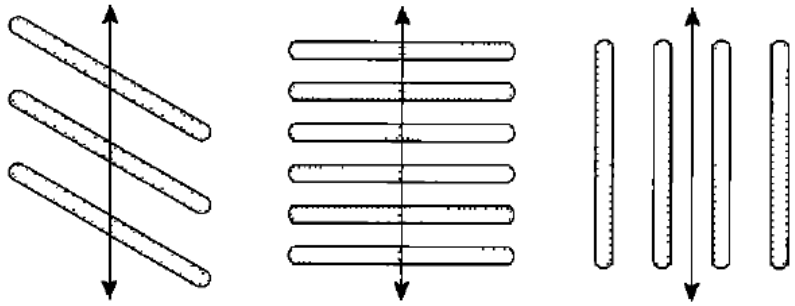

Figure 9 Crest orientation of sand banks (left), sand waves (middle) and tide-parallel ridges (right). The arrow indicates the mean tidal current (Hulscher, 1996).

2.2.3. Significance of dynamics

Growth and migration are two important factors that characterize the significance of bedform dynamics. These dynamics are distinctly different for most marine bed features, see Table 1 (Hulscher, 1996; Morelissen et al., 2003; Dorst, 2009; Van Dijk et al., 2011).

As the growth rate of large-scale bed features is very low, this property is commonly translated to a morphological timescale at which shape changes takes place. The morphological timescale of sand waves is of the order of years (Hulscher, 1996; Németh, 2003; van Dijk et al., 2011). This is rather slow compared to smaller bed-features such as ripples or megaripples, which evolve at a timescale of hours or days, respectively (Morelissen et al., 2003; Van Dijk et al., 2011). However, other large-scale bed-features such as sandbanks and *long bed waves* evolve at a much longer timescale (Hulscher, 1996; Morelissen et al., 2003; Van Dijk et al., 2011).

Sand wave migration rates are of the order of m/year. Typical observations of migration rates in various shelf seas are between 0-20 m/year (Van Dijk & Kleinhans, 2005; Lin et al., 2009; Van Dijk et al., 2011; Zhou et al., 2018). This is not significant compared to small-scale bed features such as ripples and megaripples, but it is much more significant compared to large-scale bed features such as sand banks (Morelissen et al., 2003; Van Dijk et al., 2011). It is commonly accepted that in the case of 2-D bed features in a uniform flow field, the migration direction is perpendicular to the crest (Duffy & Hughes-Clarke, 2005). However, this does not always hold as oblique and rotated migration have been observed in complex bathymetries (Zhou et al., 2018). Importantly, high migration rates are often associated with large asymmetry parameters (Knaapen, 2005).

2.3. Tidal sand waves and related physical mechanisms

2.3.1. Formation, growth, and shape evolution

By using linear stability analysis in combination with a three-dimensional model, Hulscher (1996) was the first to provide a physical explanation for the formation of tidal sand waves. By extending a depth-integrated model developed by Huthnance (1982) in the vertical direction, it was shown that the interaction between bed topography and an oscillatory tidal flow gives rise to residual vertical circulation cells. This process is visualised in Figure 10 and Figure 11. The figures show that, at both flanks, the residual near-bed current is directed toward the sand wave crest. Hence, there is a convergence of sediment transport at the crest, thereby inducing growth. In this model, the bed slope effect was identified as the main mechanism that counteracts growth and causes the damping of short wavelengths (Hulscher, 1996; Damen et al., 2018). Furthermore, the vertical structure of the flow field was found to mainly depend on two parameters: a resistance parameter ($\hat{S}$), describing the bottom

shear stress, and the vertical Stokes number (E_v). The latter in turn determines the Stokes depth, which is the part of the water column in which viscous effects influence the tidal motion significantly. Tidal sand wave only appeared for large values of the resistance parameter, which implies that their occurrence strongly depends on the bottom shear stress.

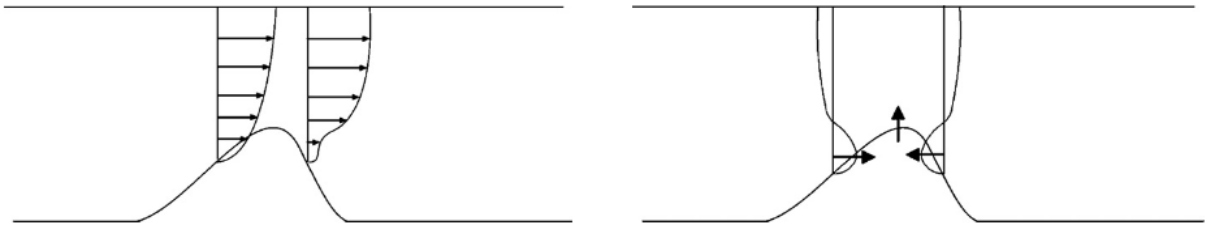

Figure 10 Velocity profile (left) and residual velocity profile (right) over a sand wave (Tonnon et al., 2007)

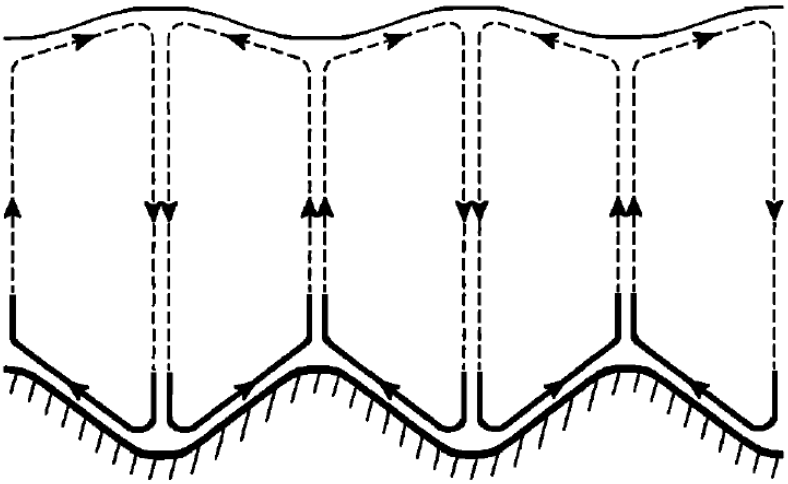

Figure 11 Residual vertical circulation cells with sediment convergence at the crest (Hulscher, 1996)

By building on these findings, Hulscher & Van den Brink (2001) developed a parametric large-scale bed form prediction model. Since the resistance parameter $\hat{S}$ and the vertical Stokes number E_v could not be determined from measurements, they were expressed as a function of the depth-averaged flow velocity (u_m), water depth (H), a viscosity variation parameter (ε) and the level of zero intercept (z_0), defined as the level above the bed where the velocity is zero. By using known water depths and flow velocities, a constant value for the viscosity term and by spatially varying the level of zero intercept, the model predicted the area where sand waves occur in the southern part of the North Sea quite well. However, the model was unable to explain small-scale variations in sand wave occurrence. Several years later, this prediction model was improved by Van der Veen et al. (2006), who accounted for the spatial variability of sediment grain size and the critical bed shear stress. It was found that the critical bed shear stress has to be sufficiently high for sand waves to occur, which matches with the fact that sand waves are mainly observed in relatively shallow coastal seas.

Borsje et al. (2014) confirmed the importance of grain size in the occurrence of sand waves. Data analysis showed that sand wave fields mainly occur where bed load transport is the dominant transport mode, which is the case when mainly large grain sizes are present. When suspended transport is dominant, sand waves are absent. This is confirmed by results from Damen et al. (2018) in Figure 12. As can be seen, the areas where bed load transport is dominant (red) coincides with areas where sand waves occur (black).

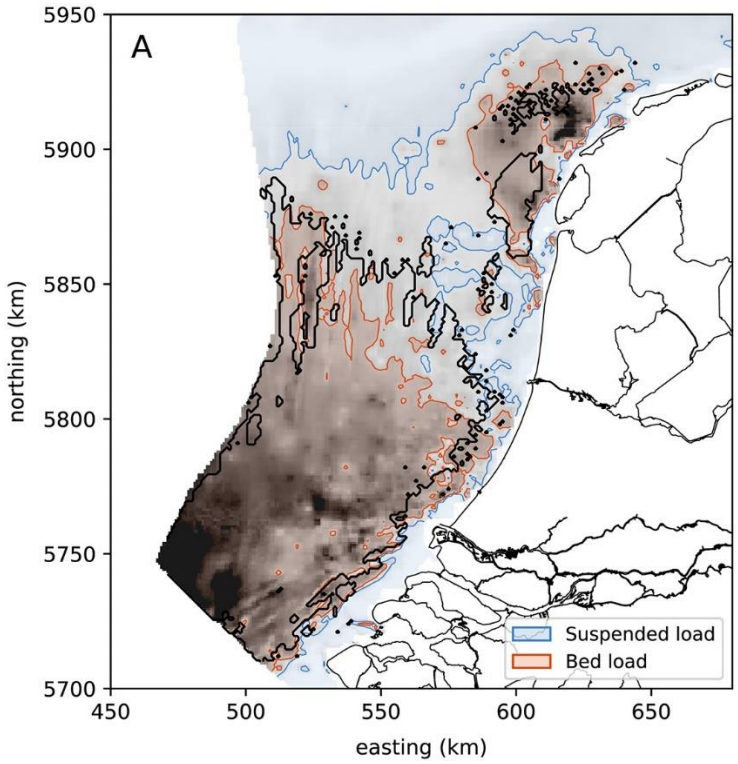

Figure 12 Bed load dominated, suspended load dominated and sand wave regions (black) (Damen et al., 2018)

Furthermore, model simulations of sand wave formation by Borsje et al. (2014) indicated that, when the bed load regime is dominant, the presence of suspended sediment increases the preferred wavelength but suppresses very long sand waves, resulting in a finite range of wavelengths. Furthermore, the inclusion of suspended transport had a damping effect on the growth rate. These findings contradict with modelling results obtained by Sterlini (2009), who found that, under calm weather conditions, the inclusion of suspended sediment shortens the sand waves and increases the growth rate. An explanation for these contradictions might be that Sterlini (2009) used a constant eddy viscosity in combination with a partial slip condition while Borsje et al. (2014) used an advanced turbulence model with a spatially and temporally variable eddy viscosity and sediment diffusivity.

Apart from sediment transport processes, storm effects also influence sand wave length in the formation stage, as was shown by Campmans (2018). By means of a linear stability approach, it was concluded that storms (wind-driven flow and surface waves) reduce growth rates in a way that favours longer sand waves more than those generated during fair weather conditions.

In addition to sand wave evolution in the formation stage, several data driven as well as modelling studies were performed to investigate the influence of environmental mechanisms on equilibrium sand waves. Based on model results and observations, Van Santen et al. (2011) showed that sand wave length decreases with increasing tidal current strength. Based on observations, Van Dijk & Kleinhans (2005) concluded that wave action near the coast causes sand wave flattening in such a magnitude and frequency that they cannot be restored by tidal currents. Further offshore, the water depth is sufficient to reduce the impact of waves, thereby allowing tidal currents to be the main process of development. Later modelling studies by Sterlini (2009) and Campmans (2018) confirmed these findings, as they showed that the inclusion of wind-driven flow, wind waves or a residual current reduce sand wave height while a wind-driven flow and a residual current increase asymmetry. An explanation for this phenomenon is that the presence of a residual current reduces the relative strength of the residual vertical circulation cells (Damen et al., 2018).

2.3.2. Migration

The mechanisms contributing to sand wave migration are divided in mechanisms inducing migration and mechanisms influencing migration.

Mechanisms inducing migration

In general, there is one basic mechanism that induces sand wave migration. It is the presence of vertical residual circulation cells that causes sand wave formation and growth, whilst it is the distortion of the symmetry of these circulation cells that induces migration. The distortion of these circulation cells can have several causes.

Németh et al. (2002) were one of the first who modelled sand wave migration in shelf seas. They conducted a linear stability analysis using a 2DV-model and found that steady residual currents, generated by wind stress or a pressure gradient, distort the symmetry of the recirculating cells, which induces migration in the direction of the steady current. Later modelling studies by Besio et al. (2003) and Besio et al. (2004) confirmed these findings. In addition, they found that the superposition of M2 and M4 tidal components also distorts the symmetry of the recirculating cells, thereby inducing migration. Although the tide-average residual current is zero, sand wave migration can occur due to the nonlinear relationship between flow velocity and sediment transport. A phase shift of 30^o to 80^o between the M2 and M4 components can lead to migration against the direction of the residual current.

Based on model results from a 2DV idealized non-linear process-based model, Sterlini (2009) concluded that surface waves can significantly influence sand wave migration. In general, they cause migration in the propagation direction of the surface waves. She also found that the effect of surface waves increases for increasing tidal currents and decreasing water depths. A few years later, Sterlini et al. (2011) came to similar conclusions based on model results and field data from Varne (UK) and a survey site 50 km of the coast near Alkmaar. They found that waves can both induce and enhance sand wave migration. Using a linear stability model, Campmans (2018) concluded that intermediate and extreme storm conditions have a significant effect on sand wave migration and that sand wave migration is larger during winter than during summer. Using a nonlinear sand wave model, Campmans (2018) showed that wind-driven flow causes sand wave migration. Furthermore, waves and wind combined result in larger migration rates compared to wind only, whilst waves alone do not cause migration. So, wind waves enhance migration but do not induce it. The latter conclusion contrasts with Sterlini (2009) and Sterlini et al. (2011), who concluded that surface waves can cause migration. Although it is not clear what causes this contradiction, it is evident that both wind-driven flow and surface waves enhance sand wave migration. Importantly, it is suggested in several studies that wind-driven flow and wind waves can cause a short-term seasonal change in sand wave shape and migration direction (Harris, 1989; Sterlini et al., 2011).

To understand the physical mechanisms behind uphill migration of sand waves on top of a sand bank, Leenders et al. (2020) used a Delft3D model to simulate the dynamics of a sand wave field when a sand bank is included in the topography. Using a schematised model set-up, they showed that it is an alteration of the tidal flow over the sand bank that induces a residual horizontal current towards the crest. This residual current leads to distortion of the vertical circulation cells which causes sand wave migration towards the crest on both sides. Roos & Hulscher (2003) explained that, on the Northern Hemisphere, Coriolis effects enhance a clockwise circulation of the tide-averaged flow around a sandbank. Hence, sand waves on the seaward and landward flank migrate to the north-east and south-west, respectively.

In their study on sand wave characteristics near the shelf break of the northern South China Sea, Zhang et al. (2019) concluded that strong currents associated with internal solitary waves were the main mechanism behind the generation and migration of the observed sand waves. These internal solitary waves occur in stratified fluid bodies and are particularly active in the northern South China Sea (Huang et al., 2016).

Finally, note that migration and asymmetry are caused by the same physical mechanism. Only measuring crest displacement can be confused with a change in asymmetry. Therefore, it is important to measure displacement of the entire sand wave.

Mechanisms influencing migration

As explained in the previous section, several studies showed that surface waves can enhance migration. Next to that, water depth and sediment characteristics are also important in explaining the magnitude of migration.

Van Dijk & Kleinhans (2005) concluded that the differences in migration rates between the coastal site and the offshore site were, among others, caused by the difference in water depth. Near the coast, a lower water depth results in higher migration rates due to interaction of wave stirring and flood-dominated longshore currents. Migration rates at the deeper offshore area were lower due to the absence of wave stirring and the dominance of the current regime. The impact of water depth is confirmed by observations near Hainan Island in the South China Sea by Li et al. (2011), where the migration rates at six different survey locations implied an inversely proportional relationship between water depth and migration rate.

Based on their sensitivity analysis of the Shields parameter for current and waves, Van Dijk & Kleinhans (2005) concluded that in current-dominated regimes, bed form dynamics and bed form mobility is controlled by grain size whereas in combined wave and current-related regimes, bed form dynamics are controlled by water depth. However, the grain size differences between the coastal site and the offshore site in their study was too small to cause major differences in sediment mobility. Furthermore, Li et al. (2011) suggested a similar relationship between grain size and migration rate. Using this relationship, their predictions agreed reasonably well with observations near Hainan Island in the South China Sea. Finally, Sterlini (2009) and Van Gerwen et al. (2018) concluded that the inclusion of suspended sediment transport increases the migration rate. Sterlini (2009) also noted that without suspended sediment transport, the effect of varying the grain size on migration rates is negligible.

It is important to note that depth, grain size, the presence of surface waves and suspended sediment are strongly coupled. After all, high waves in shallow coastal regions are better able to stir up small grains, thereby increasing the suspended sediment concentration. However, it still makes sense to distinguish between these factors because it is interesting to see which one contributes most to the magnitude of sand wave migration.

2.4. Morphology and dynamics on the Netherlands Continental Shelf

Large-scale observational studies indicate that, on average, sand waves are longer and lower in the north-eastern region of the NCS and near the coast while they are shorter and higher in the south-west and further offshore, see Figure 13 and Figure 14. Furthermore, steep, symmetric sand waves mainly occur in the south-west of the NCS while flat, asymmetric sand waves occur in the north-east and near the coast, see Figure 15 and Figure 16 (Damen et al., 2018). The crest orientation predominantly varies between 90^{o}N and 110^{o}N (Van Dijk & Kleinhans, 2005; Passchier & Kleinhans,

2005). Observations of individual sand waves on small-scale sites show that the morphological properties significantly vary on a local scale as well (Van Dijk et al., 2011).

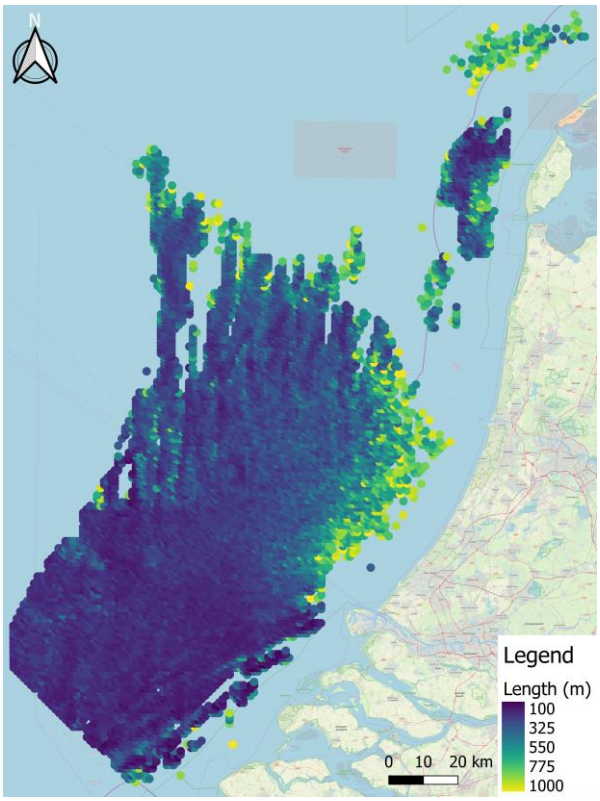

Figure 13 Sand wave length per km²

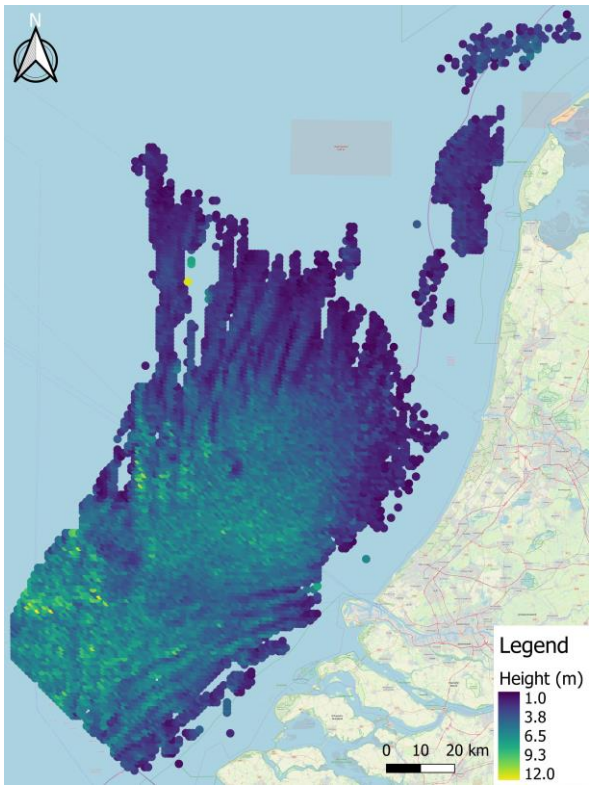

Figure 14 Sand wave height per km²

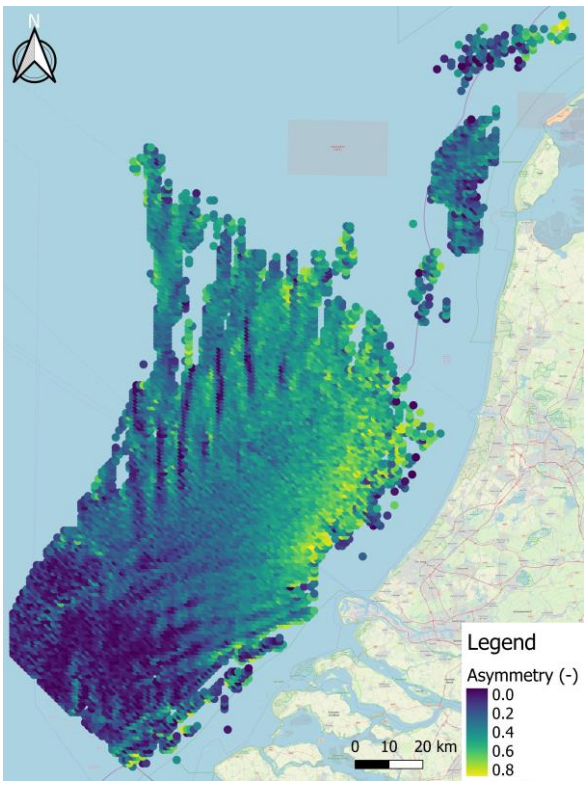

Figure 15 Sand wave asymmetry per km²

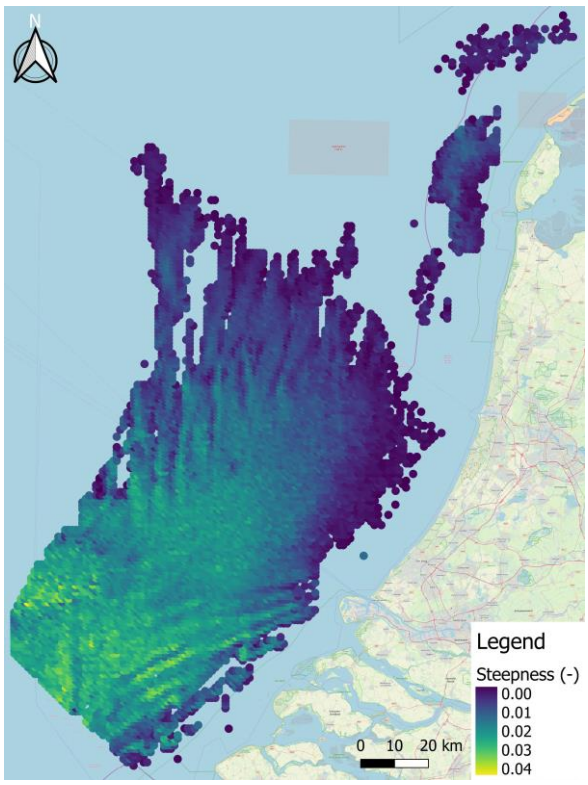

Figure 16 Sand wave steepness per km²

A similar small-scale variability is observed for sand wave dynamics. Sand waves that belong to the same section of seafloor migrate at different speeds and in different directions. This is indicated by the large range of migration rates (given in Table 2) for the survey sites in Figure 17.

Average migration on the NCS predominantly takes place in north-eastern direction or south-western direction at rates of 0-20 m/year (Knaapen, 2005; Van Dijk & Kleinhans, 2005; Van Dijk et al., 2011). Large-scale studies indicate several offshore regions of moderate to high dynamics: a large sand wave field that covers the Southern Bight and some smaller fields near the Wadden Island. Especially the latter are highly dynamic with average migration rates exceeding 12 m/year. The rest of the NCS is less dynamic as average migration rates are predominantly below 5 m/year (Van Dijk et al., 2011).

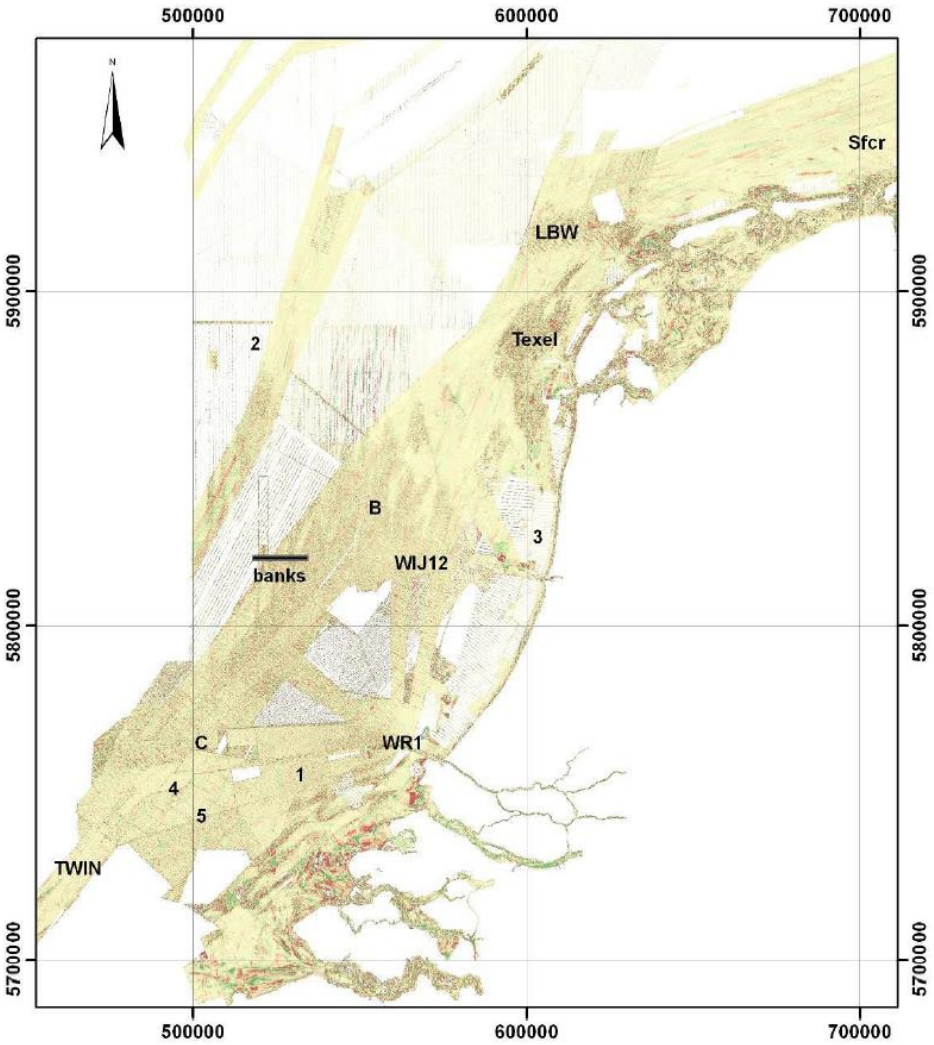

Figure 17 Survey sites where sand wave dimensions and dynamics are quantified by Van Dijk et al. (2011)

Table 2 Minimum, maximum and average migration rates of individual sand waves per survey site. A positive value means migration in north-eastern direction, a negative value means migration in south-western direction. Data by courtesy of Van Dijk et al. (2011)

	Site	1	4	5	Texel	B	C	WIJ 12	TWIN	WR1 A1	Wr1N	LBW
Migration rate (m/year)	Min	-5.4	-1.6	0.6	5.0	-	-	-2.9	-4.5	-0.09	0.2	10.5
	Av	-3.2	0.7	3.4	16.0-19.0	2.0	0.4	2.2	-1.5	4.7	3.7	12.4
	Max	1.2	4.0	5.7	37.0	-	-	6.0	0.06	8.5	15.0	18.5

2.5. Quantifying bedform or landform migration from bathymetric or terrain data

2.5.1. Non-GIS methods to estimate sand wave migration from bathymetric data

The migration detection methods in literature can be divided in two classes: methods that measure the displacement of separate sand wave components (crest and trough locations) and methods that use statistical techniques to detect migration directly, taking a full bathymetric grid as input.

Migration detection based on crest, trough and/or lee side displacement

A common approach to quantify migration is to compare the positions of crest, trough, and *lee* side in time. The main aspect that separates different approaches is the way in which the bedform components are determined.

One way to quantify the displacement of sand wave components is to measure the displacement manually, which was done by Van Dijk & Kleinhans (2005). In their study, migration was determined by measuring the displacement of the *lee* slope from 2DV profiles. The *lee* slope was preferred over the crest because the crest variability due to megaripple variation was too large. Importantly, since the horizontal displacement error of the GPS system was known, the significance of the obtained migration rates could be stated. Although this approach works for smaller sites, it is rather subjective and too labour intensive to be used for large-scale applications.

An automated procedure was applied by Knaapen (2004), Knaapen (2005) and Knaapen et al. (2005), who quantified migration from the crest and trough positions in both SBES and MBES data. The bathymetric data sets were filtered using a low-pass Bartlett window, which removed the noise related to megaripples and ripples, leaving only the crest and trough positions. Migration was measured from one (SBES) or several (MBES) crest-perpendicular profiles. The horizontal positioning error of the estimates was corrected for using markers, which were fixed at the seafloor. It was found that the migration rates from the MBES had a much lower standard deviation since multiple estimates can be done for the same crest. Generally, these markers will not be present. To reduce the impact of positioning errors on migration estimates, Knaapen (2004) therefore advised to use surveys with long periods in between or many surveys in time.

As it is not always desirable to entirely remove small-scale bed features from the bathymetric signal, several automated methods have been developed that are able to separate bathymetric data sets into different components of a particular scale. Van Dijk et al. (2008) compared the performance of a geostatistical method (factorial Kriging) and a spectral method (Fourier analysis) using two case studies. Both methods performed equally well in separating the sand wave signal and in quantifying the associated morphometric properties (length, height). Migration rates were determined by the displacement of crest, trough, and inflection points from sand wave profiles. Again, the performance of both methods was found to be comparable. According to the authors, the credibility of the geostatistical and spectral method is strong as the results strongly agree with each other as well as with the manual results obtained by Van Dijk & Kleinhans (2005) for the same region. Importantly, analysis of plan view behaviour of crest and trough lines in time revealed that significantly variable dynamics can occur along these lines, thereby showing that lateral displacement of crests and troughs can occur, see Figure 18. In a later study, Van Dijk et al. (2011) used a similar Fourier analysis to separate sand wave signals from bathymetric data. Migration rates were determined from crest and trough displacement, taken from sand wave profiles perpendicular to the crests. The obtained results agreed well with those obtained using deformation analysis in Dorst (2009) (section 2.5.2), strengthening the credibility of the method.

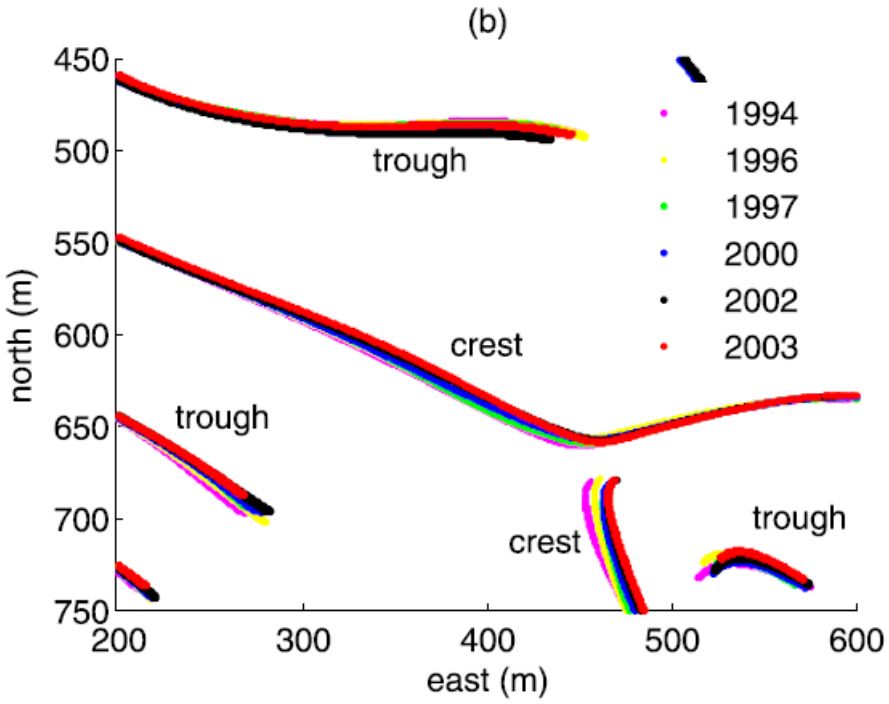

Figure 18 Variable displacement of crest and trough lines (Van Dijk et al., 2008)

The main advantage of the considered method in general is that it has proven its reliability and robustness (Knaapen, 2004). Furthermore, it is straight forward and easy to grasp compared to the statistical approaches described in section 2.5.2. A disadvantage is the fact that crest and trough detection is prone to depth and positioning errors, which play a role in the detection of local minima and maxima and their location, respectively (Dorst, 2009). The effect of these errors can be mitigated by using high resolution surveys with long periods in between or by taking multiple measurements along the same crest. In addition, detecting migration can be difficult when the migration distance is long relative to the wavelength. Finally, sand waves may deform as they migrate so that crest displacement is not necessarily equal to displacement of the centre of mass of the dune (Duffy & Hughes-Clarke, 2005). Shape changes can then be mistaken for migration of the entire bedform.

2.5.2. (Geo)statistical techniques

To resolve the issues of quantifying migration based on crest, trough and *lee* side displacement, several methods have been developed that quantify migration based on the three-dimensional bedform shape, using statistical techniques.

One such method, which also accounts for the stochastic character of bathymetric surveys, is called geodetic deformation analysis, applied by Dorst (2009). Deformation analysis describes the seafloor and the presence of bedforms in an idealised, statistical way using spatial trend functions and (sinusoidal) residual functions. Input requirements for this method to work are among others the water depth including the measurement uncertainty at equal positions for every survey, a user-defined level of significance and some a priori knowledge of the seafloor morphology (Dorst et al., 2009). By explicitly considering the uncertainty of every measured depth value, the method can estimate the type and size of seafloor dynamics (including sand wave migration) and its uncertainty from timeseries bathymetric data.

A spatial cross correlation method to detect bedform migration was developed by Duffy & Hughes-Clarke (2005) and later applied by Buijsman & Ridderinkhof (2008) and Zhou et al. (2018). This method

computes the correlation between grid cells from two Digital Terrain Models (DTMs) inside a window that moves within a search area, see Figure 19. Migration vectors are then determined based on the distance between the regions of the DTMs that are most correlated. This way, the rate of bedform migration as well its direction can be estimated, obtaining a migration map a visualised in Figure 20. Strong aspects of this method are, among others, the fact that it computes migration based on the entire sand wave body, that positioning errors are of less influence as the correlation is calculated multiple times inside a larger window and that the computation is not bound to the resolution of the bathymetric data (Duffy & Hughes-Clarke, 2005; Zhou et al., 2018). Also, this technique can detect variable migration rates along the sand wave crest. However, the original method is quite sensitive to outliers or errors in the data sets as these significantly disturb the correlation values and hence the migration estimates (Van Dijk et al., 2011; Zhang et al., 2016). Therefore, the cross-correlation technique was improved by Zhang et al. (2016), who accounted for morphological distortion and outliers in the data.

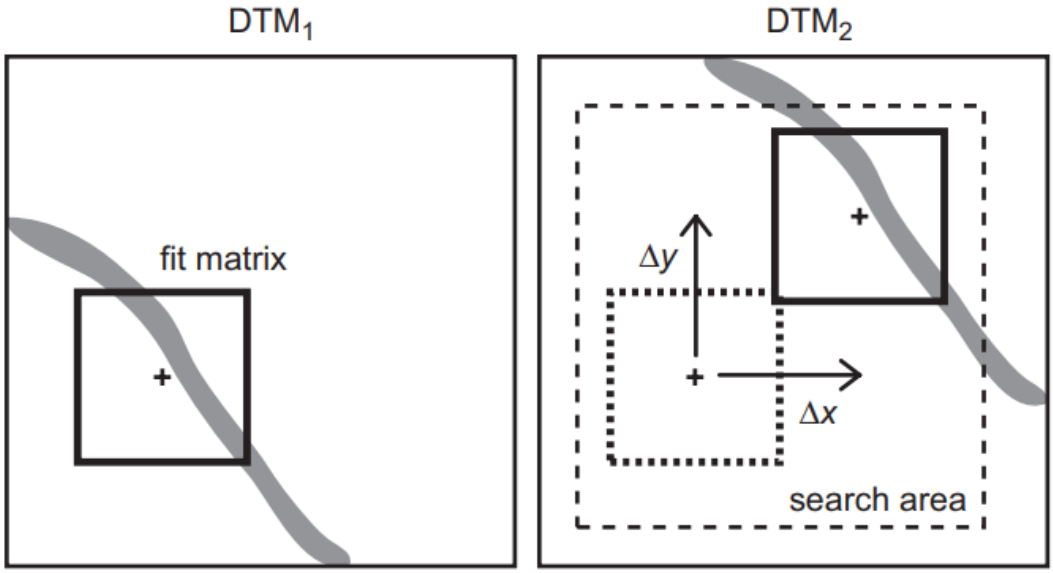

Figure 19 The highest correlation inside the search area yields the migration vector of the sand wave (shaded area) (Buijsman & Ridderinkhof, 2008)

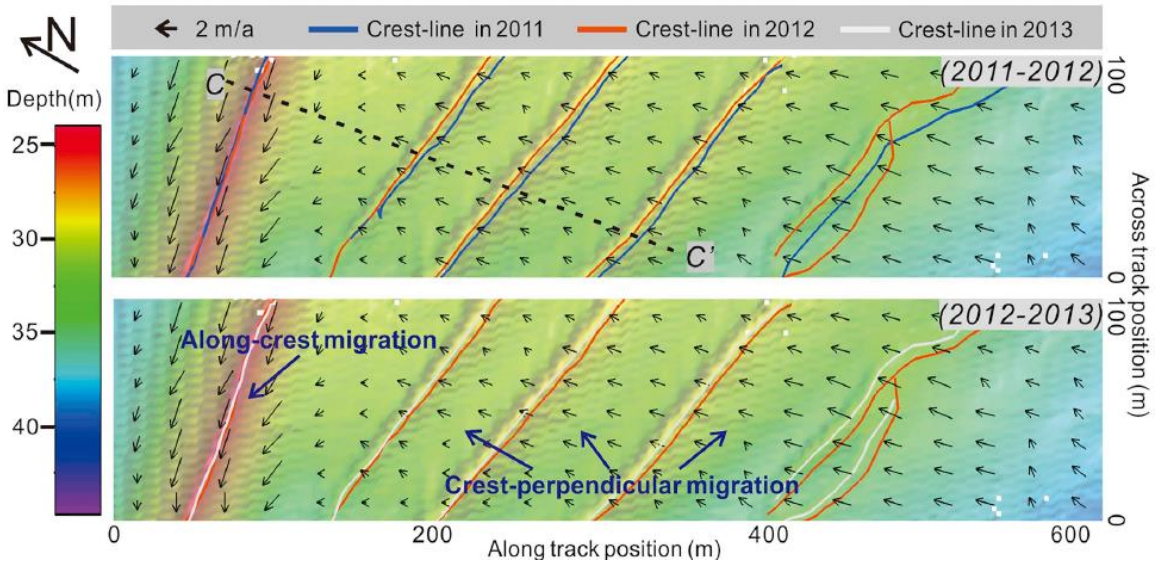

Figure 20 Migration vectors as obtained with the cross- correlation technique (Zhou et al., 2018)

2.5.3. *Using GIS to estimate bedform or landform migration from bathymetric or terrain data*

GIS are widely used for capturing, storing, analysing, and visualising geographical data. The classical static and discrete representation of reality in GIS only considers that, at a given moment, the world is composed of a set of related geographical entities. However, it is well possible to extend a spatial model to a spatiotemporal model by considering changes in location and dimensions of these entities and the changes in the relations between them (Thibaud et al., 2013).

This section concerns the use of GIS for spatiotemporal analysis of moving dunes. The marine environment as well as the desert environment are considered since GIS is also adopted in the mapping of terrestrial sand dunes.

GIS and mapping of marine sand dunes

To track to the movement and evolution or large-scale marine sand dunes on the French continental shelf, a spatiotemporal GIS model was developed (Garlan, 2009; Thibaud et al., 2013). GIS has been used over the years by the French Hydrographic and Oceanographic Office to manage records from bathymetric surveys. Comparisons between consecutive records were commonly used to define new surveys or additions to nautical charts. However, with the increase of data over time, analysing the long-term dynamics of large-scale bed features became a challenge. The GIS was therefore extended such that it is now contains the spatiotemporal relation of dunes from different surveys.

The working principle of the model is as follows. First, a software application called PARAMDUNE is used to identify marine dunes from DEMs and to extract geometric properties for each dune, see Figure 21a. The application also creates polylines and polygonal surface that define the crestline and foot slopes, respectively. These polylines can then be loaded in the GIS to visualise the geographical boundaries of the dunes, as can be seen Figure 21b. To measure and visualise dune migration, a point matching approach is used between subsequent crestlines, i.e., crestlines of the same dune in time. This approach finds a set of matching points along the crestlines that have the shortest distance between them. To this end, the tips of the polylines need to be matched such that the same features are identified on both lines. The migration distance is then readily known as it is equal to the distance between the matching points. Figure 22 gives an example of how the dune geometry and displacement *vectors* can be added as an additional layer to a nautical chart. Importantly, by measuring the displacement along the entire crestline, variable migration rates can be measured.

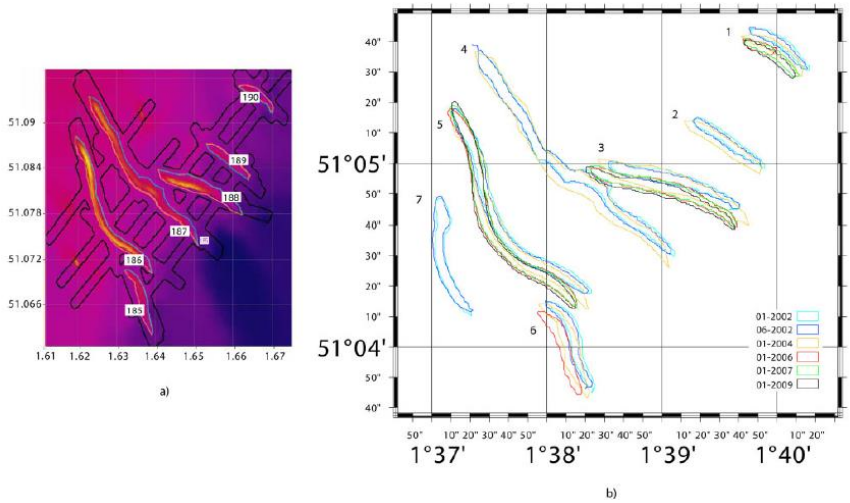

Figure 21 (a) PARAMDUNES application interface (b) Polygonal surfaces representing foot slopes (Thibaud et al., 2013)

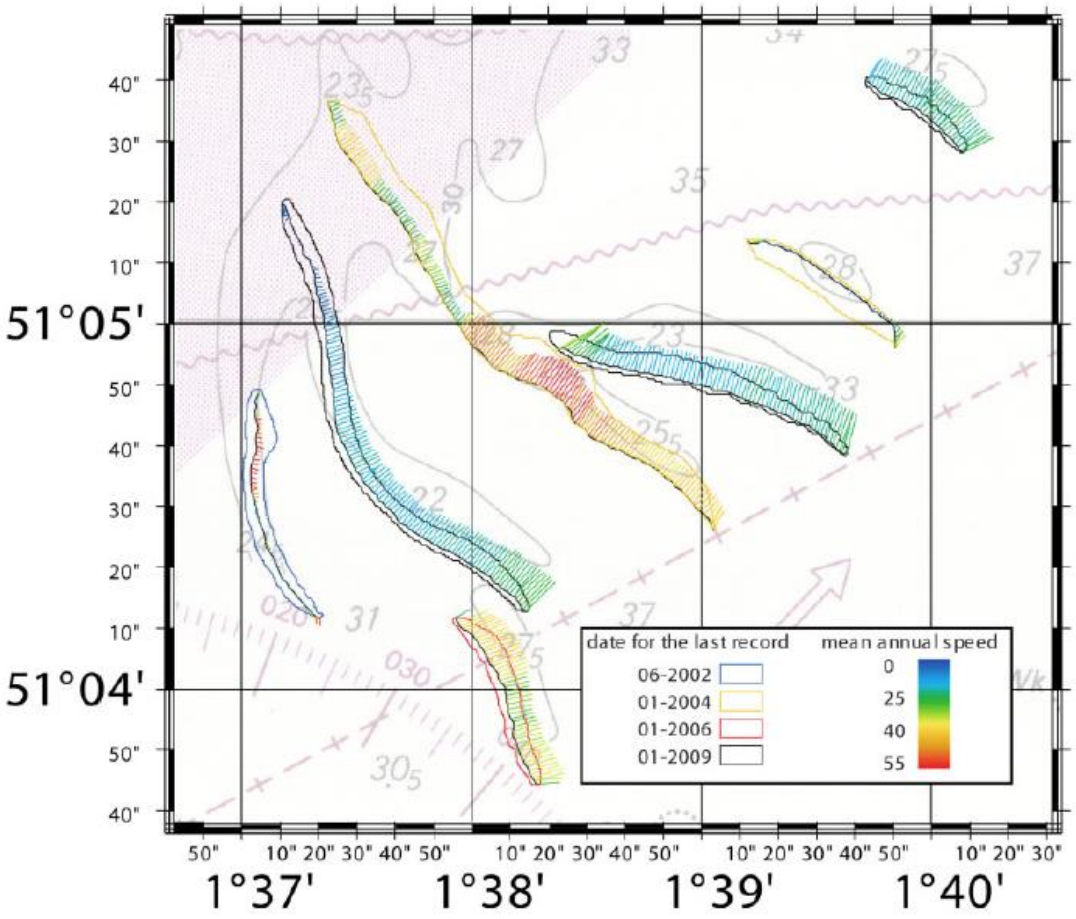

Figure 22 Dune geometry and migration vectors added to a nautical chart (Thibaud et al., 2013)

GIS and mapping of terrestrial sand dunes

Where marine bedform migration poses hazard to a variety of offshore activities, their terrestrial counterparts can cause environmental and societal problems in deserts, particularly to inhabited oases (Ghadiry & Koch, 2010). Remote sensing has since long been used for coastal and desert sand dune studies (Dong, 2015). In the past decade, the use of GIS as a complement to remote sensing data has been explored. Several automated methods are developed that quantify dune displacement from remotely sensed data. Note that, since terrestrial dunes have different shapes than marine sand waves, the techniques described below need some adjustments before they can be applied to sand waves.

One such method was proposed by Ghadiry & Koch (2010) to track the movement of desert sand dunes in Egypt. They developed an ArcGIS extension that quantified dune displacement based on direct comparison of multi-temporal high-resolution (2.5 – 10 m) satellite images. The working principle of their method is as follows. First, some data processing is required. The satellite images are enhanced such that separate classes of sand dunes can be identified. Then, the images (DTMs) are subtracted, obtaining a differential map as visualised in Figure 23. The prevailing wind is north-northwest, so dunes predominantly migrate to the south-southeast. The *raster* data in Figure 23 is then converted to a *vector* shape to mark the outer boundary of the dune displacement, visualised in Figure 24. Finally, after drawing a rectangle box with seven transects lines around the *vector* shapes, an intersect tool is applied to cut off the transect lines at the intersection with the *vector* shape, as can be seen in Figure 25. The migration distance is then equal to the remaining length of the transect lines.

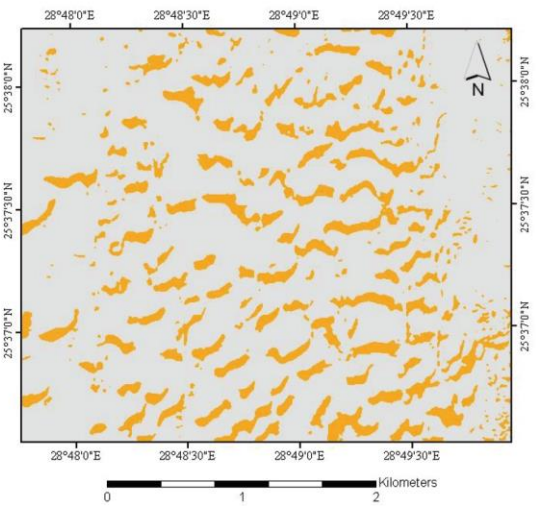

Figure 23 Differential map after subtracting two satellite images. The orange patches represent dune displacement, which is in south-south-eastern direction (Ghadiry & Koch, 2010)

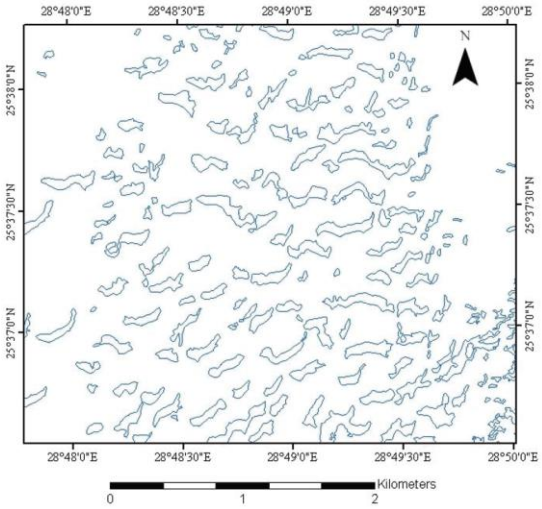

Figure 24 Vector shape files of the areas over which the dunes have moved (Ghadiry & Koch, 2010)

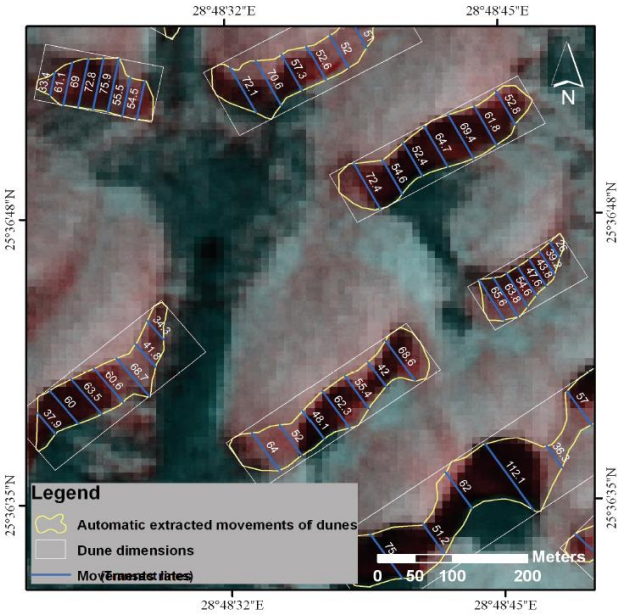

Figure 25 Extraction of the dune migration vectors (Ghadiry & Koch, 2010)

An automated method to measure sand dune migration from DEMs was developed by Dong (2015). His approach, named Pairs of Source and Target Points (PSTP), resembles the approach by Thibaud et al. (2013). The main difference is that PSTP measures the displacement of the centreline of the slip face, which is the steepest side of the dune facing in downwind direction, see Figure 26. These centrelines are called target and source lines. The target line represents the most recent centre line, and the source line represents the oldest centre line. The tips of the source and target lines are matched such that the same features are identified on both lines. Then, random target points are generated on the target line. By using a pre-defined search radius, the target points are then matched to the nearest point on the source line, see Figure 27. Based on the distance and angle between two points, the migration distance and direction of a source or target point can be determined. Figure 28 and Figure 29 contain, for 5936 target points in an area of 9 by 2.4 kilometre, the source direction and migration rate, respectively. To better distinguish spatial variability, spatial interpolation or point statistics can be applied, obtaining continuous *raster* data sets as given in Figure 30.

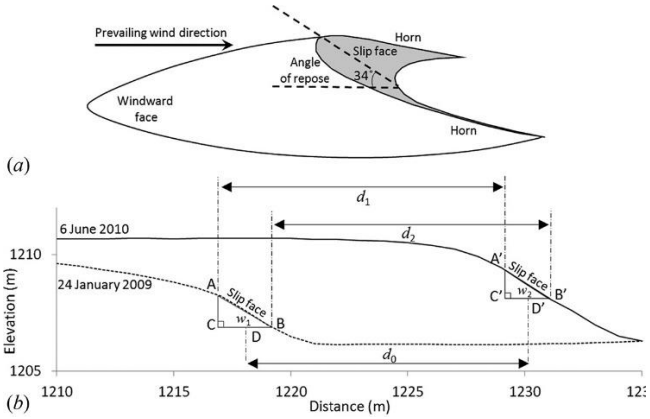

Figure 26 Quantifying dune migration based on slip face displacement (d_0) (Dong, 2015)

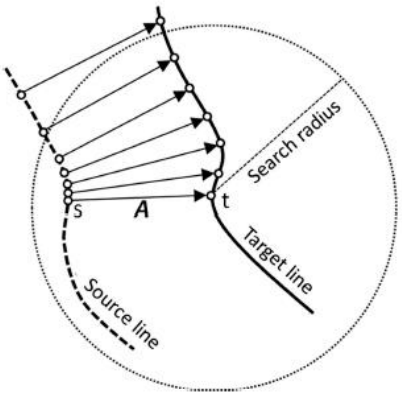

Figure 27 The concept of PSTP (Dong, 2015)

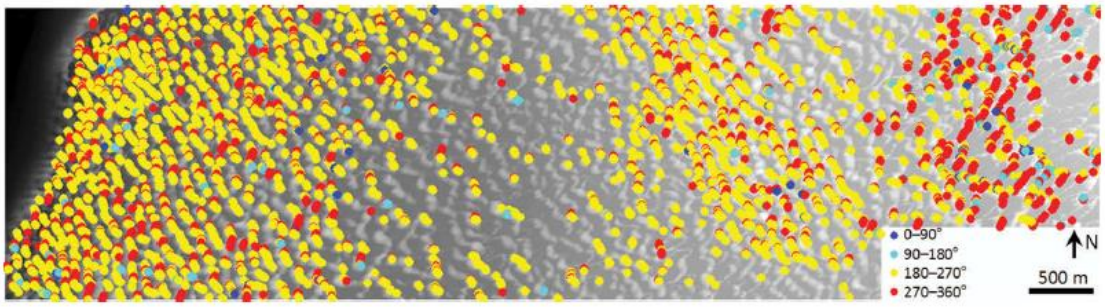

Figure 28 Source directions of 5936 target points (Dong, 2015)

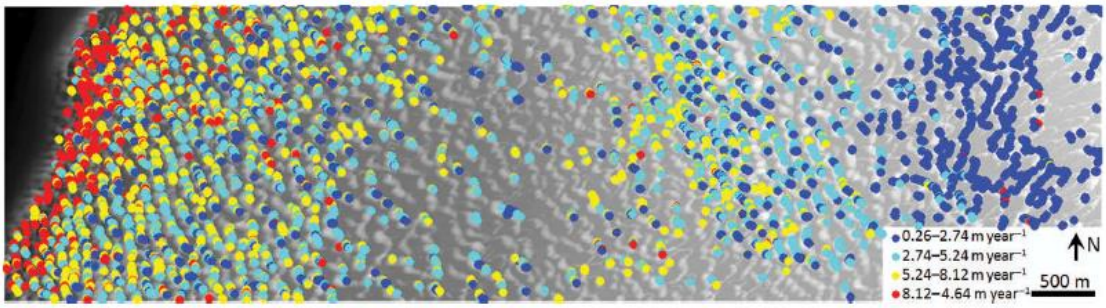

Figure 29 Migration rates of 5936 target points (Dong, 2015)

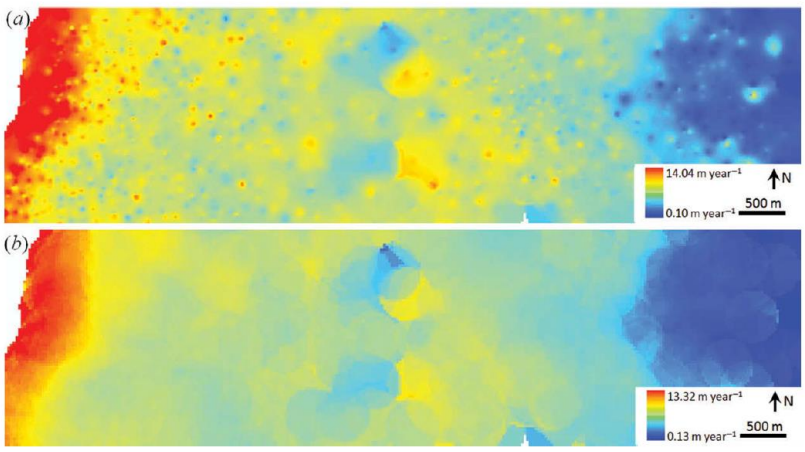

Figure 30 Raster data set of migration rates created with (a) IDW interpolation and (b) Point statistics (mean) (Dong, 2015)

2.5.4. Overview of described methods

An overview of the advantages and disadvantages of the considered migration detection methods is given in Table 3.

Table 3 Advantages and disadvantages of the considered migration detection methods

Method	Advantages	Disadvantages
Crest-perpendicular transects (Van Dijk & Kleinhans 2005; Knaapen, 2005; Van Dijk et al., 2008; Van Dijk et al., 2011)	Robust and straightforward	Lateral migration is not detected
	Has proven itself in the past	Shape changes can be mistaken for migration when only crest migration is considered
Deformation analysis (Dorst, 2009)	The uncertainty of detected dynamics is estimated as the stochastic character of bathymetric data is accounted for	Long procedure and less straightforward to grasp
	Lateral as well as crest-perpendicular migration can be detected	A priori knowledge on the uncertainty of depth measurements is required
Spatial cross-correlation (Duffy & Hughes-Clarke, 2005; Buijsman & Ridderinkhof, 2008; Zhang et al., 2016; Zhou et al., 2018)	Lateral as well as crest-perpendicular migration can be detected	Sensitive to outliers in the bathymetric data
	Relatively straightforward and fast computation	A single set of input parameters (window size, vector type) might not be optimal for all types of morphodynamics
	Quantifies migration of the entire sand wave body	
	Not bound to the resolution of the bathymetric data	
PARAMDUNE (Garlan, 2009; Thibaud et al., 2013).	Lateral as well as crest-perpendicular migration can be detected	Identifying and filtering of individual dunes is less straightforward when the sand wave pattern is more continuous, i.e. when the sand waves merge into one another
	Dune positions, migration rates and directions are instantly visible in GIS	
Raster change detection (Ghadiry & Koch, 2010)	Lateral as well as crest-perpendicular migration can be detected	Identifying and filtering of individual dunes is less straightforward when the sand wave pattern is more continuous, i.e. when the sand waves merge into one another
	Migration rates and directions are instantly visible in GIS	
Pairs of Source and Target Points (Dong, 2015)	Lateral as well as crest-perpendicular migration can be detected	Filtering centre lines of the *lee* side is not appropriate for tidal sand waves as these tend to change shape over time
	Migration rates and directions are instantly visible in GIS	
	Relatively straightforward	

3. Methodology

3.1. The use of a geographic information system (GIS)

An important component of the data-driven approach is the use of a geographic information system (GIS). These systems are widely used for capturing, storing, analysing, and visualising geographical data and are therefore highly suited for this research. The GIS which is used during this research is QGIS, which is downloaded as part of OSGeo4W, a binary distribution containing the opensource GIS desktop applications QGIS GIS and GRASS GIS and geospatial libraries such as GDAL and SAGA GIS. Since it is a free and open-source package, the steps during the MSc Thesis project can be easily reproduced. For similar reasons, the programming language Python is used as a complement to QGIS.

3.2. Approach per research question

3.2.1. Research objective 1: method development

Research question 1 aims at developing a relatively fast and accurate algorithm to quantify tidal sand wave migration from bathymetric timeseries. To achieve this, the following steps are taken:

1. **Formulation of selection criteria**. Several criteria are formulated by which detection methods found in literate are evaluated.
2. **Selection of candidates**. From the detection methods that are evaluated, two suitable options are selected for further testing. A detailed description of the methods is given in Chapter 4.
3. **Algorithm development in QGIS**. Two options are selected for further testing and are implemented in QGIS. Extensively automating the algorithms is not yet required as only few bathymetric timeseries are analysed in this phase of the research.
4. **Testing with artificial data**. To validate the results of both methods, they are tested with artificial data, in which different migration speeds are pre-defined in a uniform direction.
5. **Testing with field data**. The migration detection methods are tested with multiple sets of field data, which contain morphometries and dynamics that are representative for the NCS. The main aim is to find out how the methods cope with different types of sand wave morphology and dynamics, different types of underlying topography and differing data quality. Performance is compared by plotting the frequency distributions of the measured migration rates and directions in one figure. The median, the 10^{th} and 90^{th} percentiles are used to describe the data distributions. The median quantifies the typical value[2] and the percentiles give the boundaries which contain 80 percent of the values. These indicate the spread of the data around the median. In addition, spatial colour plots of migration rate and direction are plotted to see whether comparable spatial patterns are revealed.
6. **Selection of most suitable candidate**. The methods are evaluated on their performance with field data (are the obtained results realistic?), artificial data (are the outcomes reasonably close to the pre-defined values?) as well as their practical applicability (required steps in the procedure, computation time, ease of error sourcing, general applicability of input parameters for different bathymetric timeseries). The latter criteria are important because they determine the suitability of a method for large-scale analyses using many datasets. The method that performs best overall is selected for further use in research question 2.

[2] The median is chosen over the mean to reduce the influence of outliers. Furthermore, the median provides a better indication of a typical value when the frequency distribution is skewed (see section 6.4 to 6.6).

3.2.2. Research objective 2: migration quantification on the NCS

Research question 2 aims at quantifying tidal sand wave migration from bathymetric timeseries covering as much of the NCS as possible. Steps taken include the following:

1. **Semi-automation of preferred detection method**. Semi-automation is required such that many timeseries can be analysed without too frequent manual interference.
2. **Creation of bathymetric timeseries with data after 2000**. Initially, only the data that is collected after the year 2000 is used to create timeseries, since horizontal positioning of older data is often less accurate. Furthermore, visual inspection pointed out that most of the older data contained some random noise that could only be removed by application of a smoothing filter (see Appendix I). One survey is often collected over a period of several months up to one year. To prevent overlap at the boundaries of two surveys, the minimal time in between is one year. The preferred time in between two surveys depends on the expected magnitude of the dynamics. When the expected dynamics are high, the time between two surveys should be at least 1 or 2 years. In areas with low dynamics, time between two surveys should be at least 4-5 years (preferably longer) such that a robust estimate of migration rate can be done, and the impact of short-term seasonal changes is minimised.
3. **Migration quantification**. The semi-automated detection method is used to obtain the quantities of migration rate and direction for as much of the NCS as possible.
4. **Analysing spatial coverage**. The spatial coverage of the obtained results is analysed to identify regions without any timeseries.
5. **Creation of bathymetric timeseries with data before 2000**. New timeseries with bathymetric data sets collected before the year 2000 are created for regions where timeseries with recent data (after 2000) are absent. These are then used as input for the semi-automated detection method. Step 3-5 are repeated until the migration data covers as much of the NCS as possible.
6. **Aggregation of obtained point data per square kilometre**. To gain insight in large-scale migration patterns on the NCS, the previously obtained point data is averaged per square kilometre[3]. Considering a typical length scale of roughly 500 m, most estimates are based on two or three sand waves. For the estimates to be statistically significant, a minimum number of 10 data points is used for the calculation. The main results are colour maps with migration rates and directions for all sand wave fields on the NCS. In addition, to quantify the uncertainty of the results, the standard deviation and coefficient of variation of migration direction and migration rate are determined, respectively.

3.3. Bathymetric data

The bathymetric data which is used during the research regards the readily available Digital Elevation Models (DEMs) from the OpenEarth server managed by Deltares (Deltares, 2017b). These DEMs contain the water depth relative to the *lowest astronomical tide* (*LAT*) and are interpolated from digitized fair sheets, single beam and multibeam echo sounding data[4] using Inverse Distance Weighting at a 25 m resolution. A 25 m resolution is favourable because it is just high enough such that large-scale bed features (sand waves) are visible and small-scale features (megaripples) are smoothed out. Furthermore, it is a reasonable choice in terms of data density of SBES and MBES data (Van Dijk et al.,

[3] To compute an average value for the central node in a square of 1 by 1 km, all data points within a radius of 707 m are included.

[4] The digitized fair sheets are excluded from the research as the data resolution is too low for the identification of bedforms of a spatial scale smaller than the resolution (Van Dijk et al., 2011).

2011). It is important to note that the resolution is not increased as this would dramatically increase the computation time of the algorithms, which is not desirable when analysing many timeseries.

The search radius, which is the radius within which all depth measurements are used to interpolate the depth at the node, is set to 100 m. This way, the distance of 50-1,000 m between sailed SBES track lines means that not all SBES grids are filled. Using a larger search radius would generate a filled grid, but the uncertainty of interpolated values in between sailed track lines would be very high (Van Dijk et al., 2011). This small search radius, combined with the fact that the survey tracks of SBES and MBES data are mostly sailed perpendicular to the sand waves orientation, means that the uncertainty of the interpolated values is not significant. After all, parallel to the crests, the variability in depth is generally much lower that perpendicular to the crests.

The NLHO bathymetric data is stored as a netCDF-file, which is a data format that is suitable for storing multi-layered data. An overview of the data layers contained with each netCDF-file can be found in Appendix II.

3.4. Study area

The study area concerns the sand wave fields on the Netherlands Continental Shelf (NCS), also referred to as the Dutch Exclusive Economic Zone (EEZ), which is the area in the North Sea that falls within the jurisdiction of the Netherlands (Ministry of Defence, 2021). The area covered by the NCS as well as the bathymetry are visualised in Figure 31.

Figure 31 Bathymetry of the Netherlands Continental Shelf (EMODnet, 2021)

Figure 32 visualises the water depth of the NCS relative to the LAT. The names of regions or locations (marked with a red dot) that are often referred to in this research are indicated in Figure 32 as well.

Sand banks, which are oriented parallel or oblique to the Dutch coast, can be mainly found near Zeeland (Zeeland Banks) and far offshore of IJmuiden and the Wadden Islands (Brown Ridge and Breeveertien Banks). Shoreface connected ridges have a clockwise oblique orientation relative to the coast and are observed between the Maasvlakte and Den Helder and north of Vlieland and Texel (Van Dijk et al., 2011).

Tidal sand waves are represented by the rippled pattern perpendicular to the Dutch coast. The NCS comprises three sand wave fields, which are marked in *italics* in Figure 32. The main sand wave field covers the seafloor between the southern border of the NCS and the northern parts of the Breeveertien Banks and the Brown Ridge. In addition, two sand wave fields are present near the Wadden Islands. These are located west of Texel and north of Vlieland.

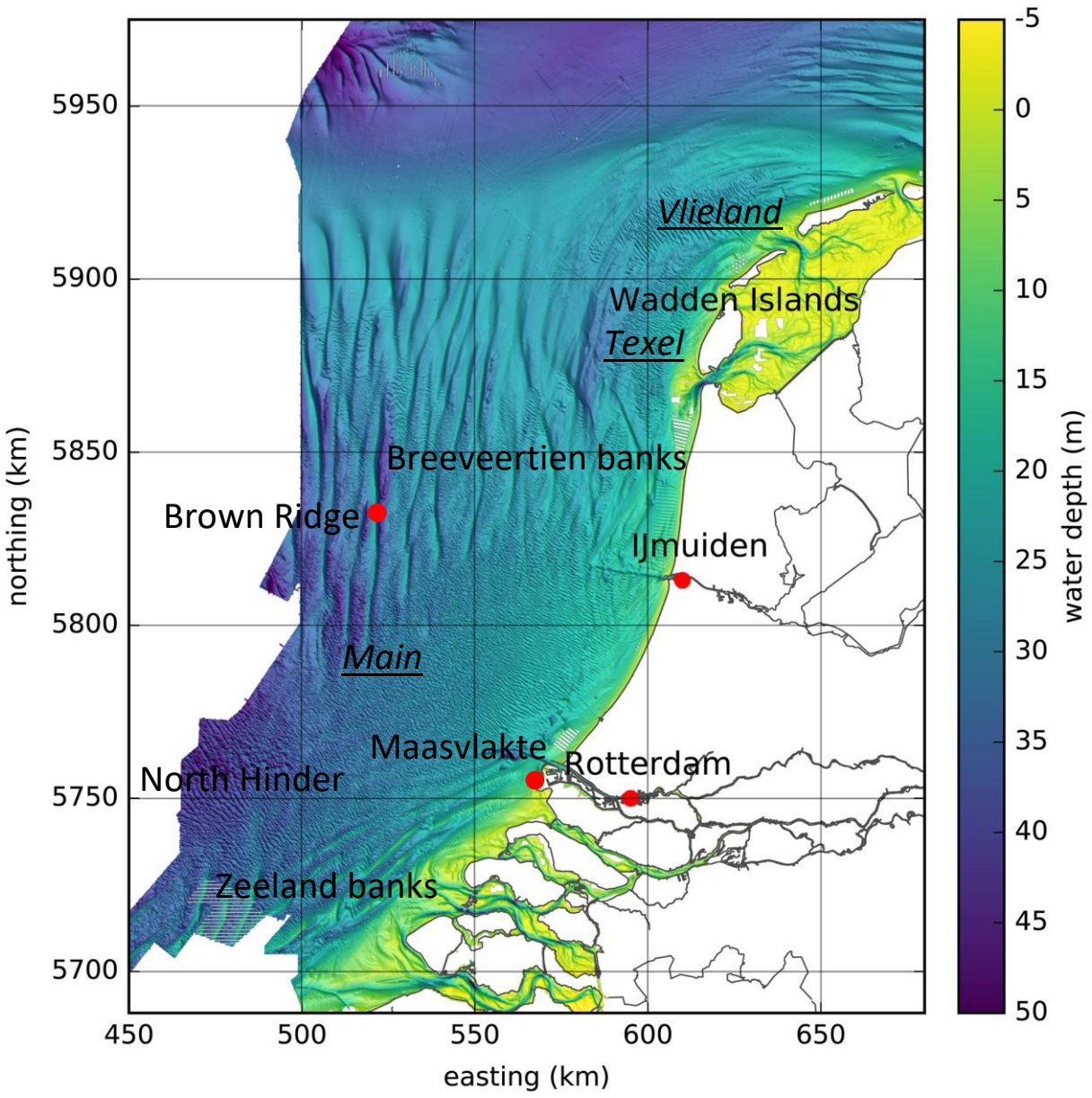

Figure 32 Water depth relative to the Lowest Astronomical Tide (Damen et al., 2018)

4. Migration detection methods

4.1. Introduction

This chapter comprises the selection and implementation of suitable methods that quantify tidal sand wave migration from bathymetric timeseries.

First, the selection procedure is described in section 4.2. Then, in sections 4.3 and 4.4, the selected methods are described in more detail. This includes, among others, the working principle, implementation in QGIS, output and sources of uncertainty.

4.2. Preliminary method selection

From the detection methods available in literature (see section 2.5), several suitable candidates are selected. These are: Pairs of Source and Target Points (PSTP, Dong (2015)), Spatial Cross Correlation (SCC, (Duffy & Hughes-Clarke, 2005; Buijsman & Ridderinkhof, 2008; Zhou et al., 2018)), Deformation Analysis (DA, Dorst (2009)) and Raster Change Detection (RCD, (Ghadiry & Koch, 2010)). These are selected because they quantify migration in two horizontal directions and because it is expected that they can be implemented in QGIS. See Appendix III for a further explanation.

In this preliminary selection phase, two criteria are formulated. See below.

Accuracy with available bathymetric data. Although the resolution of the available datasets is relatively low at 25 m, the detection method should be able to provide a reasonably accurate estimate. Resampling the *raster* data to a higher resolution is not considered for the purpose of this research.

Efficiency and upscaling. Computation time and required steps of a detection method should be manageable such that it is suitable for analysing a large number of datasets.

In Table 4, it is given whether a method does (V) or does not satisfy (X) a criterion. A detailed explanation for the assessment can be found in Appendix III. The main reason why DA is not suitable for the purpose of this research is because too many complicated steps are required and because the migration estimates are extracted from on an idealised, sinusoidal surface, instead of the bathymetric data. RCD is not suitable since sand waves have a more continuous pattern than terrestrial sand dunes. Therefore, identifying individual sand waves is more difficult and subtracting two bathymetric datasets does not result in a clear difference map as in Figure 23.

Since PSTP and SCC satisfy both criteria, these are selected for implementation in QGIS and further testing with artificial data and field data.

Table 4 Performance of detection methods per criterion

Method	Accuracy with available data	Efficiency and upscaling
PSTP	V	V
SCC	V	V
DA	X	X
RCD	X	V

4.3. Pairs of Source and Target Points (PSTP)

4.3.1. Working principle

PSTP quantifies migration by measuring the displacement of vectorised morphological components in two horizontal directions. As is described in section 2.5.3. PSTP was originally developed for the quantification of terrestrial sand dune migration (Dong, 2015). Some adjustments are required to make the technique suitable for quantifying tidal sand wave migration.

The main adaptation to the method developed by Dong (2015) is the vectorization of crest and trough lines instead of centre lines at pre-defined slope values. The latter approach is suitable for the terrestrial sand dunes studied by Dong (2015) since these tend to preserve their shape over time. However, it is not preferred for the purpose of this research since tidal sand waves can change shape. Both crest and trough displacement are quantified to distinguish shape changes from true migration. At a resolution of 25 m, crest and trough locations are generally well represented by a single *raster* cell and can therefore be vectorised to a continuous, relatively smooth line.

The main steps are as follows:

- Smoothing of DEMs. It is preferred to use the raw DEMs as well as the smoothed DEMs as input. However, in case data quality is insufficient, only the smoothed dataset is used.
- Detection of crest and trough cells with maximal curvature (crest detection, taking raw DEM as input) and convergence index (crest and trough detection, taking smoothed DEM as input).
- Filtering of crest and trough *raster* cells.
- Vectorization of filtered crest and trough cells to obtain source and target lines.
- *Buffering* and *clipping* to match the ends of the source and target lines.
- Plotting random target points on the target lines, i.e., the most recent crest and trough lines.
- Measuring distance and angle from target points to the source lines, i.e., oldest crest and trough lines.

4.3.2. Pre-processing of bathymetric data

Smoothing of the DEMs is required before detecting the crest and trough cells. The motivation is twofold:

1. As a result of, among others, horizontal positioning errors and overlapping MBES survey tracks, a DEM can be too noisy for either maximum curvature or convergence index to detect continuous linear features.
2. The convergence index produces better results when smoothed DEMs are used as input, which is due to its high sensitivity to noise.

A smoothing filter is applied to remove undesired noise. The applied filter in SAGA GIS uses a moving window to average the difference between a *raster* cell and its neighbouring cells (see Appendix I).

An important consequence of using a moving average for data smoothing is the fact that the crests are lowered and shifted towards the *stoss* side, while the troughs are elevated and shifted towards the *stoss* side of the next adjacent sand wave (see Appendix I). Hence, since PSTP relies on the measurement of crest and trough displacement to quantify migration, an additional uncertainty is introduced. To reduce the impact of smoothing on the final estimate, DEMs that belong to one timeseries are smoothed with identical settings. An advantage of this approach, regarding crest migration, is the fact that the migration estimate is based on displacement of the sand wave body instead of the highest peak. Short-term shape changes are therefore filtered out.

4.3.3. Crest and trough detection

The tools that are used to filter out crest and trough cells are Maximal Curvature (MC), which is used for crest detection from raw data, and Convergence Index (CI), which is used for crest and trough detection from smoothed data. MC and CI are both part of SAGA GIS.

CI measures the degree of convergence or divergence for a *raster* cell inside a moving window. Since the slopes of a sand wave converge at the trough and diverge at the crest, the convergence index is well suited for extracting crest and trough positions from a DEM. In this research, CI is calculated by averaging the aspect of adjacent *raster* cells relative to the centre cell and subtracting 90 degrees, see Equation (2) and Figure 33 (Kiss, 2004; Thommeret et al., 2010).

$$CI = (\frac{1}{8}\sum_{i=1}^{8}\theta_i) - 90 \quad (2)$$

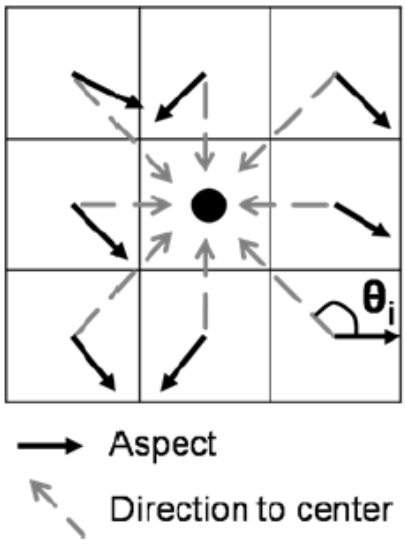

Figure 33 Aspect of adjacent raster cells to a center cell (Thommeret et al., 2010)

The CI varies between -90° and 90°. Maximum divergence (corresponding to a peak of a cone) occurs at 90°, maximum convergence (corresponding to a pit), occurs at -90° and 0° corresponds to an even slope, see Figure 34.

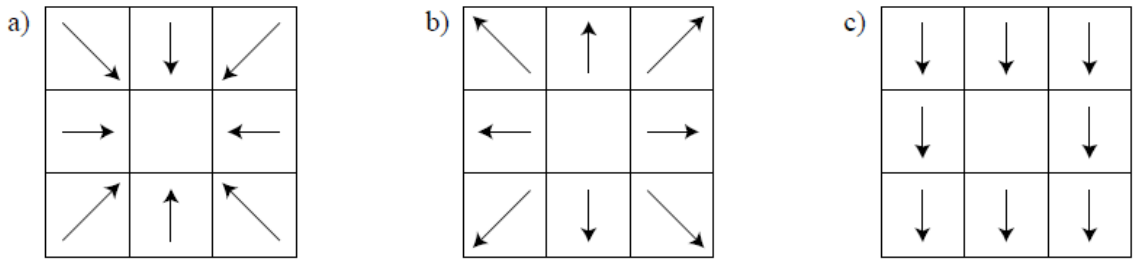

Figure 34 The convergence index is calculated based on aspect. The averages of the relative aspects are (a) 0°, (b) 180° and (c) 90°. The convergence indexes are -90° (a), 90° (b) and 0° (c) (Kiss, 2004).

While CI produces the cleanest output on a smoothed dataset, MC works better on raw data. Since the curvature of the seabed is generally the strongest at the crest of a sand wave, MC is well suited for the extraction of crest lines.

In SAGA GIS, MC is calculated as the maximum 2nd derivative of a surface that is fitted over a window of 3 by 3 *raster* cells, see Figure 35 (Environmental Systems Research Institute, Inc., 2016; Minár, 2020).

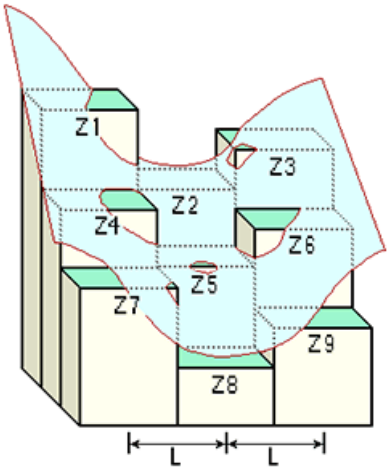

Figure 35 Surface fitted over a 3x3 raster window (Environmental Systems Research Institute, Inc., 2016)

An example of the calculation of CI with a smoothed DEM and MC with a raw DEM is given in Figure 36 and Figure 37.

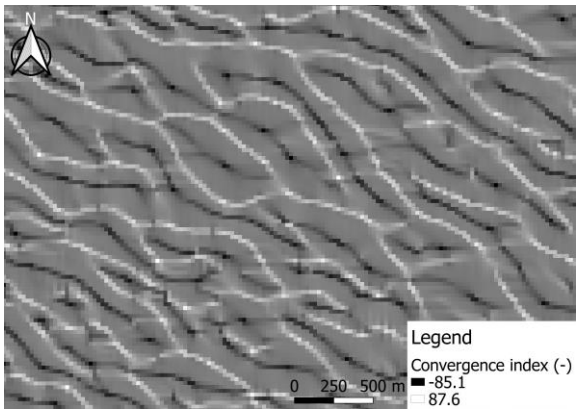

Figure 36 Example of convergence index with sand wave crests in white and troughs in black

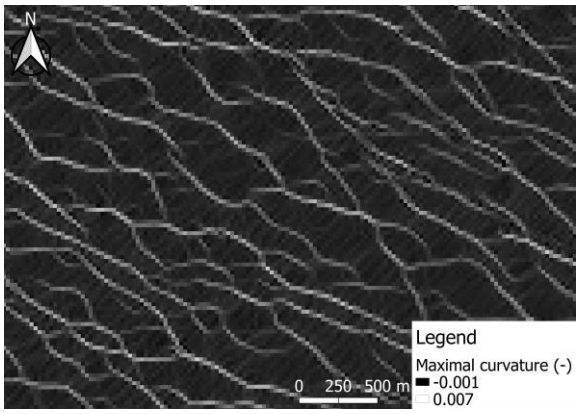

Figure 37 Example of maximal curvature with sand wave crests in white

4.3.4. Intermediate steps

When CI and MC are calculated for both DEMs, the obtained *raster* datasets are converted to a binary *raster* using the QGIS Raster Calculator. To filter out the crest and trough lines, values above or below a threshold are set to 1 and 0. For CI, a threshold of 25 (crest) and -25 (trough) produces robust results in all tests. For MC, in most cases, the optimal value for accurately filtering the crest lines is roughly 1/3 of the maximum curvature value. Setting the *raster* cells that are 0 to NAN/NULL leaves only the crest and trough cells.

Next, the filtered cells are thinned to obtain a linear feature of a single cell width, after which the thinned cells are vectorised to a line geometry. The obtained lines are smoothed using a small tolerance and minimal number of iterations as to represent the crest and trough lines with a smooth line but without changing the *vector* geometry. Lines that do not represent a real crest or trough line are removed manually.

Before displacement of crest or trough lines can be measured, it is important that the ends of the lines are matched. This way, similar features are identified on the source and target lines. This is achieved by *buffering* both lines and consecutively *clipping* the source line to the *buffer* of the target line and the target line to the *buffer* of the source line.

4.3.5. Final output

The final output of PSTP consists of randomly placed target points along the target lines. Since these are placed randomly, a certain number of points per feature and a minimum distance between the points is entered to prevent clustering. These parameters are chosen such that an area of 5 by 5 km contains is covered by at least a few thousand data points. The optimal parameters depend on whether the sand wave pattern is two-dimensional (10 points) or three-dimensional (20 points). A minimum distance of 50 m in between the data points is used in most analyses.

For each target point, the minimum distance to the nearest source line as well as the coordinates of the source and target points are added to the attribute table of the *vector* layer. A maximum distance between the source and target points (which is larger than the expected migration distance) is defined to prevent outlier values from occurring. An annual migration rate (m/year) is then determined by dividing the distance by the difference in time. The source direction (degrees), i.e., the migration direction, can be calculated based on the coordinates of the source and target points.

4.3.6. Known uncertainties

When using PSTP to quantify tidal sand wave migration, note the following sources of uncertainty:

Integer position of raster cells. Migration distances are measured along the integer positions of the *raster* cells in x and y direction. Hence, when dynamics are insignificant in the time between two surveys, measured distances are mostly 0 m. It is therefore important to use long-term timeseries to obtain robust estimates for migration.

DEM smoothing. Smoothing the DEMs results in a minor shift of the crest and trough positions, especially in the case of sharp-crested, steep-sloped sand waves. The effect on the quantitative output should however not be significant since the DEMs that belong to a single timeseries are smoothed with identical settings. Moreover, one could argue that a more robust estimate of migration is obtained since migration is quantified closer to the sand waves' centre of mass instead of at the peak. This way, short-term shape changes are filtered out.

Irregularity of crest and trough lines. The relatively low resolution of the DEMs means that the vectorised crest and trough lines are irregular rather than smooth, see Figure 38. Since this applies to the target lines as well as the source lines, the lines alternately converge and diverge, where they should be more parallel.

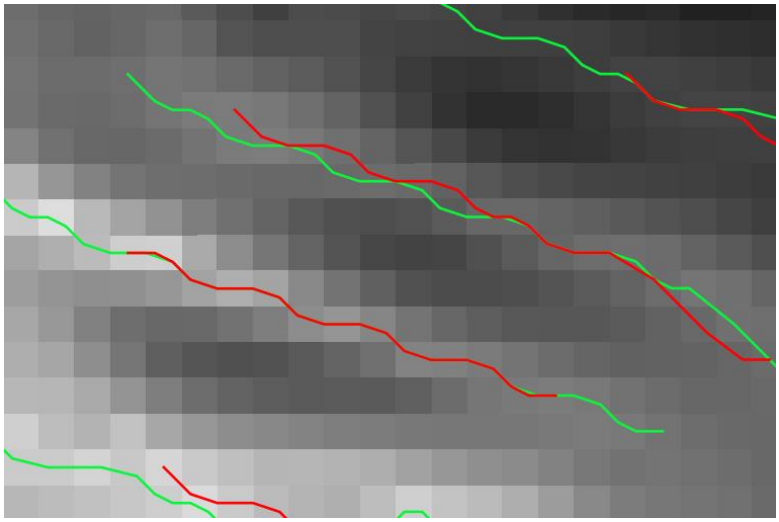

Figure 38 Source (green) and target (red) crest lines

As a result, when plotting the migration rates in a histogram, relatively sharp peaks occur at the beginning and the end of the distribution. Furthermore, several peaks might occur for migration direction, depending on whether migration occurs in one or two directions. In case the displacement is low relative to the data resolution, some target points are located on the wrong side of the closest source points, which implies migration in two directions.

In case dynamics are high, the problem that is described here does not significantly change the overall conclusion regarding average migration rate or direction, especially when many points are used. However, in case dynamics are low, aggregating the point data leads to an average migration direction that is perpendicular to the actual migration directions. Average migration rates are still realistic but show strong variability in the form of high standard deviations and coefficients of variation (see sections 8.3 and 8.4).

4.4. Spatial Cross Correlation (SCC)

4.4.1. Working principle

In essence, the SCC technique determines the location where two datasets are most similar. Displacement is estimated by finding the best fit of a template, which is a section of DEM 1, inside a larger image, which is a section of DEM 2. In Duffy (2005), a slope *raster* was used as input rather than an elevation map. For this research, the elevation maps gave robust results.

The main steps are as follows:

- *Clipping* the DEMs to each other's extent to match the number of rows and columns.
- Defining window size and search zone. The template is the region within the window and the image is the region within the search zone.
- Filling the normalized cross correlation matrix by incrementing and decrementing the window around the search zone.
- Locating the point or region of highest correlation between the template and the image.
- Migration quantification using three different vector types.
- Incrementing and decrementing the window and search zone over the DEMs with pre-defined steps.

4.4.2. Pre-processing of bathymetric data

For two DEMs to be represented by one rectangular grid, the number of rows and column need to be equal. This is achieved by *clipping* DEM 1 by the extent of DEM 2 and *clipping* DEM 2 by the extent of DEM 1.

No difference is noted between raw and smoothed datasets during testing, which is probably because the window is sufficiently large such that the normalized correlation calculation is not distorted by small scale bed features and minor data anomalies. Smoothing of the DEMs is therefore not required.

4.4.3. Defining window size, search zone and step size

Window size, and hence template size, is defined by an integer number of grid cells. For this research, only a squared window shape was tested such that the width and height can be changed using a single input prior to each run.

Conceptually, the optimal window size depends on the dominant sand wave length in an area. If the window is too small, the technique has difficulty tracking displacement of larger bed features, especially when the window does not include a crest. In that case, a chaotic vector field is obtained. On the other hand, when the window is too large, migration of smaller sand waves is not detected accurately, and the estimates are based on the generalized displacement of multiple sand waves together. In practice, the optimal window size is found by trial and error. Based on the range of wavelengths in an area, the smallest wavelength is used as a first attempt. The window size is then increased until a relatively smooth and uniform vector field appears.

The search zone, which is defined by an integer number or grid cells that is added to the window at each side, must be larger than the expected migration distance such that the image includes the template. See Figure 39. The step size determines the grid spacing of the final *raster* output. Its value is chosen such that an area of 5 by 5 km is covered by at least a few hundred data points. To this end, a step size of ¼ the window size suffices in most cases.

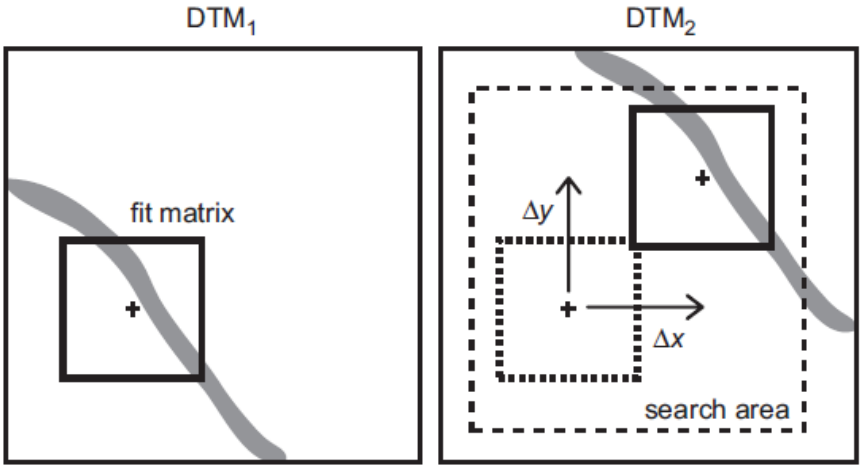

Figure 39 Illustration of the cross-correlation technique. To obtain the migration vector of the sand wave (shaded area) the following procedure is followed. For every grid point, the fit matrix on DTM_1 on time t_1 is shifted in x and y directions within the search area on DTM_2 on time t_2. For every displacement, a correlation between the height in the fit matrices on DTM_1 and DTM_2 is calculated. The highest correlation within the search area yields the displacements D_x and D_y of the fit matrix (Buijsman & Ridderinkhof, 2008).

4.4.4. Normalized cross correlation

The normalized cross-correlation coefficient quantifies the correlation strength of two discrete data sets. It is the sum of the products of overlapping pixels, which is normalized by subtracting the mean and dividing by the standard deviation. The coefficient varies between -1 (template and image are in antiphase) and 1 (template and image are in phase).

The normalized cross correlation coefficient is calculated with Equation (3)[5] (Lewis, 1995; Duffy, 2005). The calculation is iterated by incrementing and decrementing the relative displacement in the x and y directions by u and v, respectively.

$$\gamma(u,v) = \frac{\sum_{x,y}[f(x,y) - \bar{f}_{u,v}][t(x-u,y-v) - \bar{t}]}{\left\{\sum_{x,y}[f(x,y) - \bar{f}_{u,v}]^2 \sum_{x,y}[t(x-u,y-v) - \bar{t}]^2\right\}^{0.5}} \quad (3)$$

f = the *raster* cells in the image
$\bar{f}_{u,v}$ = the mean of $f_{x,y}$ in the region under the template
t = the *raster* cells in the template
$\bar{t}$ = the mean of t

The reasoning to prefer normalized cross correlation over simple cross correlation is twofold (Duffy & Hughes-Clarke, 2005).

1. Outliers in the DEMs tend to bias the maximum correlation towards these locations so that high correlation values reflect data anomalies instead of truly matching patterns.
2. The magnitude of the non-normalized correlation coefficient is linked to the window size. It is therefore not useful for comparing results obtained with different window sizes.

The normalized cross correlation procedure with image A (size M_a,M_b) and template B (size N_a,N_b) results in a matrix C of size (M_a+M_b-1, N_a+N_b-1).

[5] The Python implementation of normalized cross correlation uses Fast Fourier Transform convolution rather than correlation for speed purposes. The results are similar up to 3 significant digits.

4.4.5. Vector types

The location of highest correlation in the normalized cross correlation matrix is the location where the DEMs are most similar. By measuring the distance to the zero-lag position, the migration rate and direction of the features inside the window can be estimated. However, since a linear feature is correlated to another linear feature that has been displaced, a clear point of maximum correlation will not always occur. Rather, depending on the sinuosity of the sand wave crest, the correlation matrix contains an elliptical region of high correlation values, as can be seen in Figure 40(c) (Duffy & Hughes-Clarke, 2005).

Three different vector types can be used to estimate sand wave displacement from the normalized cross correlation matrix, see Figure 40(a)(b).

Maximum correlation. The position of maximum correlation is located, and displacement is measured by the offset in x and y direction relative to the zero-lag position. An important downside is the fact that displacement can only be expressed by integer grid cells in x and y-direction.

Weighted centroid. This method considers the cross-correlogram as a continuous correlation surface (see Figure 40(c)) with a peak that may lie between the pixels. The correlation peak is found by taking the weighted centroid, or centre of mass, of a region with correlation values above a certain threshold value, also called the threshold region. The optimal threshold value lies between $\gamma_{max}/1.1$ and $\gamma_{max}/2$ in most cases and is found by trial and error, in the same way as the optimal window size is determined. The weighted centroid can be located reliably when the threshold region is an enclosed ellipse, which is the case when the sand wave pattern is three-dimensional.

Weighted regression line. This method draws a regression line through the *raster* cells that make up the threshold region. The displacement of the zero-lag position to the closest point on the regression line represents the migration distance. This way, the direction of the migration vector is always perpendicular the orientation of the sand waves, which is a valid assumption in a two-dimensional flow field with straight-crested sand waves.

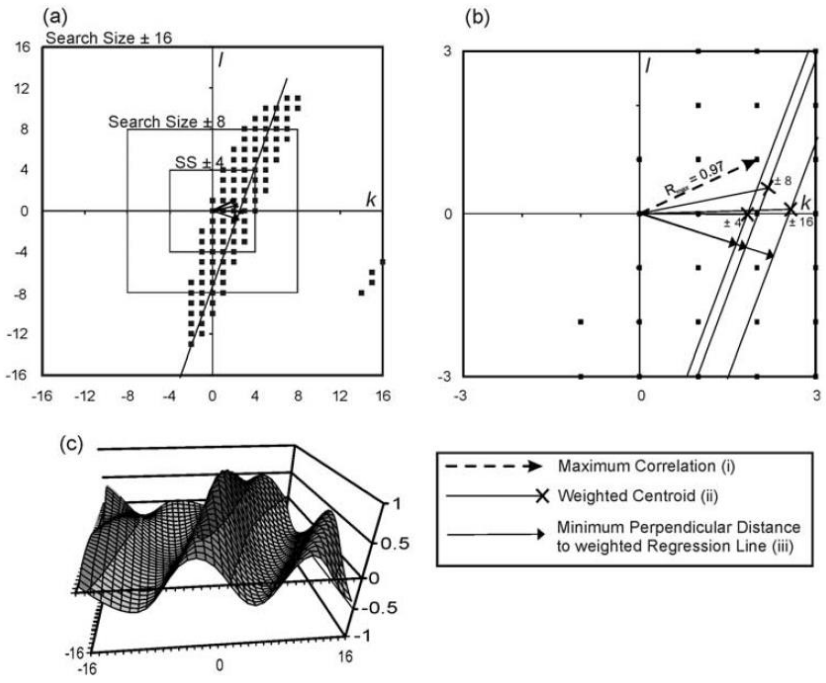

Figure 40 (a) Threshold region for different search sizes (b) Close-up view of cross-correlation picks by different vector types and (c) Variogram shape (Duffy & Hughes-Clarke, 2005)

4.4.6. Final output

The final output consists of a field of regularly spaced data point, for which each data point contains a migration rate (m/year) and a migration direction (degrees).

An important difference with the output of PSTP is the fact that the grid covers the entire DEM, rather than solely the bedform patterns. This means that, in some cases, estimates are given for areas where no sand waves are present. Some post-processing is required to remove these grid points. The same holds for outlier values that result from incorrectly matching patterns.

4.4.7. Known uncertainties

When using SCC to quantify tidal sand wave migration, note the following sources of uncertainty:

Using a single window size. Finding a single optimal window size is challenging when there is strong variability in terms of *morphometry*. A window that is too small does not detect migration of larger sand waves while a window that is too large gives a generalized estimate for multiple small sand waves combined. A general rule of thumb is to increase the window size until a relatively uniform vector field is obtained, but then it is still likely that the window size is not optimal for all sand waves.

Bathymetric data resolution. A low resolution of the bathymetric data hampers accuracy and precision of the SCC method, which is because this technique tracks three-dimensional shapes (Buijsman & Ridderinkhof, 2008). To obtain higher accuracy, the standard DEMs (with 25 m resolution) can be regridded using interpolation techniques. This is however not considered because this significantly increases computation time and adds an extra source of uncertainty.

5. Testing with artificial data

5.1. Introduction

This chapter comprises the testing of PSTP and SCC with artificial bathymetric timeseries. The aim is to validate if the methods can provide the correct quantitative results for several pre-defined migration distances.

The artificial bathymetry and the considered scenarios are described in sections 5.2 and 5.3, respectively. Subsequently, the results are given in section 5.4.

5.2. Artificial bathymetry

An artificial bathymetric dataset is prepared, in which tidal sand waves are constructed from a one-dimensional sinusoidal function, see Equation (4). This function is applied to the X coordinates of a two-dimensional grid (WGS 84/UTM 31N coordinate reference system) to create an initial wavy surface. For the artificial dataset to be representative for the field data to be used, the spacing between the grid coordinates is set to 25 m.

$$\boldsymbol{Z = 5 * \sin(0.0125x) + 5} \tag{4}$$

The artificial sand waves on the initial surface have heights of 10 m and wavelengths of roughly 502 m. To add some variance in terms of morphology, a tapering is added to the initial surface, which increases the height in the positive y-direction to 12 m and decrease the height in the negative y-direction to 1 m. The shape is strongly simplified, as the sand waves are symmetrical and have a rounded surface. Finally, some random noise is added to mimic small-scale bedforms and measurements errors. See Figure 41.

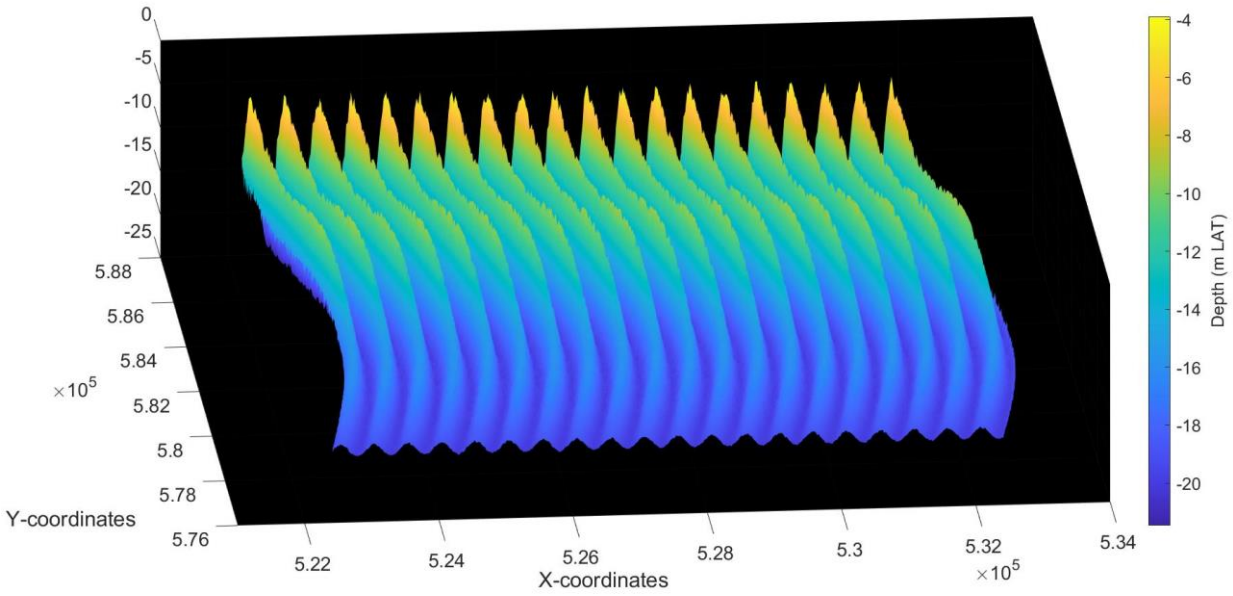

Figure 41 Example of an artifical bathymetric dataset (Y-axis = south-north, X-axis = west-east). The coordinate system is World Geodetic System 84 / Universal Transverse Mercator 31°N.

5.3. Test scenarios

A uniform horizontal shift is applied in the positive X direction. It is hypothesised that the relatively low data resolution of 25 m hampers the accuracy of the detection methods, especially when the migration distance is small relative to the resolution. To test this, a range of migration distances lower than 25 m is applied: 0 m, 5 m, 10 m, and 20 m. In addition, migration distances one time (25 m) and two times (50 m) the *raster* resolution are tested. Finally, to show the importance of carefully choosing the survey frequency for a timeseries based on the expected dynamics, a migration distance that is larger than half the sand wave length (300 m) as well as a distance larger than the sand wave length (550 m) are applied.

Two different methods are used for applying the migration distances to the datasets:

Shifting the X coordinates (PSTP). The migration distance is added to the X coordinates of the initial bathymetric surface. Hence, the initial surface and the shifted surface have similar Z values, see Figure 42. Since PSTP retains the geographic location of the crest and trough positions, it should be capable of producing the correct output. However, SCC considers the datasets as having the same X and Y coordinates. This method of shifting is therefore not suitable to validate the performance of SCC.

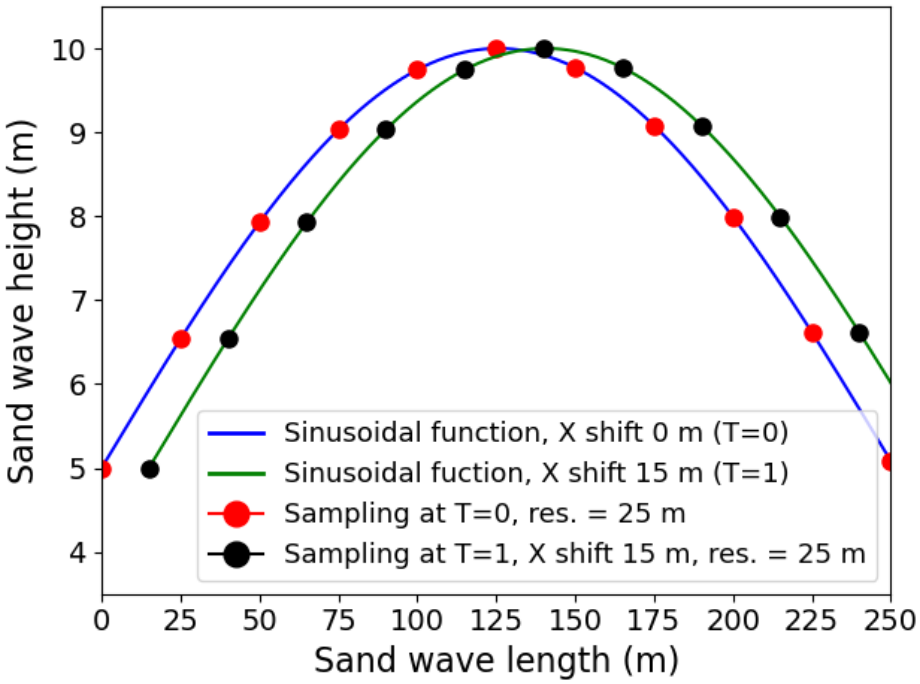

Figure 42 X and Z values of the original and shifted surface (X coordinate shift)

Phase shifting the sinusoidal function (SCC). A phase shift is applied to the one-dimensional sinusoidal function underlying the fixed bathymetric grid, see Figure 43. Equation (5) results in a phase shift of 5 m in the positive X direction. Other scenarios can be applied by substituting multiples of 0.0625.

$$\boldsymbol{Z = 5 * \sin(0.0125x - 0.0625) + 5} \quad (5)$$

Since only the Z values of the surface are changed, this method can be applied to validate the performance of SCC. Moreover, it is a good way of testing whether the technique is indeed capable of measuring the correct migration distances of the underlying (continuous) sand wave surface, regardless of the course sampling resolution of 25 m. In theory, the weighted regression and weighted centroid vectors can do this (see section 4.4.5). As opposed to SCC, PSTP only measures the migration

distance along the integer positions of the *raster* cells in the X and Y direction. Applying a horizontal shift by shifting the underlying sinusoidal function therefore mainly results in migration distances of 0 m, 25 m, 50 m, etc. (see Appendix IV). This method is therefore not suitable to validate the performance of PSTP. However, the examples in Appendix IV clearly show the limited accuracy that can be obtained with PSTP for small distances due to its restriction to the grid cell positions.

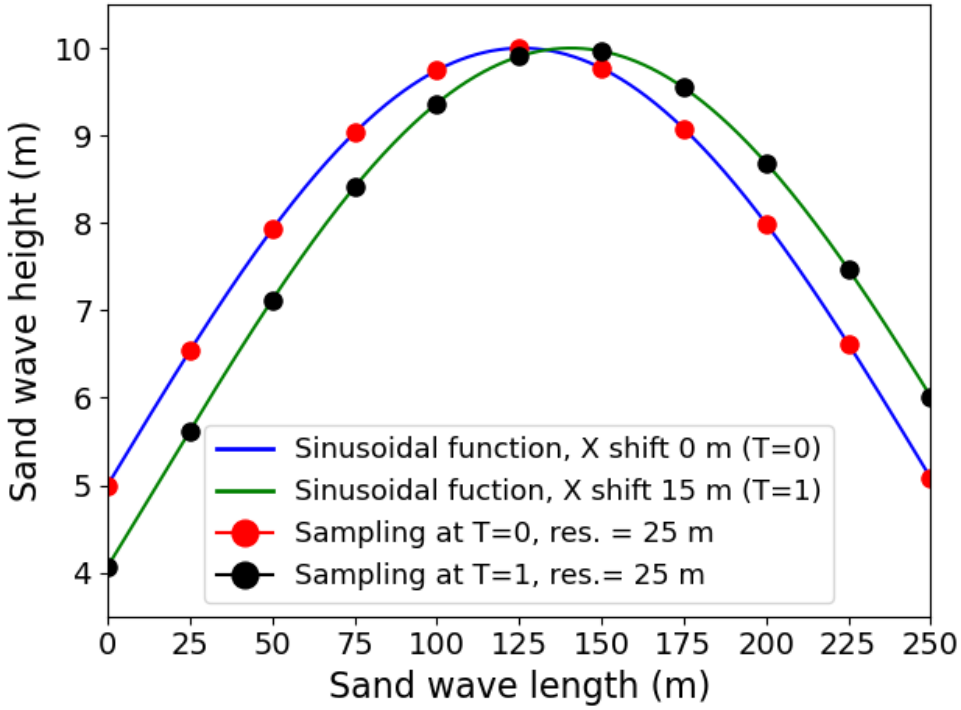

Figure 43 X and Z values of the original and shifted surface (phase shifting sinusoidal function)

5.4. Results

With PSTP, due to the rounded surface of the artificial sand waves, the Maximal Curvature tool is unable to detect the crest lines with a single cell width. Therefore, only the Convergence Index is used to filter the crest and trough positions. For SCC, the weighted regression vector is preferred over the maximum correlation and weighted centroid vectors, since the migration field is uniform and the sand waves have straight, two-dimensional crests. A window size of 24 grid cells is used for all scenarios.

Table 5 contains the median migration distances as measured by PSTP and SCC. The distribution[6] of the measured migration distances by PSTP and SCC are visualised in Figure 44. A positive value corresponds to a measured shift in the positive X-direction (which is applied in all cases).

Table 5 Median migration distances for PSTP and SCC including the percentage error

		Pre-defined migration distance (m)								
		0.0	5.0	10.0	15.0	20.0	25.0	50.0	300.0	550.0
PSTP	Median	0.0	5.0	10.0	15.0	20.0	25.0	50.0	-198.5	50.0
	% error	0.0	0.0	0.0	0.0	0.0	0.0	0.0	33.8	90.9
SCC	Median	1.3	4.0	9.4	14.2	19.5	24.1	48.2	-203.6	43.9
	% error	-	20.0	6.0	5.3	2.5	3.6	3.6	32.1	92.0

[6] Starting from 0 on the Y axis, the boxplots comprise the following horizontal lines: "minimum" (1st quartile - 1.5*Interquartile range, 1st quartile, median, 3rd quartile, "maximum" (3rd quartile + 1.5*Interquartile range).

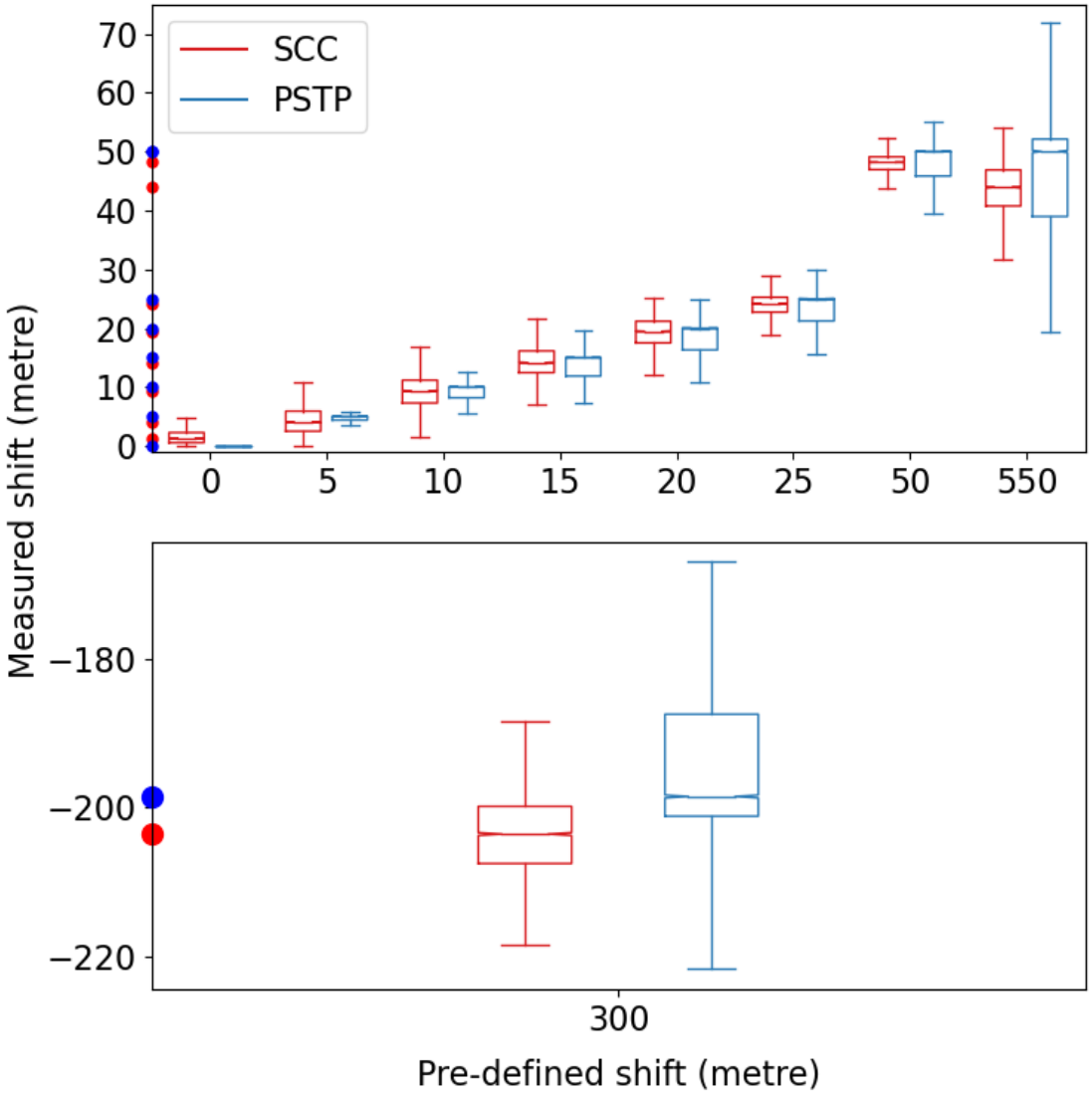

Figure 44 Boxplots of measured migration distances for pre-defined scenarios

For the scenarios between 0-50 m, the results by PSTP are accurate. Although the spread of the measurements becomes larger with increasing migration distances, the distributions are tightly centred around the correct median migration distance. For a pre-defined migration distance of 300 m, a median distance of 198.5 m in the negative X direction is obtained. This is explained by the fact that PSTP measures the shortest distance to the nearest source line, which belongs to the next sand wave to the right as the applied migration distance is larger than half the wavelength of 502 m. Note that, regardless of direction, the actual migration distance that should be measured here is rather close to 202 m, which is the remaining distance between adjacent crests or troughs. However, because PSTP is bound to the *raster* resolution of 25 m, the technique considers the sand waves as having wavelengths of 500 m (the closest multiple of 25 m). Given this, a median migration distance of 200 m makes more sense. The obtained median value of 198.5 m is explained by the larger spread of the data. For a pre-defined distance of 550 m, a median distance of 50 m in the positive X direction is measured. Here, the migration distance is larger than the wavelength of 502 (or 500 for PSTP) m, which means the shortest distance of the target lines to the nearest source line is 47.3 (or 50 for PSTP) m. For both the scenarios of 300 m and 550 m, the values are distributed within one grid cell of the median. All distributions are right-skewed, since the definition of a maximum distance to the nearest source line (which is larger

than the expected migration distance) prevents the measurement of values that significantly exceed the pre-defined distance. Furthermore, the measurements are slightly biased towards the lower end of the distribution because the shorter distances are favoured over the longer distances.

For the scenarios between 5-50 m, the median migration distances of SCC are just below the pre-defined value. The percentage error is large when the migration distance is small relative to the data resolution. It is especially notable that a median migration distance of 1.3 m is measured when 0 m is pre-defined. This might be explained by the fact that the sand wave crests are not fully straight. As a result, the weighted regression line through the threshold region does not intercept with the zero-lag position of the template. The percentage error is significantly lower, and hence accuracy is higher, for the pre-defined migration distances that are close to, or larger than the *raster* resolution. The explanation for the obtained results with pre-defined migration distances of 300 m and 550 m is comparable to the one given for PSTP. For a migration distance of 300 m, a negative migration distance is measured because the nearest threshold region is located on the left side of the zero-lag position of the template. However, as opposed to PSTP, the weighted regression vector considers the sand waves as a continuous surface. The wavelength of 502 m is therefore retained and a migration distance close to 202 m is measured. For the scenario of 550m, apart from the fact that the distance to the wrong threshold region is considered, the median distance is relatively close to the net distance of 47.3 m with which the sinusoidal function is shifted.

6. Testing with field data

6.1. Introduction

This chapter comprises the testing of the migration detection methods with field data. The aim is to find out how the methods cope with different types of sand wave morphology and dynamics, different types of underlying topography and differing data quality. Since the focus is not on obtaining the most accurate estimation, only one timeseries (comprising two DEMs) is used for each location.

Four field locations are selected. First, a reasoning on why a particular location is chosen is given in section 6.2, after which the migration results for each location are described in sections 6.3 to 6.6.

6.2. Field data locations

The field locations are picked from different regions on the NCS to thoroughly cover the situations that can occur in an NCS-wide analysis. A brief description of the locations and the expected sand wave morphodynamics is given below.

West of Texel (WT). This area covers a long, narrow transect over the entire length of Texel. Water depths range between 22-31 m. The sand waves are relatively two-dimensional, symmetrical, and short compared to the coastal site IJmuiden – Hoek van Holland (Damen et al., 2018). Average migration is in north-eastern direction at a rate of 16-19 m/year (Van Dijk et al., 2011). See Figure 45. Migration is quantified over a period of 5.5 years, between November 2008 and May 2014.

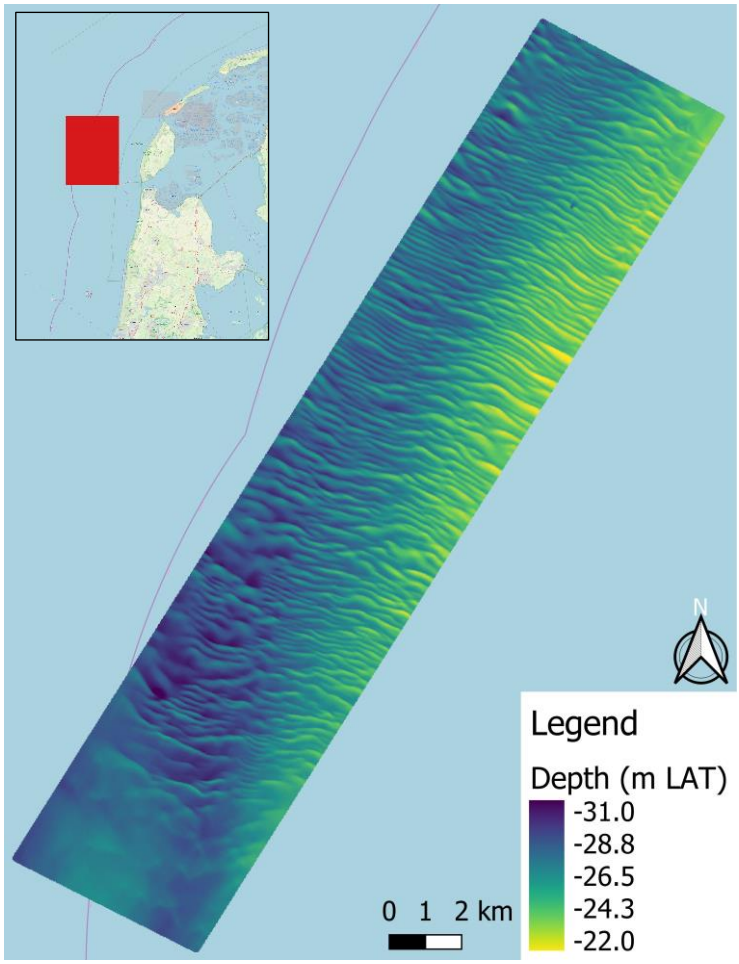

Figure 45 Bathymetry at field site West of Texel

Schaar – Rabsbank (SRB). The sand waves in this region are superimposed on several sand banks. It is therefore expected that bilateral migration occurs because of the alternation of the tide averaged flow over the sand banks (Leenders et al., 2020). The sand waves are three-dimensional, symmetrical and have wavelengths strongly vary between the sand waves on top of and in between the sandbanks (Damen et al., 2018). Migration rates at nearby locations are estimated between 0-2 m/year (Deltares, 2015). Also, besides sand waves and sand banks, areas of flat seabed are present. Water depths range between 7-35 m. See Figure 46. Migration is quantified over a period of 5 years, between June 2010 and April 2015.

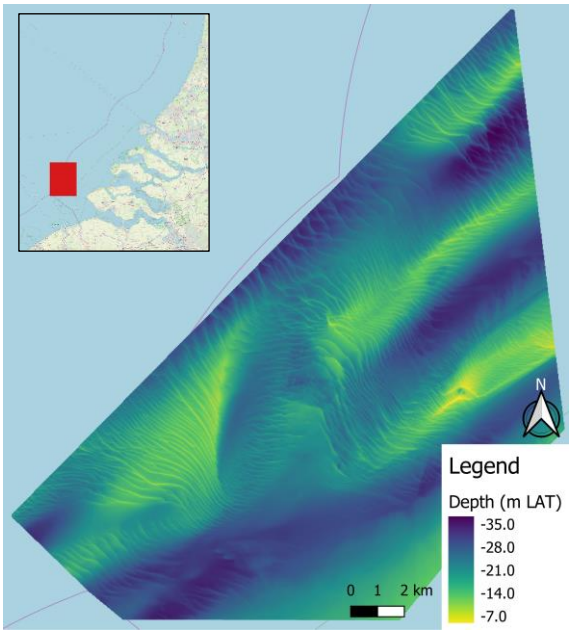

Figure 46 Bathymetry at field site Schaar-Rabsbank

North Hinder (NH). The North Hinder Bank is located offshore in water depths of 28-47 m. The sand waves in this area are three-dimensional, symmetrical, and relatively short compared to the rest of the NCS (Damen et al., 2018). The area is described as relatively non-dynamic with migration rates mostly below 0.5 m/year. The sand waves migrate both in north-eastern and south-western direction (Knaapen, 2005). See Figure 47. Migration is quantified over a period of 8 years, between May 2001 and June 2009.

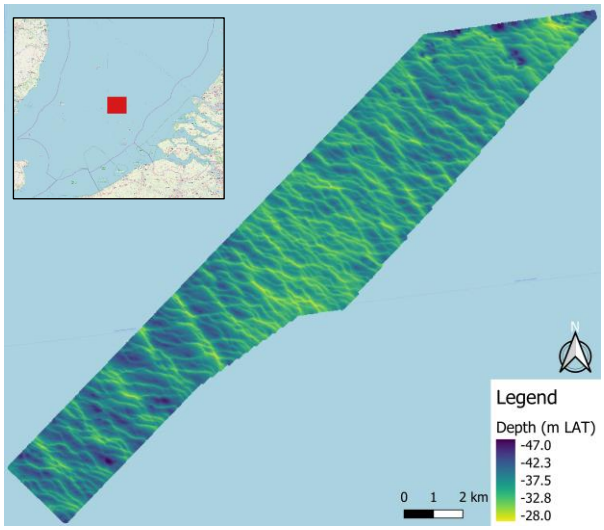

Figure 47 Bathymetry at field site North Hinder

IJmuiden – Hoek van Holland (IJHVH). The sand waves in this area are located relatively close to the shoreline in water depths between 12-26 m. They are straight-crested, strongly asymmetric and wavelengths are long compared to the rest of the NCS (Damen et al., 2018). Migration rates in the area are quantified at 6.5-20 m/year in north-eastern direction (Van Dijk & Kleinhans, 2005). An interesting aspect is the fact that several sand extraction pits have appeared in the period between both surveys, which are indicated by the dark blue patches in Figure 48. Furthermore, several shoreface connected ridges are present in the north-eastern corner of the site.

Migration is quantified over a period of 9.6 years, between November 2001 and July 2011.

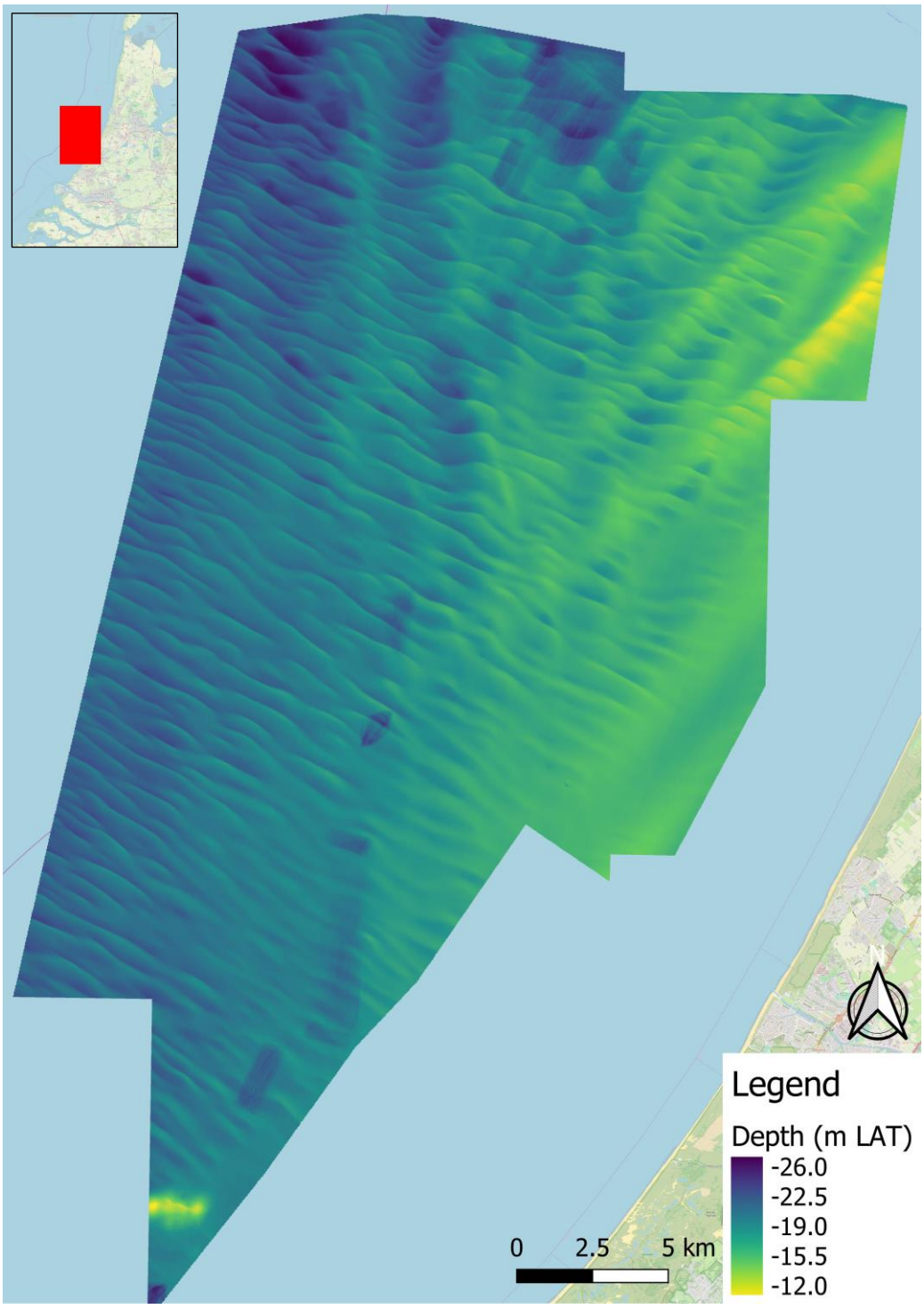

Figure 48 Bathymetry at field site IJmuiden-Hoek van Holland

6.3. West of Texel

The normalized frequency distributions of migration rate and direction are plotted in Figure 49 and Figure 50, respectively. Figure 51 to Figure 54 present the spatial distributions of migration rate and direction.

The parameter settings for each method are given in Table 6. For SCC, the weighted regression vector is preferred over the maximum correlation and weighted centroid vectors. It is more appropriate because the sand waves are straight-crested and the migration direction (and hence the tide averaged flow field) is uniform in north-eastern direction. For PSTP, the quality of the DEMs is sufficient such that both Maximal Correlation and Convergence Index can be used for crest and trough detection.

Table 6 Parameter settings and properties of the timeseries for West of Texel

Pairs of Source and Target Points		**Spatial Cross Correlation**	
Crest/trough detection	Convergence index (C/T) and Maximal Curvature (C)	**Vector type**	Weighted regression line
Points per feature	10	**Window size**	36 *raster* cells
Minimum distance between points	100 m	**Step size**	9 *raster* cells
Total number of data points	5,676	**Total number of data points**	1,620
Survey date 1	November 2008		
Survey date 2	May 2014		
Time between surveys	5.5 years		

Figure 49 indicates that SCC and PSTP give comparable results regarding migration rate. Whereas the median (PSTP: 3.8 m/year, SCC: 3.9 m/year) is almost identical for both methods, the frequency distributions are shaped differently. The distribution of SCC has a single peak, while the distribution of PSTP has a single large peak at the centre and two smaller peaks at the edges. These smaller peaks result from the low data resolution of 25 m and its restriction to integer cell positions. The spatial distributions in Figure 51 and Figure 53 both indicate that the migration rates are highest close to the shoreline. The overall picture provided by SCC is smoother because by taking a snapshot of a larger area, outlier values are filtered out. Furthermore, the data points are regularly spaced whereas for PSTP, they are placed randomly and, since both the Maximal Curvature and the Convergence index are applied, stacked on top of each other.

As is indicated by Figure 50, PSTP and SCC both detect migration to the northeast. The median directions (PSTP: 117 degrees, SCC: 115 degrees) and the percentiles do not differ significantly. The distribution of SCC is narrower, which is due to the use of the weighted regression vector, which forces the migration direction to be perpendicular to the uniformly orientated crest lines. For PSTP, two peaks occur instead of one (see section 4.3.6). The spatial distributions in Figure 52 and Figure 54 both show a deflection of the migration direction as one approaches the shoreline, especially in the upper half of the area. The sand waves closer to the shore tend to migrate more parallel to the shoreline, which is indicated by a dark purple colour. SCC shows some noisy data points in the southwestern corner of the region, where relatively deep holes are present, and sand wave *morphometry* and orientation are more irregular.

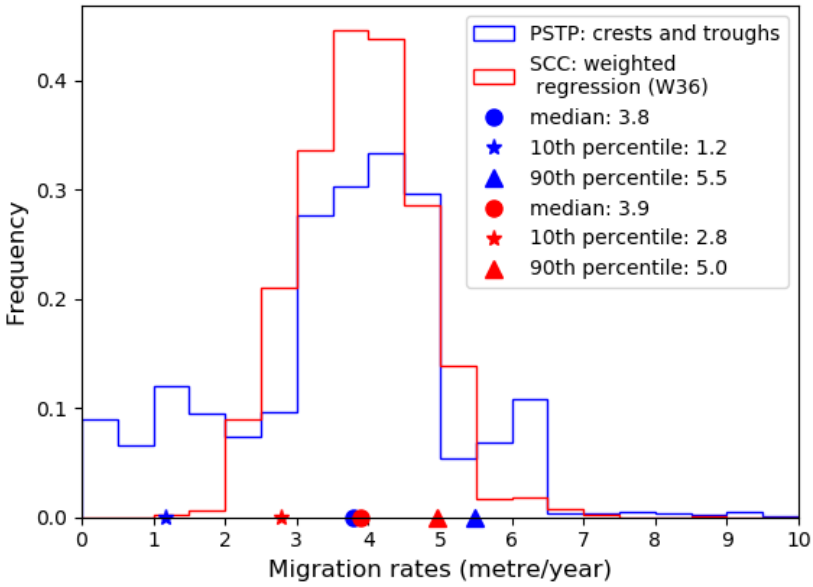

Figure 49 Frequency distribution of migration rates for West of Texel

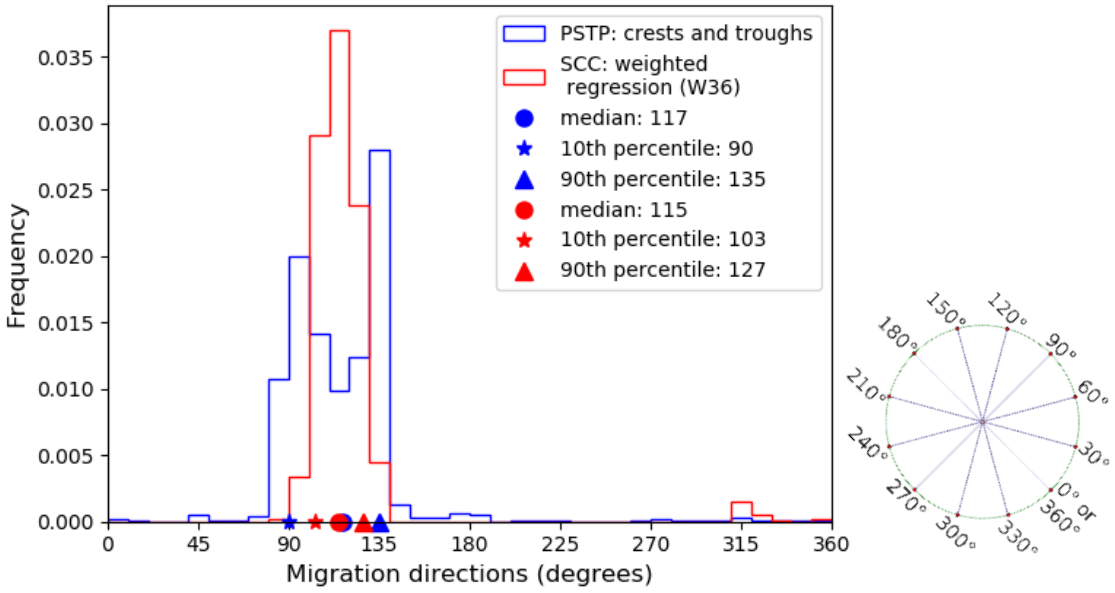

Figure 50 Frequency distribution of migration directions for West of Texel

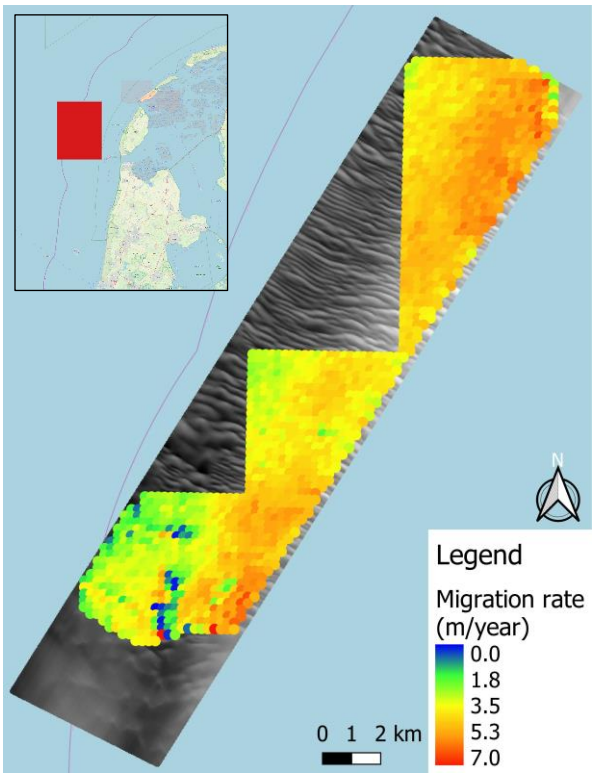

Figure 51 Spatial distribution of migration rates by SCC (weighted regression vector, window size 36) for West of Texel

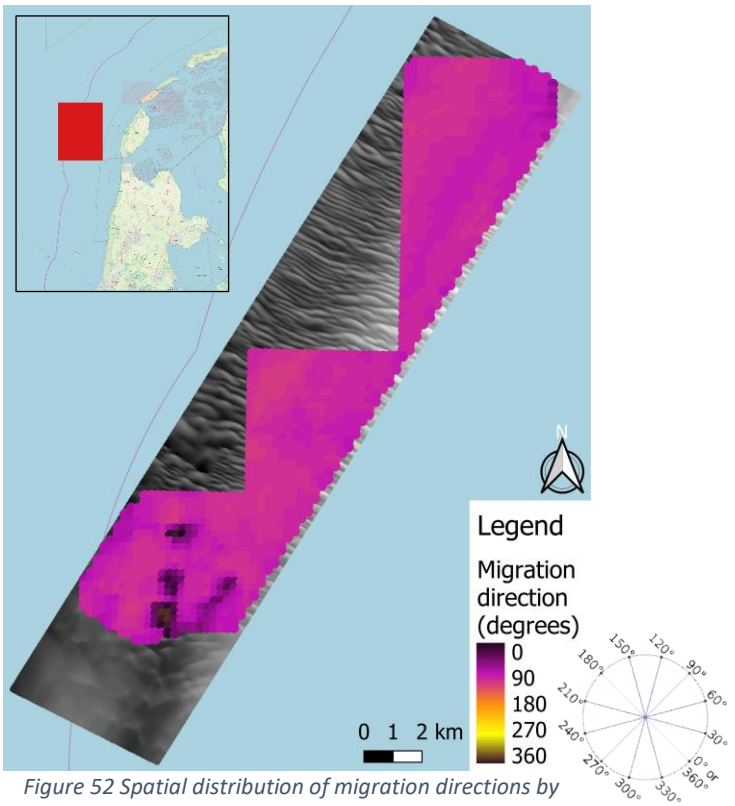

Figure 52 Spatial distribution of migration directions by SCC (weighted regression vector, window size 36) for West of Texel

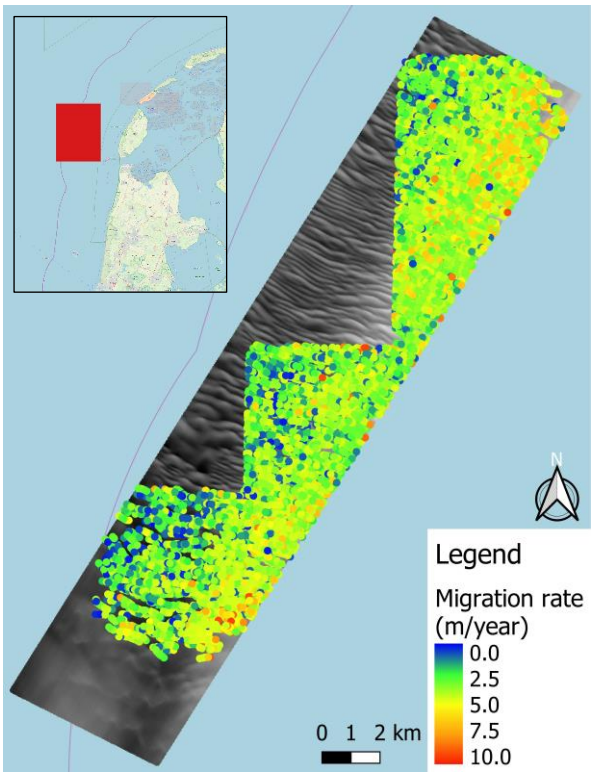

Figure 53 Spatial distribution of migration rates by PSTP for West of Texel

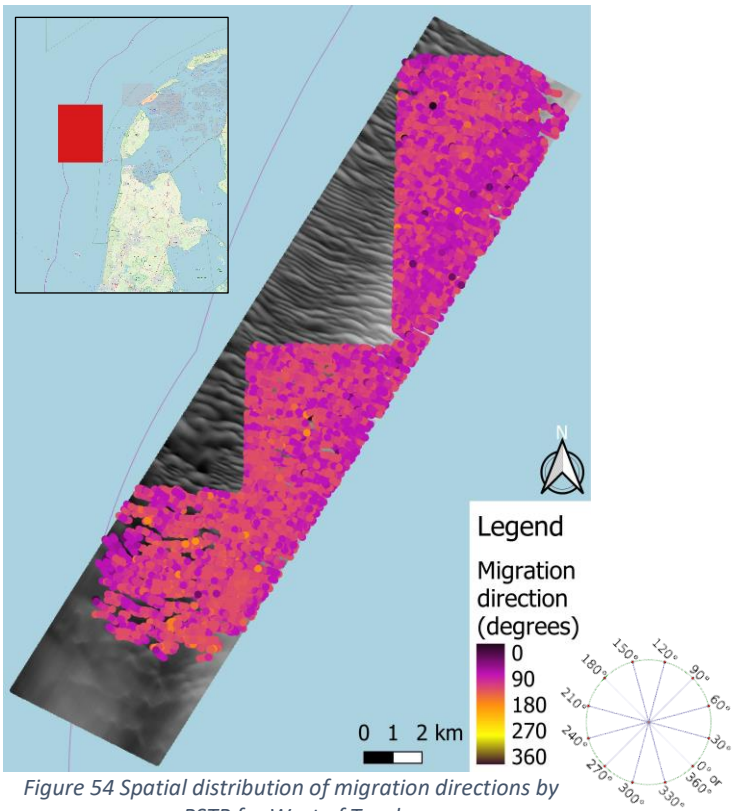

Figure 54 Spatial distribution of migration directions by PSTP for West of Texel

6.4. Schaar Rabsbank

The normalized frequency distributions of migration rate and direction are plotted in Figure 55 and Figure 56, respectively. Figure 57 to Figure 60 present the spatial distributions of migration rate and direction.

The parameter settings for each method are given in Table 7. Theoretically, the weighted centroid vector is most appropriate to use for SCC since the flow field is three-dimensional. However, except for the sand waves on top of the sandbanks, it produces migration directions mostly parallel to the crest lines. The maximum correlation vector measures migration distances along the integer grid cells in the X and Y direction, which does not lead to any realistic results, neither for migration rates nor directions. Although it is developed to be used mainly for straight crested sand waves in a uniform flow field, the weighted regression vector detects bilateral migration around the sandbanks as well. The window size of 12 cells might not be optimal for all sand waves, as wavelengths strongly vary between the sand waves that are located on top of and in between the sandbanks. For PSTP, the quality of the DEMs allows for the use of both Maximal Correlation and Convergence Index.

Table 7 Parameter settings and properties of the timeseries for Schaar Rabsbank

Pairs of Source and Target Points		**Spatial Cross Correlation**	
Crest/trough detection	Convergence index (C/T) and Maximal Curvature (C)	**Vector type**	Weighted regression line
Points per feature	10	**Window size**	12 *raster* cells
Minimum distance between points	50 m	**Step size**	4 *raster* cells
Total number of data points	12,890	**Total number of data points**	21,363
Survey date 1	June 2010		
Survey date 2	April 2015		
Time between surveys	5 years		

The frequency distributions in Figure 55 indicate a left-skewed distribution. PSTP has a sharp peak near 0 m/year, which is explained by the fact that the migration distance is measured along integer grid cells in the X and Y direction. SCC is slightly more skewed to the centre, which is also indicated by the higher median value (PSTP: 0.4 m/year, SCC: 0.9 m/year) and percentiles. This difference is explained by the tendency of SCC to overestimate migration distances near 0 m and the bias of PSTP towards the lower end of the distribution. The latter is explained by the restriction of PSTP to the integer positions of the *raster* cells. In an area of low dynamics, like Schaar-Rabsbank, migration distances insignificant relative to the *raster* resolution are measured as 0 m. The spatial distributions in Figure 57 and Figure 59 are comparable, as both methods detect the highest migration rates on top of the sandbanks and the lowest in between the sandbanks.

As is indicated by Figure 56, PSTP and SCC give qualitatively comparable results regarding migration direction. Both methods detect migration to the north-east and the south-west. The frequency distribution of SCC comprises two large peaks and some remaining noise parallel to the crest lines, PSTP comprises two peaks in each direction, so four in total. The spatial distribution in Figure 58 and Figure 60 are comparable in the sense that directionally uniform and bilateral migration is observed for the same regions. The distribution by SCC is noisier however since the algorithm covers the entire area instead of only the sand waves. This way, wrongly matching patterns are included where the search window does not fully cover a sand wave body. Furthermore, the weighted regression vector seems to have more trouble producing smooth and uniform vectors on the landward flanks of the sandbanks, where the migration directions are oblique rather that perpendicular to the crest.

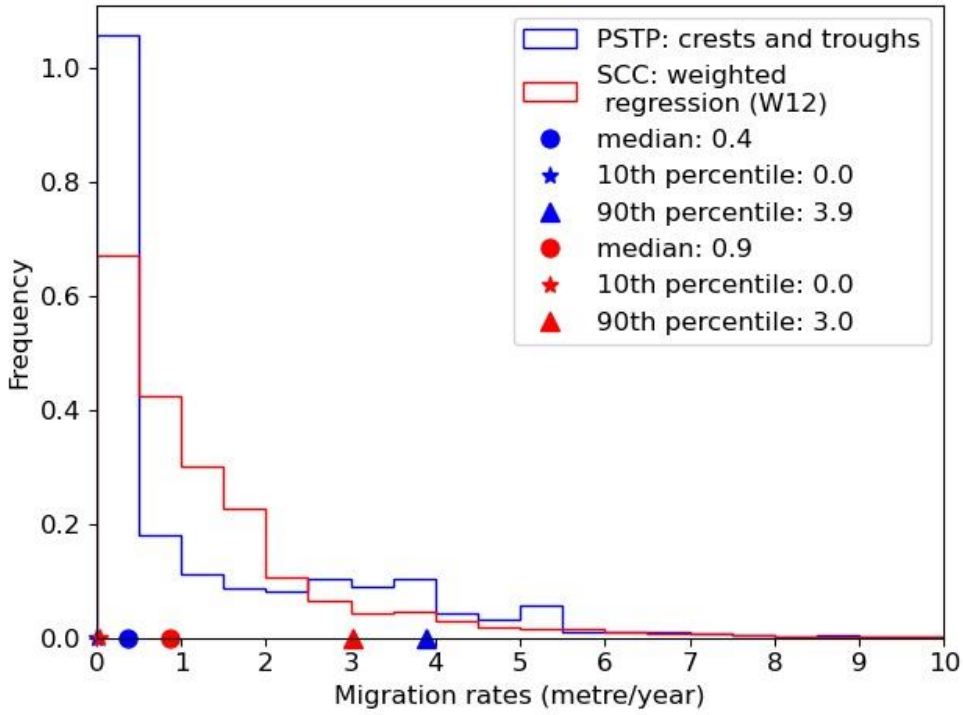

Figure 55 Frequency distribution of migration rates for Schaar-Rabsbank

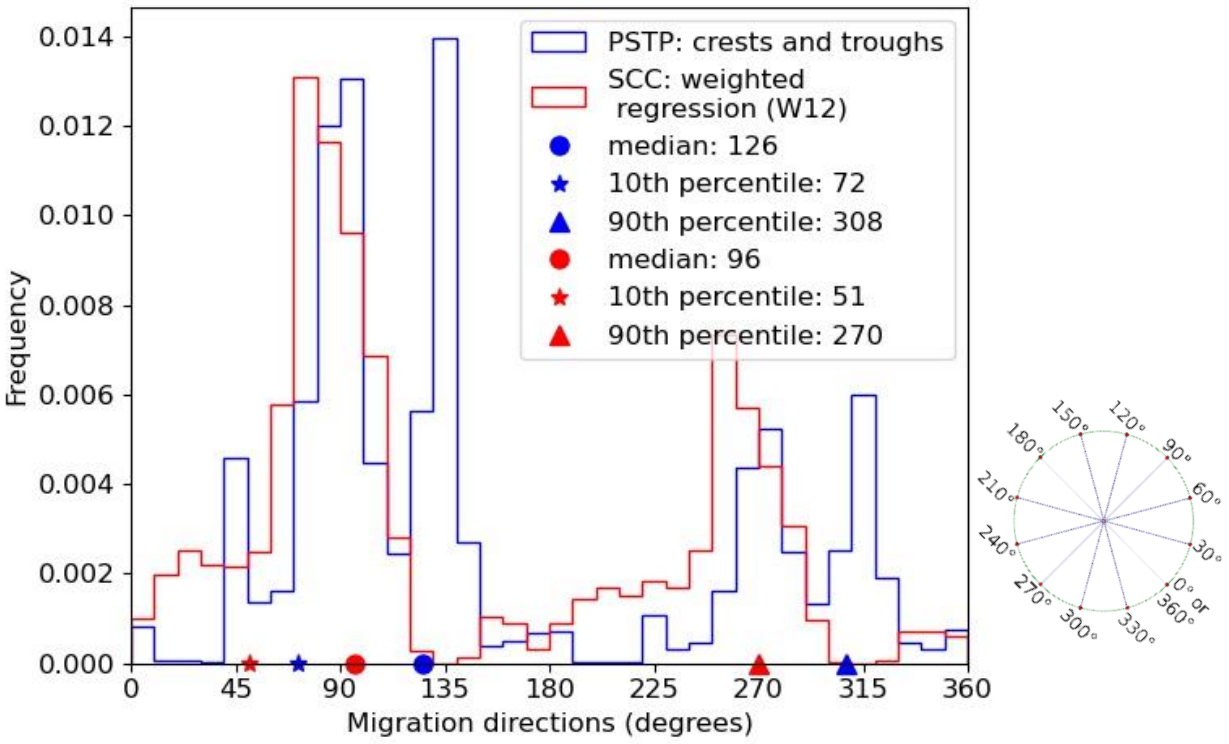

Figure 56 Frequency distribution of migration directions for Schaar-Rabsbank

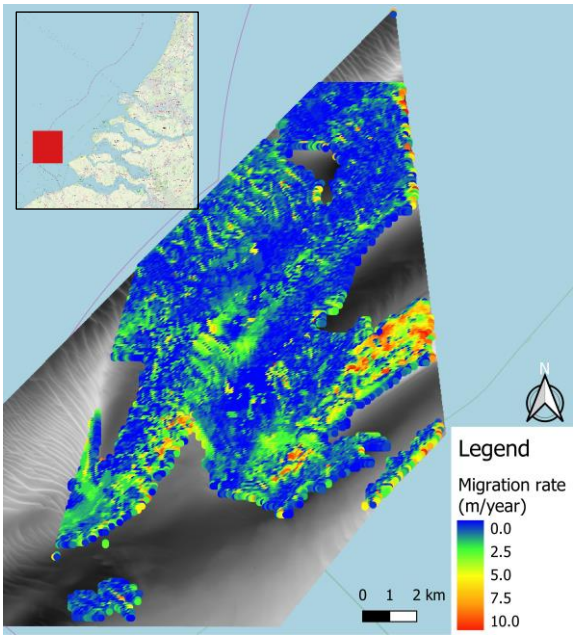

Figure 57 Spatial distribution of migration rates by SCC (weighted regression vector, window size 12) for Schaar-Rabsbank

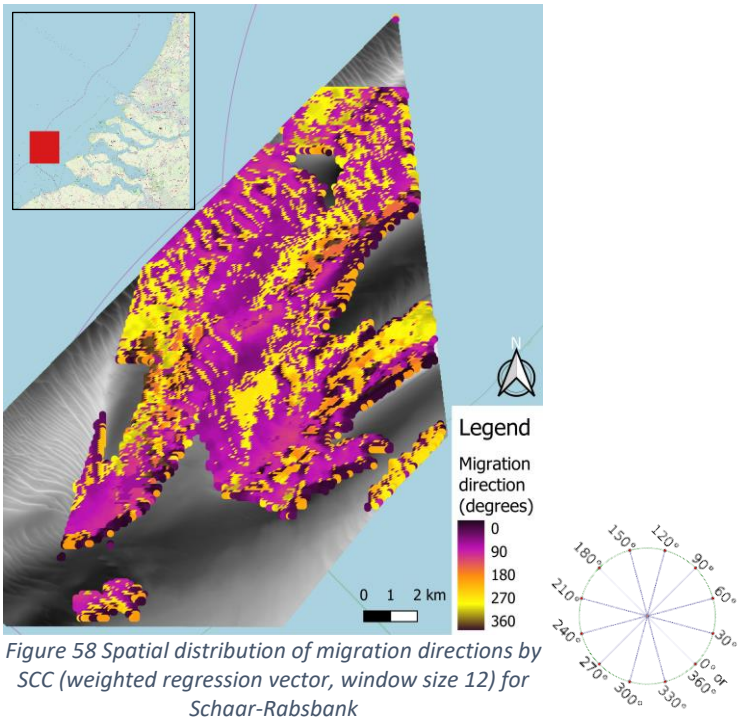

Figure 58 Spatial distribution of migration directions by SCC (weighted regression vector, window size 12) for Schaar-Rabsbank

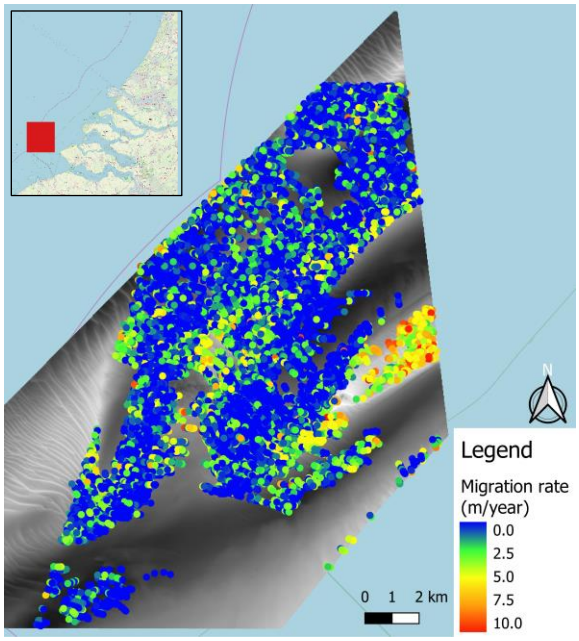

Figure 59 Spatial distribution of migration rates by PSTP for Schaar-Rabsbank

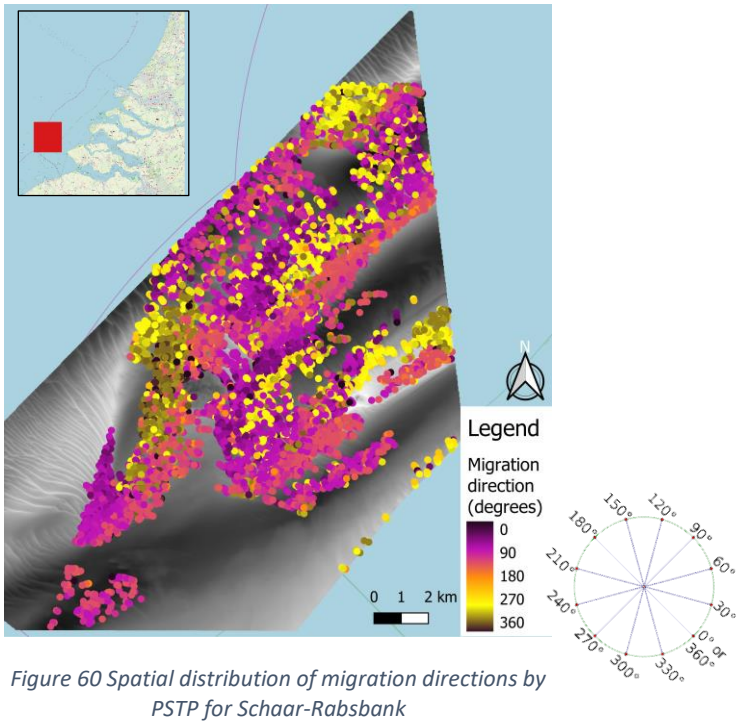

Figure 60 Spatial distribution of migration directions by PSTP for Schaar-Rabsbank

6.5. North Hinder

The normalized frequency distributions of migration rate and direction are plotted in Figure 61 and Figure 62, respectively. Figure 63 to Figure 66 present the spatial distribution of migration rate and direction.

The parameter settings for each method are given in Table 8. Theoretically, the weighted centroid vector is appropriate for SCC because of the three-dimensional shape of the sand waves. However, testing with this vector type persistently gave migration directions parallel to the crest lines. The maximum correlation vector does not provide any results for most of the area, as migration rates are too low to be represented by the displacement of a single *raster* cell. Hence, the weighted regression vector is selected as it produces migration directions perpendicular to the crest lines and migration rates that are comparable to PSTP. DEM quality is sufficient such that both Maximal Curvature and Convergence Index can be used for crest and trough detection.

Table 8 Parameter settings and properties of the timeseries for North Hinder

Pairs of source and target points		**Spatial cross correlation**	
Crest/trough detection	Convergence Index (C/T) and Maximal Curvature (C)	**Vector type**	Weighted regression line
Points per feature	10	**Window size**	12 *raster* cells
Minimum distance between points	50 m	**Step size**	4 *raster* cells
Total number of data points	6,923	**Total number of data points**	7,791
Survey date 1	May 2001		
Survey date 2	June 2009		
Time between surveys	8 years		

The migration rates from PSTP and SCC are comparable, as both produce a strongly left-skewed distribution, plotted in Figure 61. The median (PSTP: 0.7 m/year, SCC: 0.5 m/year) and 90th percentile of PSTP are higher by 0.2 m/year and 0.8 m/year, which is explained by the presence of a minor peak in the centre of the frequency distribution. This peak is caused by the restriction to the integer positions of the *raster* cells and the more prominent contribution of the crest migration rates. Separate histograms of the crest and trough migration rates in Appendix V show that the measurements for the crests are slightly higher than those for the troughs, which indicates that asymmetry changes are present. The spatial distribution of SCC in Figure 63 indicates higher dynamics at the northern edge of the region, whereas the spatial distribution of PSTP in Figure 65 does not indicate a trend or pattern.

As is indicated by Figure 62, PSTP and SCC produce comparable results for the migration direction. Both methods detect migration to the north-east and the south-west for large parts of the area. In the frequency distribution of PSTP, two peaks are present in each migration direction. As a result, the median, 10th and 90th percentiles of PSTP are slightly higher. The spatial distributions in Figure 64 and Figure 66 do not indicate a certain trend of pattern, except for the fact that migration seems to be more directionally uniform to the north-east in the upper right corner of the area.

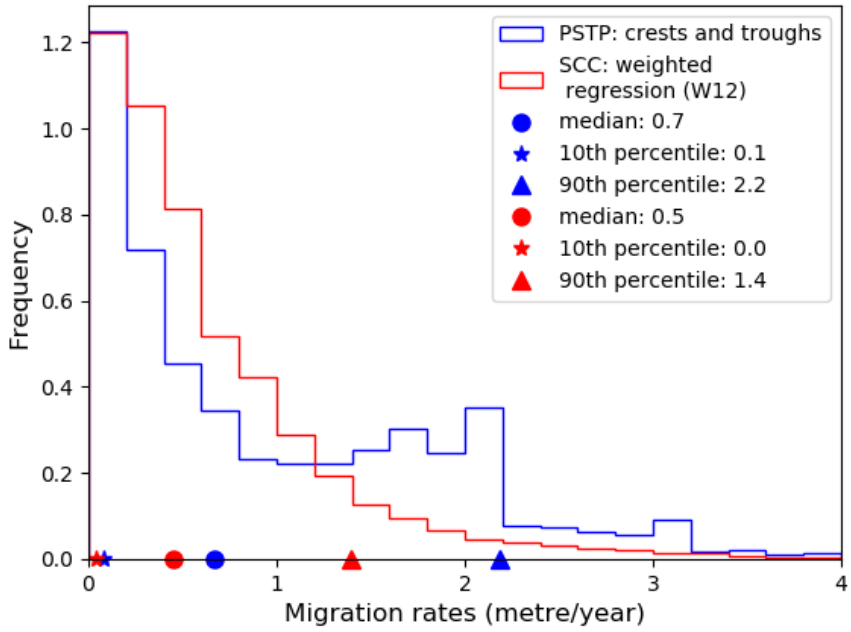

Figure 61 Frequency distribution of migration rates for North Hinder

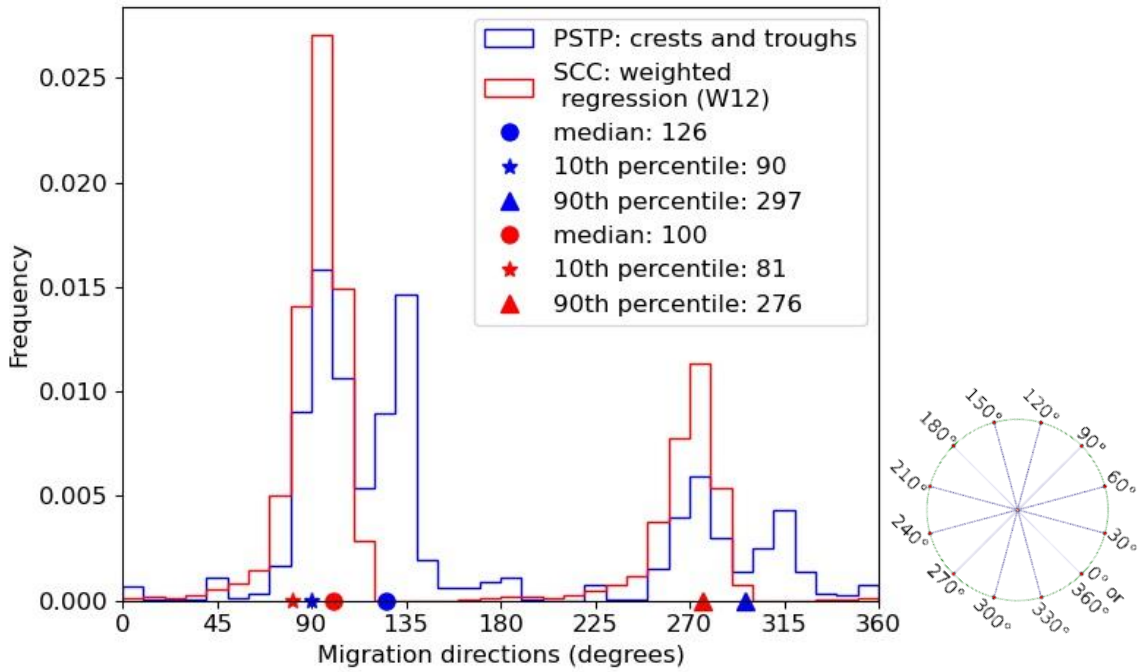

Figure 62 Frequency distribution of migration directions for North Hinder

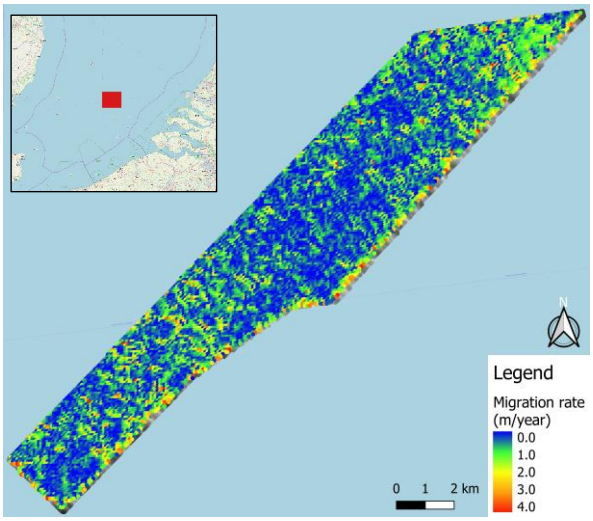

Figure 63 Spatial distribution of migration rates by SCC (weighted regression vector, window size 12) for North Hinder

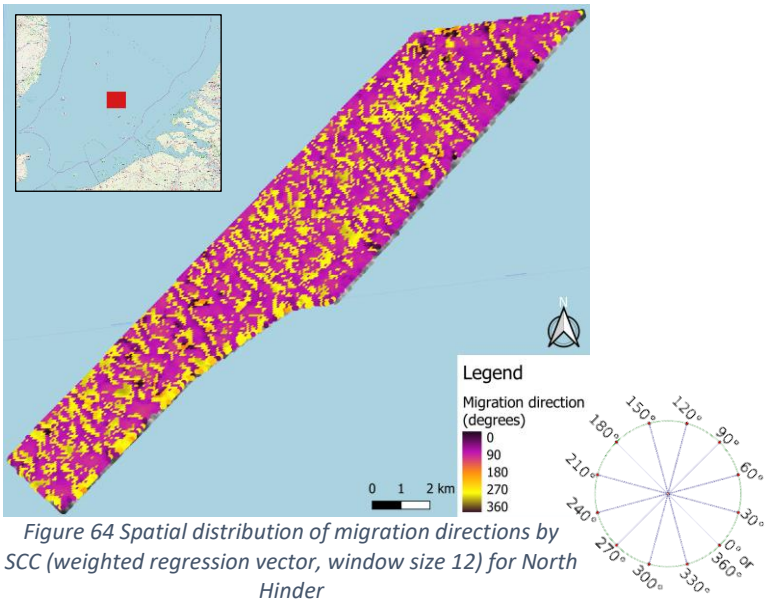

Figure 64 Spatial distribution of migration directions by SCC (weighted regression vector, window size 12) for North Hinder

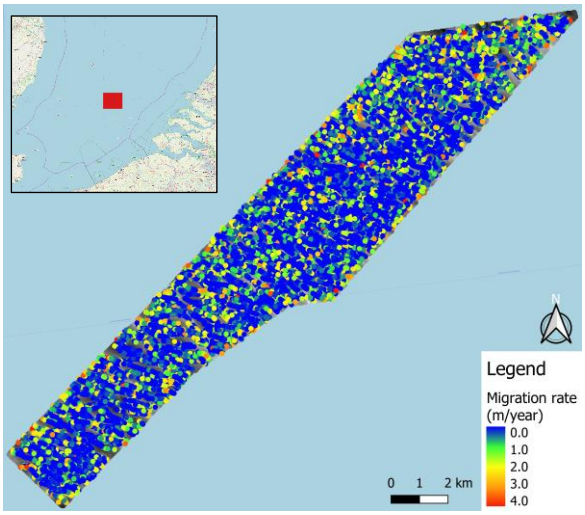

Figure 65 Spatial distribution of migration rates by PSTP for North Hinder

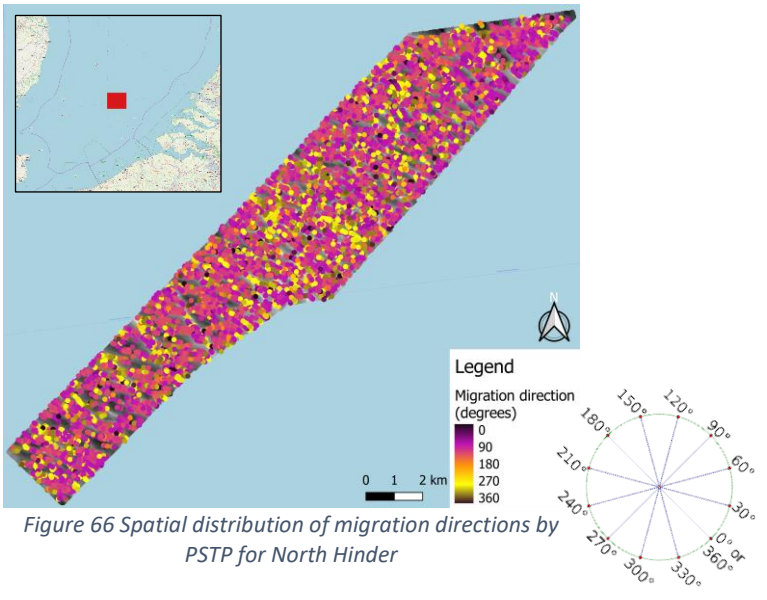

Figure 66 Spatial distribution of migration directions by PSTP for North Hinder

6.6. IJmuiden - Hoek van Holland

The normalized frequency distributions of migration rate and direction are plotted in Figure 67 and Figure 68, respectively. Figure 69 to Figure 72 present the spatial distributions of migration rate and direction.

The parameter settings for each method are given in Table 9. For PSTP, the Maximal Curvature tool is not used for crest detection since the quality of the oldest DEM is not sufficient for it to be used without smoothing. For SCC, the weighted regression vector is preferred over the maximum correlation and weighted centroid vectors. The former is most appropriate because the sand waves are straight-crested, and the migration direction (and hence the tide-averaged flow field) is uniform to the north-east.

Table 9 Parameter settings and properties of the timeseries for IJmuiden-Hoek van Holland

Pairs of Source and Target Points		**Spatial Cross Correlation**	
Crest/trough detection	Convergence index (C/T)	**Vector type**	Weighted regression line
Points per feature	20	**Window size**	35 *raster* cells
Minimum distance between points	50 m	**Step size**	7 *raster* cells
Total number of data points	8,496	**Total number of data points**	17,214
Survey date 1	November 2001		
Survey date 2	July 2011		
Time between surveys	9.6 years		

PSTP and SCC provide comparable results regarding migration rate, as can be seen in Figure 67. Both distributions are slightly left-skewed and the median (PSTP: 2.0 m/year, SCC: 1.7 m/year) differs only by 0.3 m/year. SCC shows a single sharp peak while PSTP also shows some smaller peaks near the edges of the distribution, which explains why the 10th percentile is lower (by 0.3 m/year) and the 90th percentile is higher (by 0.6 m/year) for PSTP. The spatial distributions in Figure 69 and Figure 71 indicate an upward trend from southwest to northeast. High migration rates are especially observed on top of the shoreface connected ridges and around the sand extraction pits. The presence of the latter results in bright spots in regions where natural dynamics are low, especially with SCC. At these locations, PSTP has less noisy data points because crest and trough lines are either not detected or removed, prior to the plotting of the target points. Finally, for PSTP, the crests migrate slightly faster than the troughs, which is indicated by the colour difference between adjacent crest and trough points.

As is indicated by Figure 68, PSTP and SCC both detect migration mainly in the north-eastern direction. The median, 10th and 90th percentiles of SCC from SCC are lower than from PSTP since the former still contains some data points that incorrectly imply migration to the south-east, mainly around sand extraction pits and on sections of bare seafloor in the upper right corner of Figure 70. The sharp peak around 90 degrees is better defined for SCC due to the use of the weighted regression vector. PSTP shows well defined peaks at 90 degrees as well as 135 degrees. The spatial distributions in Figure 70 and Figure 72 do not indicate a certain trend or pattern.

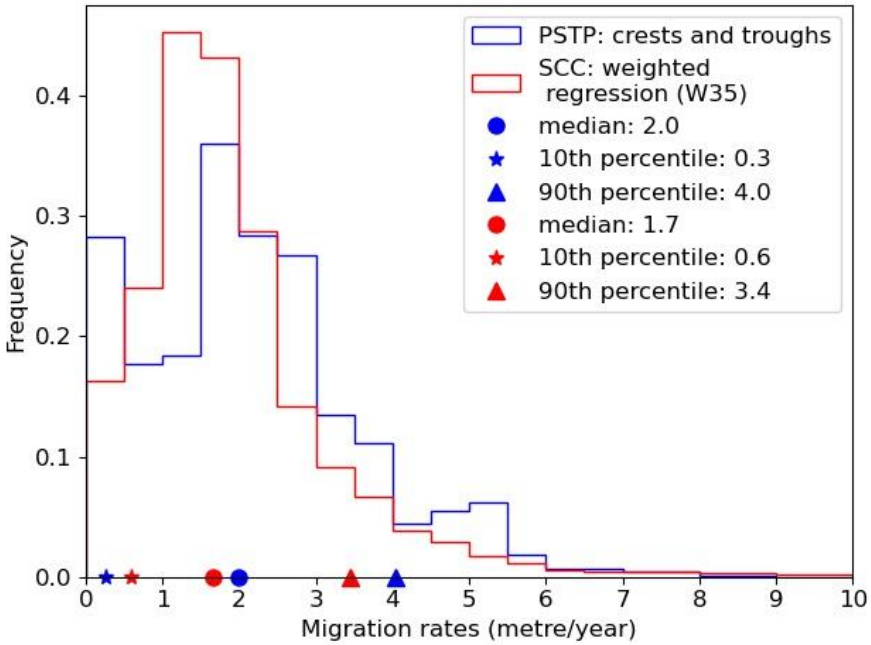

Figure 67 Frequency distribution of migration rates for IJmuiden-Hoek van Holland

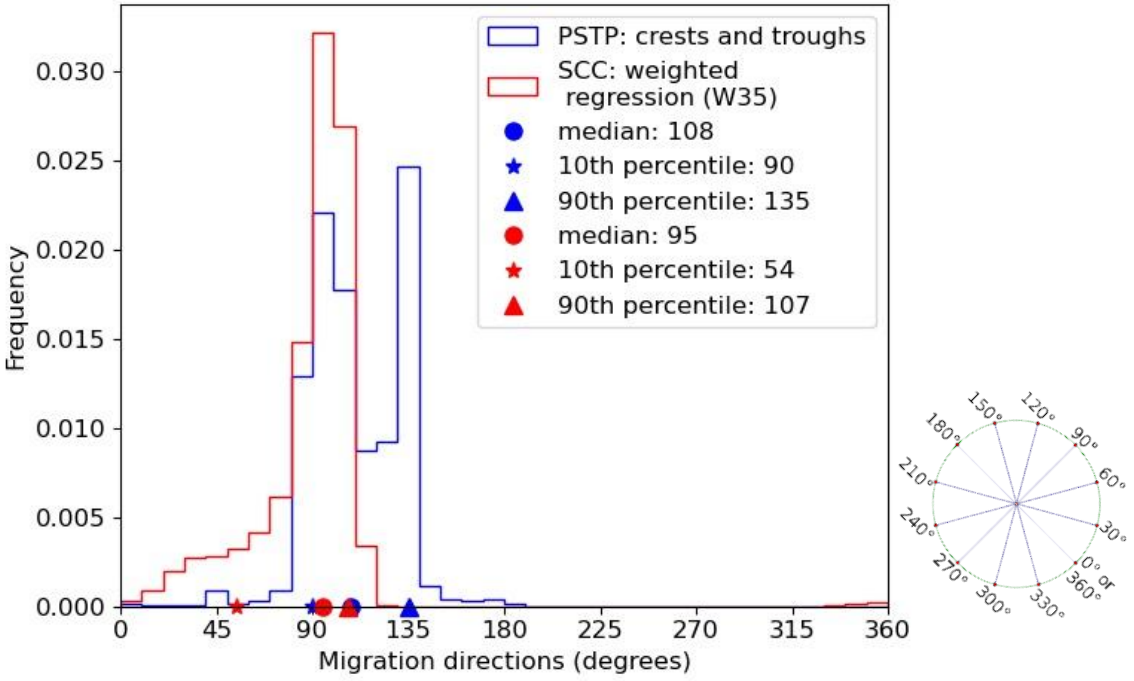

Figure 68 Frequency distribution of migration directions for IJmuiden-Hoek van Holland

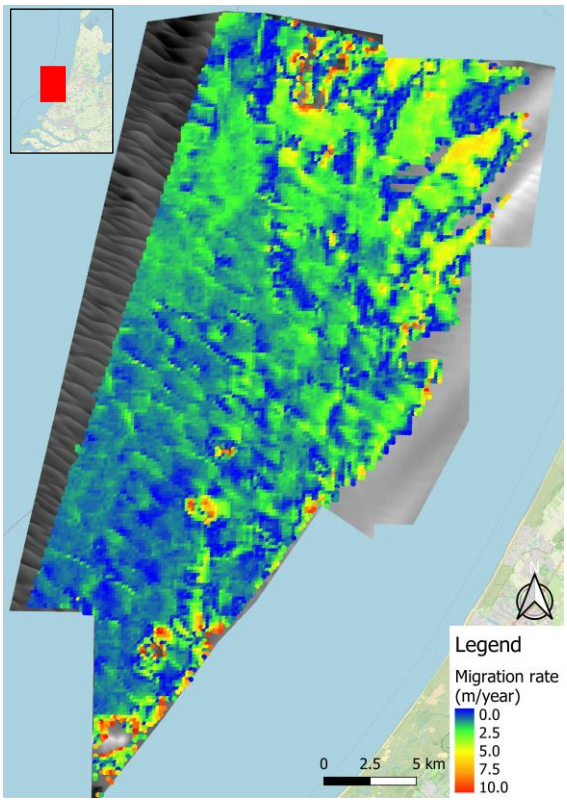

Figure 69 Spatial distribution of migration rates by SCC (weighted regression vector, window size 35) for IJmuiden-Hoek van Holland

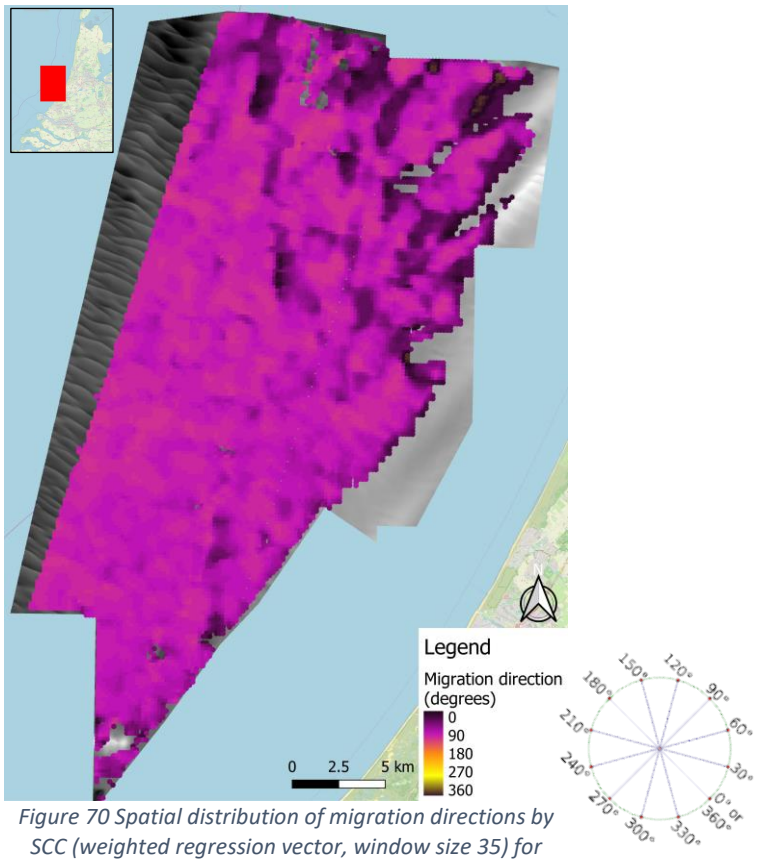

Figure 70 Spatial distribution of migration directions by SCC (weighted regression vector, window size 35) for Schaar-Rabsbank

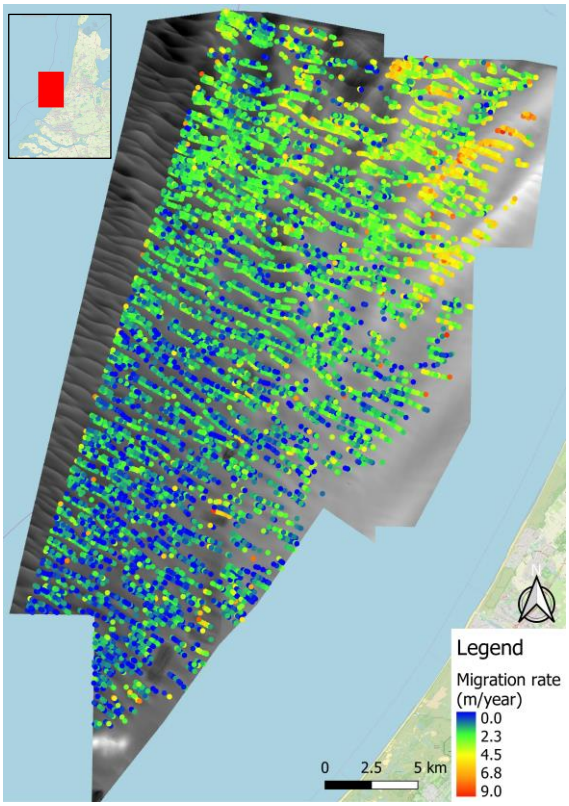

Figure 71 Spatial distribution of migration rates by PSTP for IJmuiden-Hoek van Holland

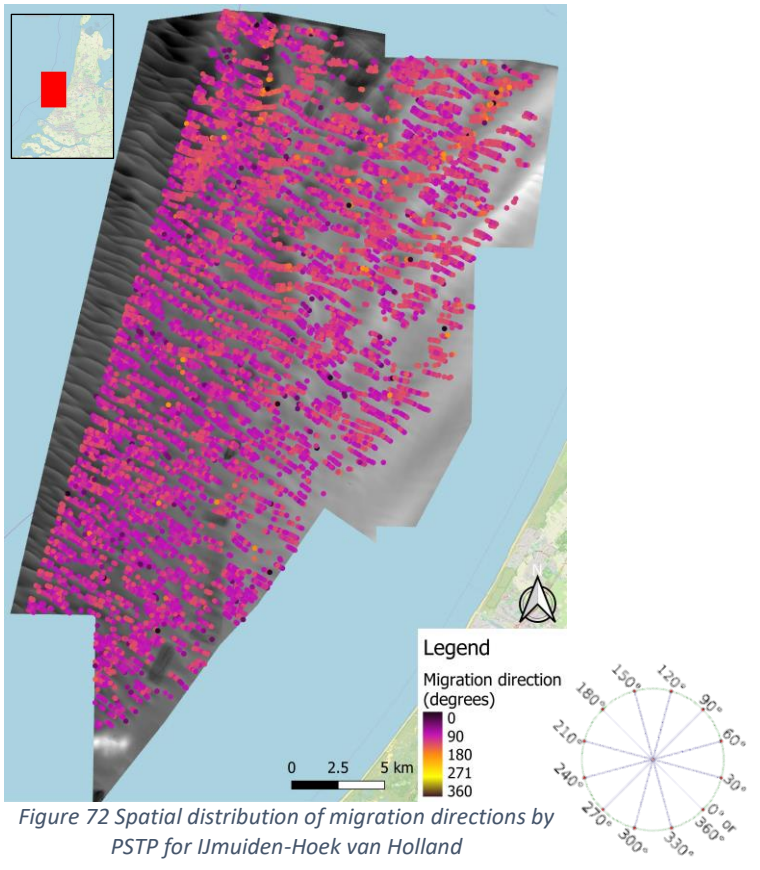

Figure 72 Spatial distribution of migration directions by PSTP for IJmuiden-Hoek van Holland

7. Evaluation and final method selection

7.1. Introduction

This chapter comprises the evaluation of the detection methods based on the results obtained with artificial data and field data as well as the practical applicability. The aim is to select the most suitable method for further use during the large-scale analysis of sand wave migration on the NCS.

First, the performance of PSTP and SCC with artificial data and field data are addressed in section 7.2 and 7.3, respectively. Subsequently, the usability of each method is evaluated in section 7.4. Finally, the pros and cons are compared, and the most suitable method is selected in section 7.5.

7.2. Performance with artificial data

The validation tests with artificial bathymetric timeseries show that PSTP and SCC can measure the pre-defined migration distances smaller than half the wavelength of the (artificial) sand waves with relative accuracy. However, when the migration distance is between half the wavelength and the wavelength, migration is measured in the opposite direction. For pre-defined migration distances larger than the wavelength, migration distances are measured in the correct direction but have a magnitude that is roughly a wavelength lower than the one pre-defined. Hence, in future field data analyses, it is important that the time in between two surveys comprising a timeseries is not too long such that the sand waves have migrated past half the wavelength.

However, the tests also show that the time in between two surveys should not be too short. With actual field data, sand wave migration can be seen as the horizontal shifting of a sinusoidal-like surface underlying a fixed bathymetric grid. PSTP can therefore only measure migration along the integer positions of the grid cells in X and Y direction, due to which its accuracy is hampered. As opposed to PSTP, SCC is not bound to the *raster* resolution, but its measurements are inaccurate when the migration distance is close to 0 m. Hence, for both methods, the time in between two surveys should be such that the expected migration distance is close to or larger than the *raster* resolution (20-25 m)[7]. This way, besides increasing the relative accuracy of the measured distances, dividing by a large number increases the robustness of the estimated migration rates (m/year). In most cases, considering the average migration rate on the NCS is mostly below 5 m/year, this comes down to a time of at least 4-5 years (Van Dijk et al., 2011).

7.3. Performance with field data

The results by PSTP and SCC are qualitatively comparable for all field sites. Regarding SCC, a notable result is that, even though it is mainly to be used for straight-crested sand waves in a uniform flow field, the weighted regression vector is the only vector that provides realistic results for all considered types of morphodynamics. The weighted centroid and maximum correlation vector fail to do so.

Except for the sand waves on top of the sandbanks at Schaar-Rabsbank, the weighted centroid vector mainly measures migration parallel to the crest lines. This is not a strange result for the straight-crested sand waves in between the sandbanks at Schaar-Rabsbank, but it is rather unexpected for the sand waves at North Hinder, which are more three-dimensional. The results indicate that this vector type has more trouble detecting the correct qualitative behaviour when dynamics are insignificant relative to the *raster* resolution. As opposed to the weighted regression vector, migration directions are not

[7] In practice, meeting this requirement is not straightforward when migration rates are close to 0 m/year. For these locations, a minimum requirement of at least 8-10 years in between two surveys can be used instead.

forced to be perpendicular to the crest, which makes it more sensitive to data quality and resolution and to slight changes in the input parameters.

The reason for the limited performance of the maximum correlation vector is that, when correlating two linear features in time, the cross-correlation matrix often has an elliptical maximum (correlation ridge) instead of a point maximum (Duffy & Hughes-Clarke, 2005).

Finally, although the qualitative results do not differ significantly, small differences in smoothness and quantitative output are observed in all field data tests. These can be explained as follows:

Data resolution. For PSTP, the filtered crest and trough lines are irregular due to its restriction to the integer *raster* cell positions of a relatively low-resolution grid. Sequential lines therefore converge and diverge where they should be parallel. Eventually, when plotting the migration rates for each of the random target points in a frequency distribution, sharp peaks appear at the edges of the plot. When plotting the migration directions, two peaks occur just around the true migration direction. In the spatial plots, the outlier values at both ends of the value range are evenly distributed over the map. Their presence adds to the chaoticity of the spatial distributions.

Window size. A single window size is often not optimal for locations with strongly variable wavelengths, such as Schaar-Rabsbank. By taking a snapshot of a collection of *raster* cells, a window that is too large generalizes the migration estimate over multiple smaller sand waves, creating a relatively smooth map. However, dynamics that occur on a scale smaller than the search window are not detected. On the contrary, a window that is too small is unable to accurately track the movement of large sand waves, which results in a more chaotic map.

Regularly and randomly placed points. Most of the spatial distributions of SCC are smooth as opposed to the more chaotic distributions of PSTP. Besides the presence of outlier values for PSTP, this is explained by the fact that the data points of SCC are placed as a two-dimensional grid whereas the target points of PSTP are placed more randomly. In addition, since two methods of crest detection are used in some cases, the target points can be stacked.

Weighted regression vector. As opposed to the weighted centroid and maximum correlation vector, the weighted regression vector provides realistic results for all field sites. However, since it is developed for straight-crested sand waves in a uniform flow field, this vector type has trouble providing a smooth, uniform vector field on top of sandbanks, where migration is oblique rather than perpendicular to the crest-lines.

7.4. Usability

Besides the differences in performance with artificial data and field data, PSTP and SCC also differ in terms of their usability. Some key factors affecting each method's suitability for large-scale analyses are described below:

Computation time. The computation time with SCC is much shorter than with PSTP. For SCC, a single analysis takes seconds to a minute as opposed to minutes with PSTP. For both, the exact time depends on the degree of data cleaning required. This significant difference is mainly due to the many consecutive steps that PSTP requires, which include *raster* smoothing, crest and trough detection, migration quantification for crests and troughs and data cleaning. Although SCC's computation time is shorter, it takes multiple runs before the correct window size is found. In addition, some post-processing is required since the algorithm also covers regions where no sand waves are present.

A brief comparison of the computation times for an artificial timeseries with bathymetry datasets of 10 by 10 km, results in 1 minute and 8 seconds for SCC (procedure includes: computation and data cleaning for one vector type) and 4 minutes and 31 seconds for PSTP (procedure includes: DEM smoothing, crest detection, crest migration and data cleaning).

Despite the significant difference in computation time between PSTP and SCC, obtaining quantitative results within minutes can still be considered as fast. Especially when compared to process-based modelling, which can take much longer before any results are obtained.

Algorithm generality. PSTP comprises more steps, but the settings and input parameters are relatively similar for different parts of the NCS. Only the curvature value above which the crest lines are filtered, the maximum distance between sequential crest and trough lines and the number of target points to be plotted are different for differing types of *morphometry* and dynamics, but these only vary on a large spatial scale. The correct settings are relatively easy to find as the range of potential options is rather narrow. The input parameters of SCC are less generally applicable, as only the weighted regression vector can provide a realistic vector field with limited changes to the input parameters. The optimal window size largely depends on the dominant wavelength of the sand waves. Some prior knowledge of these wavelengths helps with finding the optimal window size quickly, but trying a few different options is still required in most cases. Finally, for the purpose of this research, an 'optimal' window size is defined as the window size that results in a realistic, uniform flow field. However, for regions where wavelengths strongly vary, a single window size might not be optimal as a large window generalizes the measurements over multiple smaller sand waves and a small window does not fully cover the larger sand waves.

Interpretation of obtained output. As a result of the lengthy procedure of PSTP, many output files (around 80 for crest or trough migration) are generated, whereas SCC generates much less (around 40). Identifying errors and anomalies in the output is slightly easier with PSTP, as outlier values in migration rate and direction usually result from irregularities in the crest and trough lines. Vector cleaning and entering a maximum distance between subsequent crest and trough lines prevents extreme outlier values in the final output from occurring. For SCC, error sourcing is more difficult as only the final output in the form of a two-dimensional grid is visible. One should plot the correlogram to identify where an outlier value might come from. Potential error sources might the window size, threshold value and quality issues with the DEM. On the other hand, spatial patterns are readily revealed with SCC whereas the spatial distributions of PSTP are usually noisier. Aggregation is in most cases required to identify spatial patterns.

7.5. Preferred method for NCS-wide analysis

Table 10 summarizes the pros and cons of PSTP and SCC as techniques to quantify sand wave migration from timeseries of bathymetric data. It is important to note that these are based on the tests that are done during this research. However, since sand wave morphodynamics worldwide are comparable, it is expected that Table 10 is also valid when PSTP and SCC are applied for analysing sand wave migration in other shelf seas than the NCS.

Table 10 Pros and cons of Pairs of Source and Target Points and Spatial Cross Correlation

	PSTP	SCC
+	Input parameters are generally applicable	Short computational time
	Error sourcing is relatively easy	Measurements are not bound the to the resolution of the bathymetric grid
	Provides realistic results for differing types of *morphometry* and dynamics	Weighted regression vector provides realistic results for differing types of *morphometry* and dynamics
-	Longer computational time	Input parameters are less generally applicable
	Measurements are bound to the resolution of the bathymetric grid	Error sourcing is more difficult
	Spatial distribution of data points can be chaotic	Accuracy is limited for migration distances near 0 m
		A single set of input parameters is often not optimal when wavelengths vary strongly

Based on the obtained findings in the testing phase, PSTP is selected as the preferred method for the quantification of sand wave migration on the NCS. The preference for PSTP is mainly based on its ability to provide robust and realistic results for a wide range of sand wave morphodynamics. Moreover, compared to SCC, the input parameters are more generally applicable, and sources of errors and anomalies are easier to identify. Although the computation time is longer than with SCC, a computation time of several minutes is still considered as fast. The generality of the algorithm allows for the consecutive analysis of many timeseries without changing anything to the input parameters. Finally, the accuracy of the measurements is limited due to the restriction to the integer cells position. This can however be dealt with by using surveys that are collected with a sufficiently long time in between.

The rejection of SCC for a large-scale, NCS-wide analysis is mainly caused by the fact that its (optimal) input parameters are less generally applicable and are less straightforward to determine. The sensitivity of the results to the correct input parameters also means that error sourcing is not as straightforward as with PSTP. However, its rejection does not mean that the technique not suited for other purposes. The weighted regression vector performs well in terms of detecting the correct qualitative and quantitative behaviour for different types of morphodynamics. Accuracy is limited when the migration distance is nearly 0 m, but this might improve with high-resolution bathymetric data. Furthermore, improving the process of finding the correct input parameters or even allowing for variable input parameters (window size, vector type) can strongly improve the usability and generality of the technique.

8. Sand wave migration on the NCS

8.1. Introduction

This chapter comprises the results regarding sand wave migration on the NCS. PSTP is used to analyse over 300 timeseries. To gain insight in the spatial variability of migration rate and direction, the resulting 1,900,000 data points are aggregated to an average value per square kilometre.

Section 8.2 first addresses the coverage of the bathymetric data in space and time. Then, section 8.3 and 8.4 comprise the results of the aggregated migration direction and migration rate, respectively.

8.2. Data coverage in space and time

The number of timeseries used for aggregation is given in Figure 73. As can be seen, virtually the entire NCS is covered with at least one timeseries (which equals at least 2 observations).

Areas of seafloor that are of high priority for shipping, such as the approach routes to the Maasvlakte and IJmuiden and the *traffic separation schemes* (TSS) that cross the Breeveertien Banks, Texel and Vlieland are clearly visible. Estimates of migration rate and direction for these areas are robust as most are based on at least three timeseries. For regions of low priority, such as the coastal area between IJmuiden and Hoek van Holland and the sand banks near Zeeland, only one or timeseries are used.

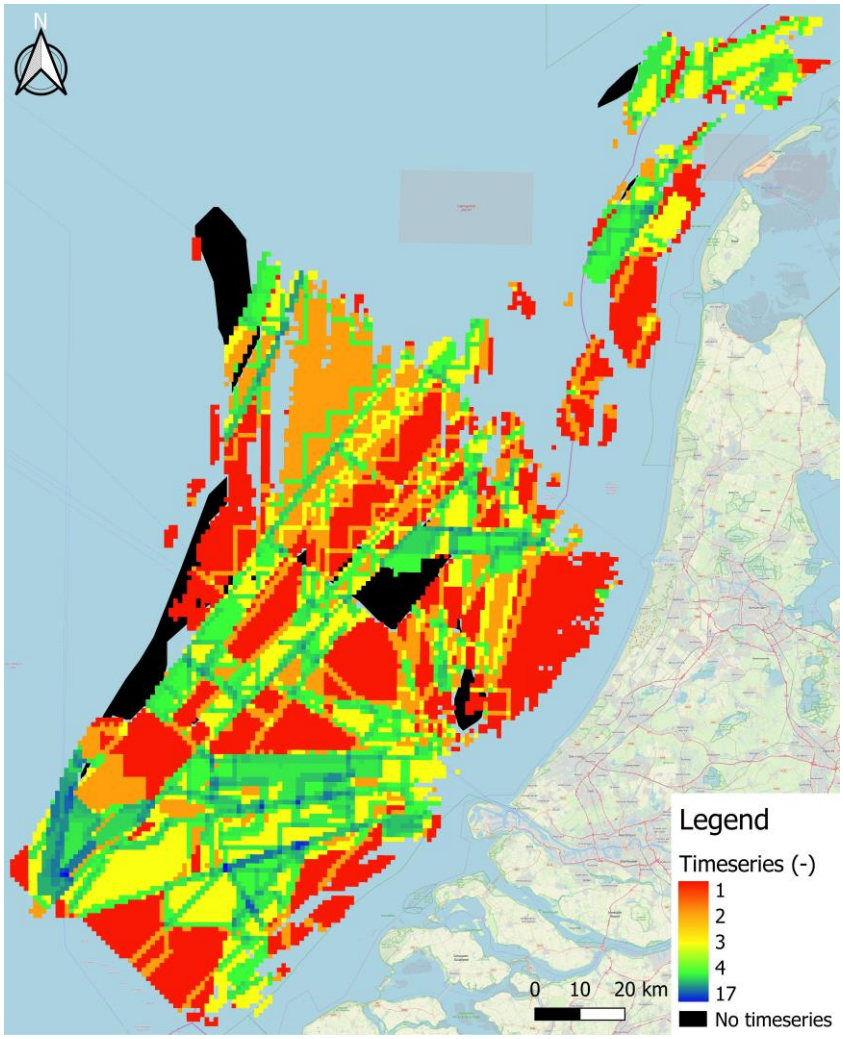

Figure 73 Number of timeseries per km² (1 timeseries = 2 bathymetric datasets)

The number of timeseries is to some extent coupled with the number of data points, visualised in Figure 74. In general, more data points are present for regions where multiple timeseries are available. The number can be lower due to the absence of multiple timeseries or because the wavelengths are long (and hence the spatial frequency is low), which is the case for the sand waves between IJmuiden and Hoek van Holland and north of Vlieland.

The 10th percentile, median and 90th percentile of the number of available data points per square kilometre are 50, 206 and 568, respectively. Hence, most estimated average values for migration rate and direction are considered significant.

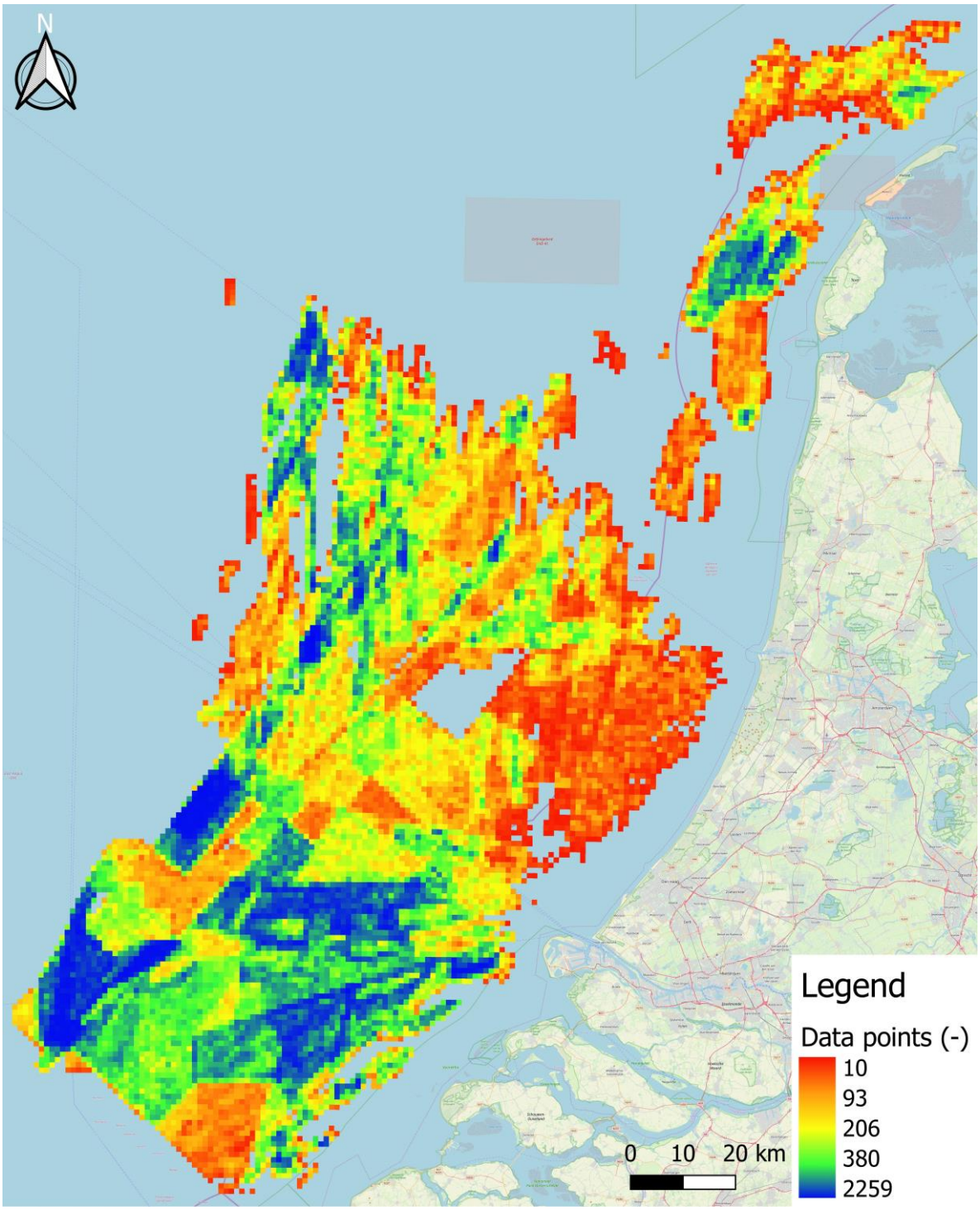

Figure 74 Number of data points per km^2

8.3. Spatial variability of migration direction

A colour map with the average migration direction per square kilometre is given in Figure 75. The uncertainty of the average direction is expressed by the standard deviation in Figure 76. From the colour plots, three types of behaviour are distinguished.

Migration in northern or north-eastern direction is observed for most of the sand waves located at the level of Rotterdam and further north. For a large part of the NCS, the sand waves migrate roughly parallel to the Dutch coastline. A deviation of this general pattern is seen at the Breeveertien Banks and the southern parts of the Brown Ridge. Here, the migration direction on the seaward flank of the sand banks is deflected to the east. Since the sand waves generally migrate in a uniform direction, the standard deviations are low. An exception is seen at the most northern edge of the Breeveertien Banks, where migration directions vary on a scale smaller than a square kilometre due to the presence of some relatively narrow sandbanks.

Different behaviour is observed at the Zeeland Banks and on top of the Brown Ridge. The presence of multiple large sandbanks causes the sand waves on different flanks to migrate in either north-eastern or south-western direction. Note that sand waves on either the landward or the seaward flank do not necessarily migrate in a certain direction, see the encircled sandbanks in Figure 75. Standard deviations are relatively high, which comes from the fact that the *raster* cells are sometimes located on the crest line of a sandbank. As a result, the data points within the *raster* cell have opposite directions. Furthermore, migration rates between the sand banks are low, which increases the amount of noise in the data.

Finally, in the south-western corner of the NCS, the colour plot wrongly implies migration to the north-west, which is roughly parallel to the sand wave orientation. This can be explained by the fact that, within a *raster* cell of a square kilometre, the number of data points that measures migration to the north-east (± 90 degrees) is comparable to the number of data points that measures migration to the southwest (± 270 degrees). Moreover, this region is less dynamic (see section 2.4 and 8.4), which, combined with the low data resolution, increases the amount of noise in the results. Averaging these data points per square kilometre therefore leads to values of around 180 degrees and standard deviations of up to 115 degrees. A colour plot that shows the chaoticity of the raw data in this region is given in Appendix VI.

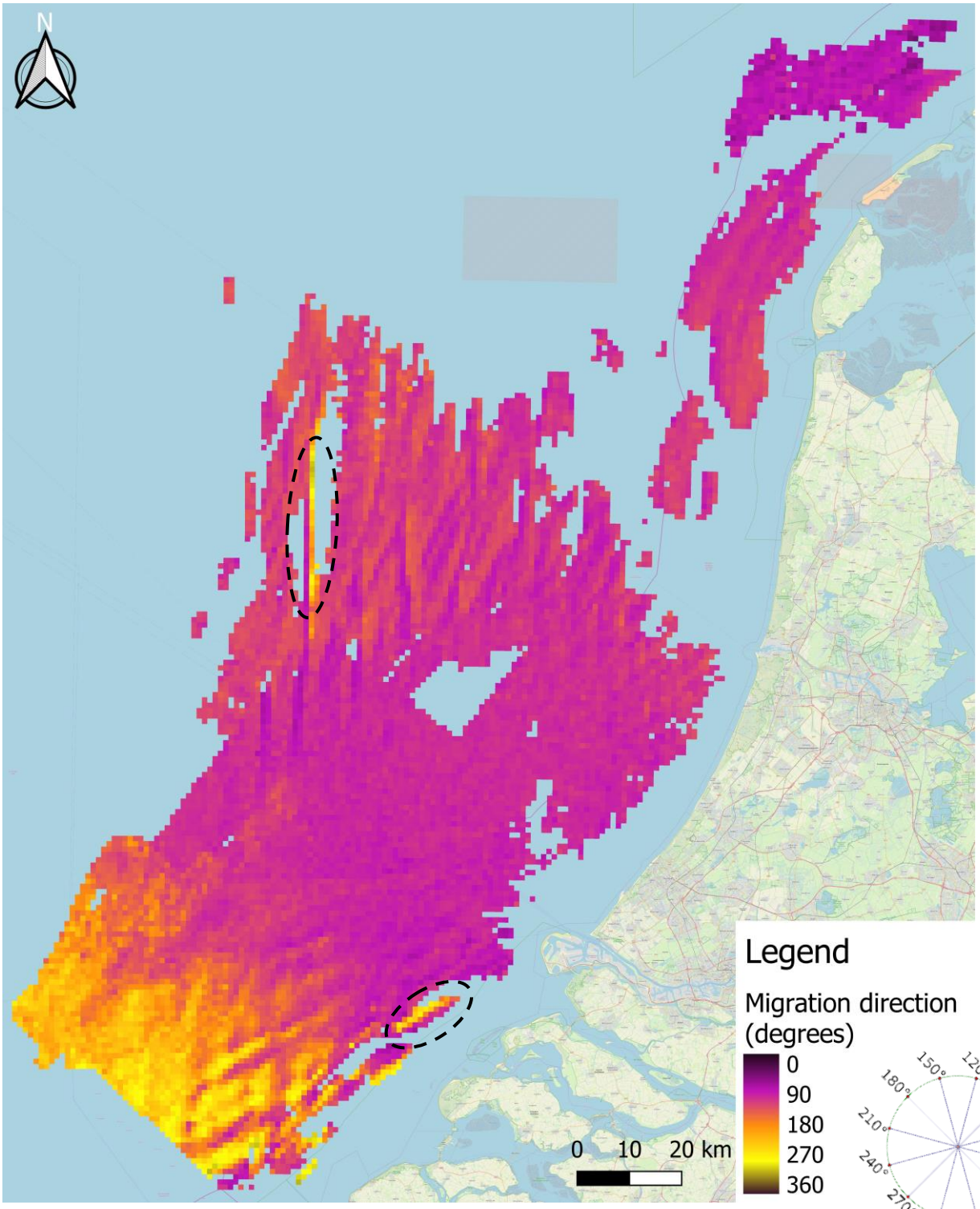

Figure 75 migration direction averaged per square kilometre

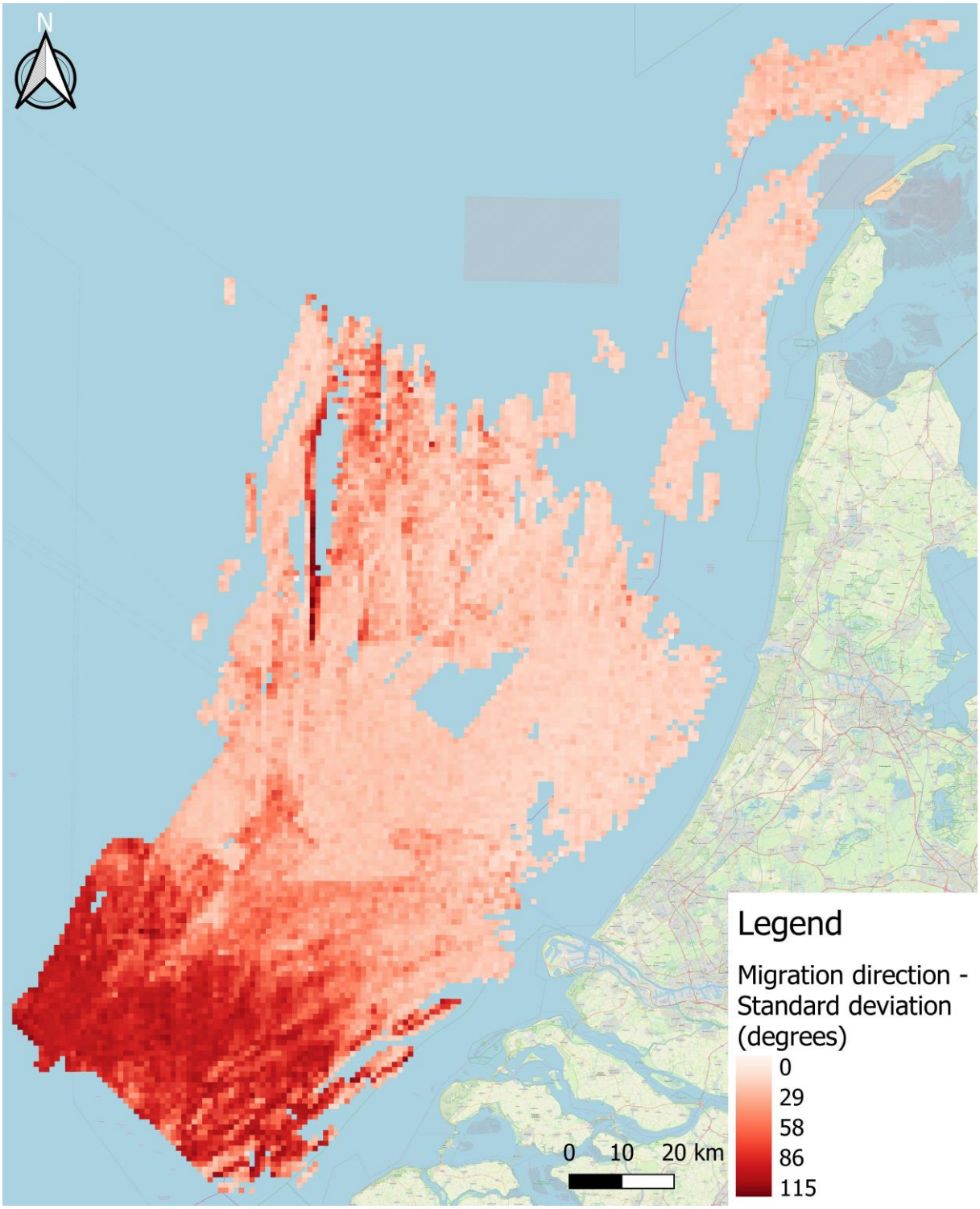

Figure 76 Standard deviation of migration direction per km²

8.4. Spatial variability of migration rate

Colour maps of the average migration rate per square kilometre are given in Figure 77 and Figure 78. A linear as well as nonlinear colour scale are used to clarify spatial differences. The uncertainty of the estimates is expressed by means of the coefficient of variation (standard deviation relative to the mean), visualised in Figure 79, which is preferred over the standard deviation (Appendix VII) as it allows for comparison of locations with differing mean values.

Table 11 indicates that the average migration rates at the main sand wave field typically range between 0-3 m/year, although migration rates of up to 12 m/year are observed at the Zeeland Banks. The fields at the Wadden Island are more dynamic, with average migration rates typically ranging between 2-8 m/year. For this region, the highest migration rates of 10-21 m/year are observed near the coast. Frequency distributions for the three sand wave fields are given in Appendix VIII.

Table 11 Statistics for the average migration rates per square kilometre

Sand wave field	Main	Texel	Vlieland
Median (m/year)	1.2	3.9	3.1
min (m/year)	0.2	1.6	1.5
10% (m/year)	0.5	2.6	2.1
90% (m/year)	2.6	7.4	5.7
max (m/year)	12.3	13.4	21.1

Three spatial patterns can be deduced from Figure 77 and Figure 78.

First of all, migration rates are lowest (< 0.5 m/year) at the North Hinder bank and highest at the Wadden Islands. The upward trend from south-west to north-east increases non-linearly, as large parts of the main field are below 5 m/year. Migration rates exceeding 10 m/year are only observed for a small section of the sand wave fields at the Wadden Islands.

Furthermore, migration rates are generally highest near the coast and decrease in the offshore direction. This can be clearly seen near IJmuiden, the Maasvlakte and the Wadden Islands.

Finally, migration rates locally increase where sand waves are located on top of a shoreface connected ridge or sandbank, as is seen at ridge in the approach route to the Maasvlakte, the Zeeland Banks and the Breeveertien Banks. For the latter, the sand waves on the seaward flank migrate significantly faster than on the landward flank. An example where this can be clearly seen is encircled with a solid line in Figure 77 and Figure 78.

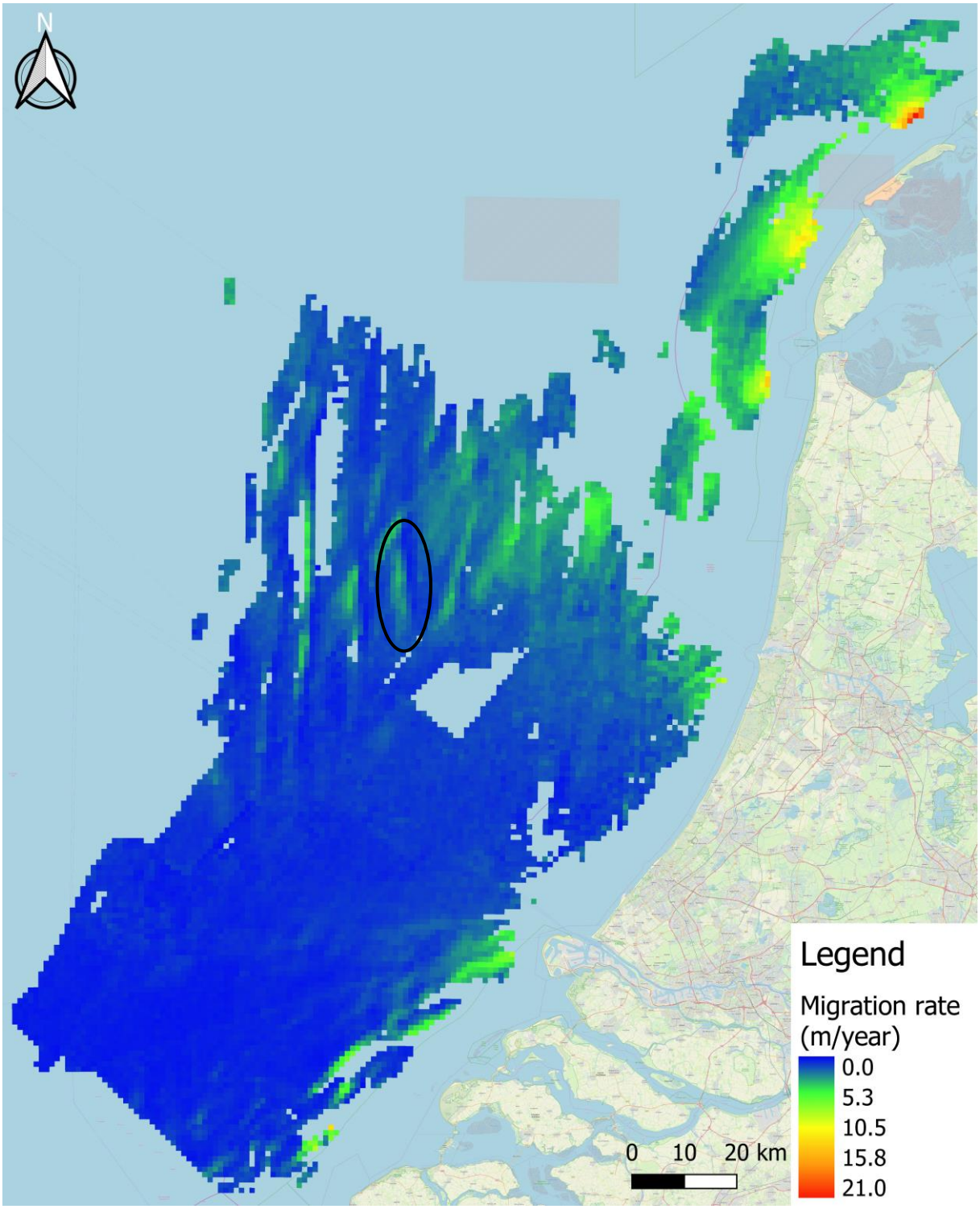

Figure 77 Migration rate per km² (linear colour scale)

By using a nonlinear colour scale, spatial differences in the non-dynamic regions are clearly revealed. However, it also makes the colour plot more chaotic as small deviations from the surrounding dynamics become visible. The blue patches (encircled with a dashed line in Figure 78) in the coastal region between IJmuiden and Hoek van Holland and further offshore are clear examples. These artefacts are caused by fact that only one timeseries (comprising only two surveys) is used for which the time in between both surveys is relatively short. Future analyses with additional timeseries should improve these estimates.

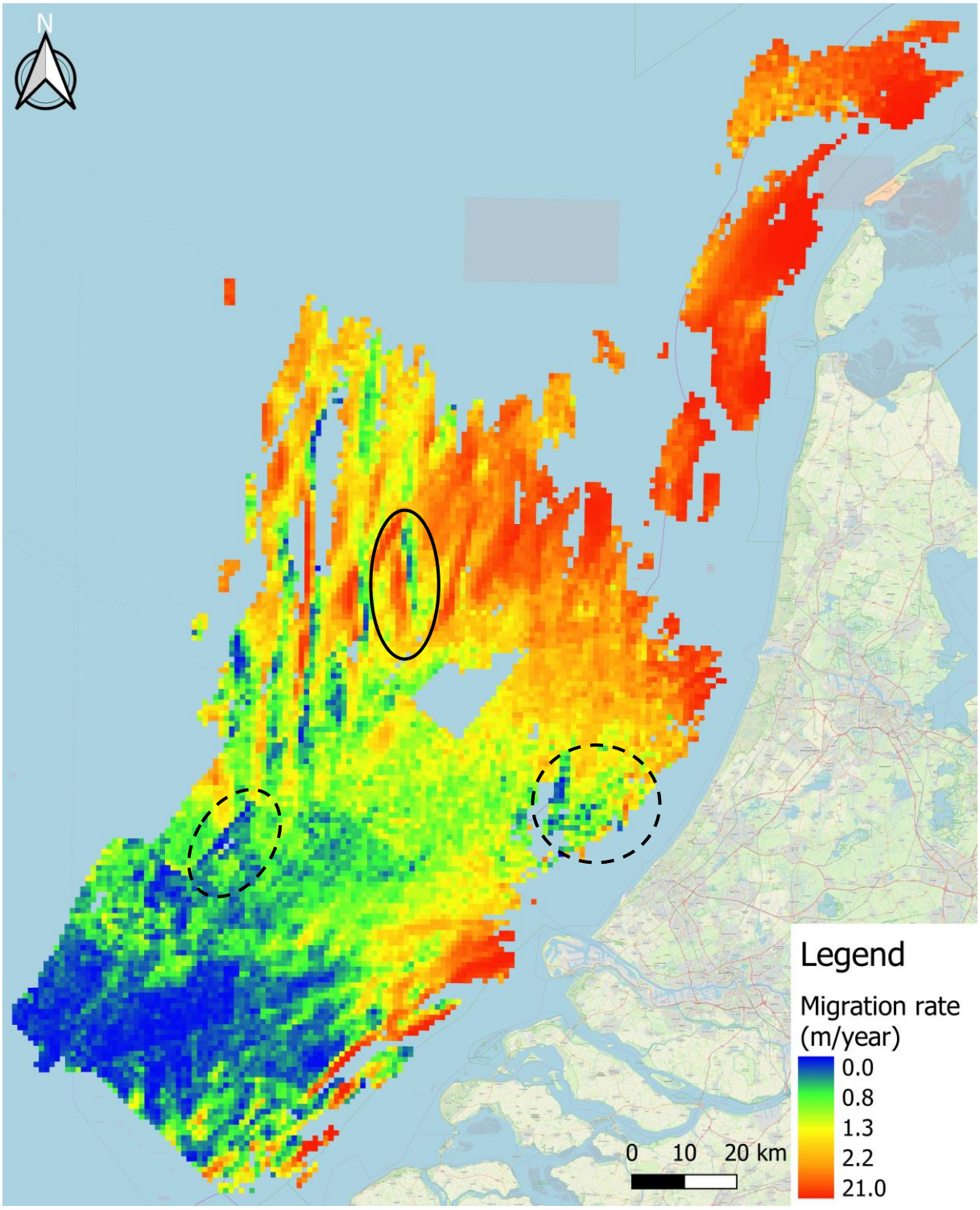

Figure 78 Migration rate per km² (nonlinear colour scale)

The coefficient of variation in Figure 79 shows an opposite pattern as the average migration rate. The colour plot indicates that the relative dispersion of the data points around the mean migration rate is highest in regions of low dynamics, such as at the North Hinder banks and at the landward flank of the Breeveertien Banks. Hence, the relative uncertainty of the estimates is largest here.

In regions where migration is in uniform direction and at a high rate, such as near the Wadden Islands, the relative dispersion of the data points is much lower.

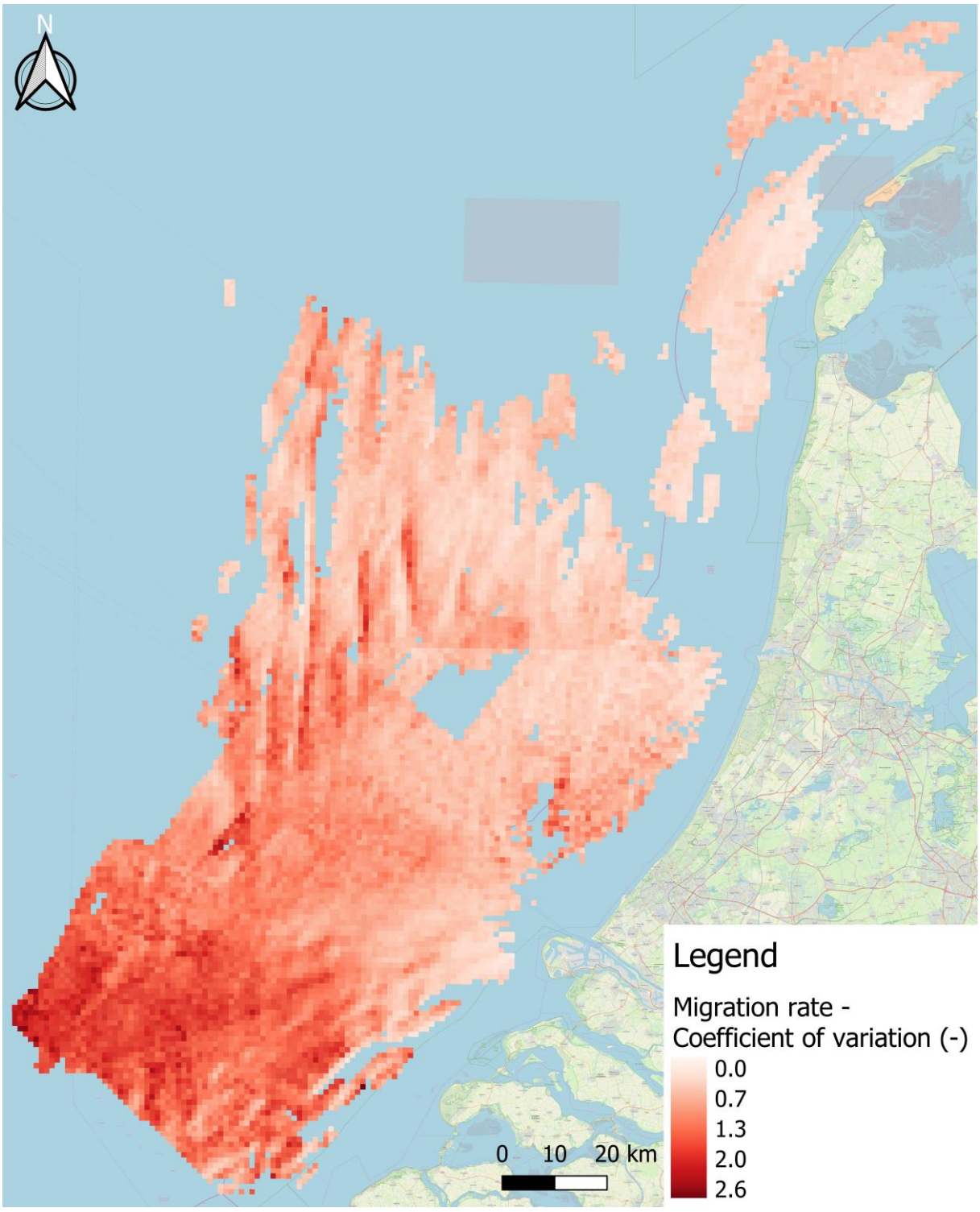

Figure 79 Coefficient of variation (standard deviation/mean) of migration rate per km²

9. Discussion

9.1. Explanation and interpretation of obtained results

The aim of this research is to gain insight in the spatial variability of sand wave migration on the NCS. To facilitate an analysis on that scale, a 2D measurement methodology was developed in QGIS which quantifies migration rate and direction based on timeseries of bathymetric data.

9.1.1. Selection, testing and evaluation of detection methods

After a preliminary selection procedure, two migration detection methods were implemented in QGIS: Pairs of Source and Target Points (PSTP) and Spatial Cross Correlation (SCC). Testing with field data and artificial data showed that PSTP is favourable for doing a large-scale analysis at the NCS.

The version of PSTP used during this research is adapted from a version that quantifies the migration of terrestrial sand dunes (Dong, 2015). Although accuracy of the quantitative results is not specifically mentioned, it is likely that the application of PSTP by Dong (2015) provided more accurate results as the 1 m resolution of the LIDAR data is much higher than the 25 m resolution used in this research. For the current application, a resolution of 25 m is sufficient since most crest and trough positions can be nicely represented by a single *raster* cell. Provided the time in between two surveys is long enough such that displacement is large relative to the *raster* resolution, the restriction of PSTP to measuring displacement along integer cell positions in the X and Y direction is sufficient for gaining a general insight in large-scale, NCS-wide migration patterns. Plotting several hundred data points per square kilometre provides a good insight in how migration rates and directions are distributed for a particular location. Aggregating these points to an average value per square kilometre then reveals spatial differences on a large scale. However, for engineering purposes for instance, it might be desirable to accurately track the movement of specific sand waves (or other bedforms) using many timeseries and a higher survey frequency. Using high-resolution bathymetric data is then required since a 25 m data resolution is too low for doing these accurate measurements. Performance wise, the current application of PSTP differs from the application by Dong (2015). For a test region of 2.4 by 9 km, Dong, (2015) and Jisheng & Dong (2016) obtained results for 8707 target points within two minutes. It takes the current version of PSTP longer in most cases to deliver a comparable performance. This difference is partly explained by the fact that more pre- and post-processing is required, whereas PSTP used by Dong (2015) is fully automated. Furthermore, some additional intermediate steps are required in QGIS. However, obtaining quantitative results within several minutes can still be considered as fast, especially when compared to process-based modelling, which generally take much longer.

In the application of SCC by Duffy & Hughes-Clarke (2005), it was also found that a single vector type is unable to correctly detect all sand dune migration directions around a sandbank. When using this method at locations where *morphometry* and dynamics strongly vary, it is required to use multiple vector types to detect the correct qualitative behaviour. In addition, finding the optimal input parameters in the form of window size, search zone and threshold value is not always straightforward. Improving the process of finding the correct input parameters or even allowing for variable input parameters (window size, vector type) can strongly increase the usability and generality of the technique. Quantitative migration rates are described by Duffy & Hughes-Clarke (2005) as relatively accurate, which is partly explained by the fact that a higher data resolution (1 m) is used. Using high-resolution bathymetric data is beneficial for obtaining a higher accuracy, since SCC tracks three-dimensional shapes (Buijsman & Ridderinkhof, 2008). In the application of SCC by Zhou et al. (2018) at the Taiwan Banks, using a 1 m resolution even allows for the maximum correlation vector to provide

sufficiently accurate results. In testing SCC with migration distances near 0 m (see sections 5.4), the data resolution of 25 m was too low for the technique the deliver quantitatively correct results. However, it was also shown that the accuracy is much higher when dynamics are significant relative to the data resolution. Provided the usability of SCC is improved, it might also become a suitable technique for large-scale analyses of sand wave migration.

The added value of the first part of this research to the existing knowledge base is mainly the adaptation of PSTP to make it suitable for analysing tidal sand wave migration. The technique was originally developed to analyse terrestrial sand dune migration and until now, it was never applied to marine bedforms. The current research has shown that PSTP is well suitable for analysing the large-scale spatial differences of sand wave migration at the NCS. However, its applicability is not restricted to the NCS. Provided there is a sufficient spatial and temporal coverage of bathymetric (or topographic) timeseries, it can be used for large-scale analyses of bedform and landform migration around the world. Significant adaptations for PSTP to be applied elsewhere are not required as the detection of crest and trough positions using Maximal Curvature and Convergence Index can be done for all types of harmonic bed- and landforms.

9.1.2. Observed sand wave dynamics at the NCS

Average migration directions as obtained during this research largely agree with those reported in literature. For the sand wave fields north of Rotterdam, migration is mostly in north-eastern direction (Knaapen, 2005; Van Dijk & Kleinhans, 2005; Dorst et al., 2011; Van Dijk, et al. 2011). As opposed to the results here, Van Dijk & Kleinhans (2005) found migration to the southwest for a sand wave field 50 km offshore of Egmond. The fact that this seasonal variability is not reported in the current research is mainly because only timeseries are used which comprise surveys with multiple years in between. This way, the measurements are less affected by seasonal weather processes, such as increased wind and waves, which can significantly influence sand wave migration (Sterlini et al., 2011; Campmans, 2018). For the south-western corner of the NCS, local variability of migration directions to the north-east or south-west is also reported by Knaapen (2005) and Van Dijk et al. (2011). The bidirectional migration of sand waves superimposed on sandbanks as reported by Van Dijk et al. (2011) at some sections of the Brown Ridge and by Deltares (2015) at the Borssele Wind Farm Zone is also observed in this research. However, it is notable that the presence of a sandbank does not necessarily lead to bidirectional sand wave migration, as the Breeveertien Banks only show a strong deflection of migration to the east on the seaward flank.

A notable observation is that, at the Zeeland banks, the sand wave migration direction is not linked to the landward or seaward side of the sandbank (see section 8.3). This contradicts the physical explanation by Roos & Hulscher (2003) and the modelling results by Leenders et al. (2020). Roos & Hulscher (2003) explained that, on the Northern Hemisphere, Coriolis effects enhance a clockwise circulation of the tide-averaged flow around a sandbank. Hence, sand waves on the seaward and landward flank migrate to the north-east and south-west, respectively. This phenomenon was modelled by Leenders et al. (2020) for a symmetrical as well as an asymmetrical tidal flow. It is not exactly clear what causes this contradiction. It is possible that some measurements are faulty. When the time in between two surveys is sufficiently long for sand wave displacement to be larger than half the wavelength, both PSTP and SCC can detect migration in the wrong direction (see section 5.4). However, the credibility of the analysis is strenghtened by the fact that anti-clockwise migration is observed for multiple sandbanks and for multiple different timeseries. Adding to the plausibility of the obtained results, is the fact that the observed migration directions match with the observed sand wave pattern. The migration directions over one of the sandbanks at Schaar Rabsbank are indicated in Figure 80. From above, it can be seen that the crest lines of the sand waves point in the direction in which

they migrate. It is unlikely that this particular orientation would occur when the sand waves migrate in a clockwise direction around the sandbank. The opposite pattern is visible at the Brown Ridge in Figure 81. Here, observations agree with theory as the superimposed sand waves migrate in a clockwise direction.

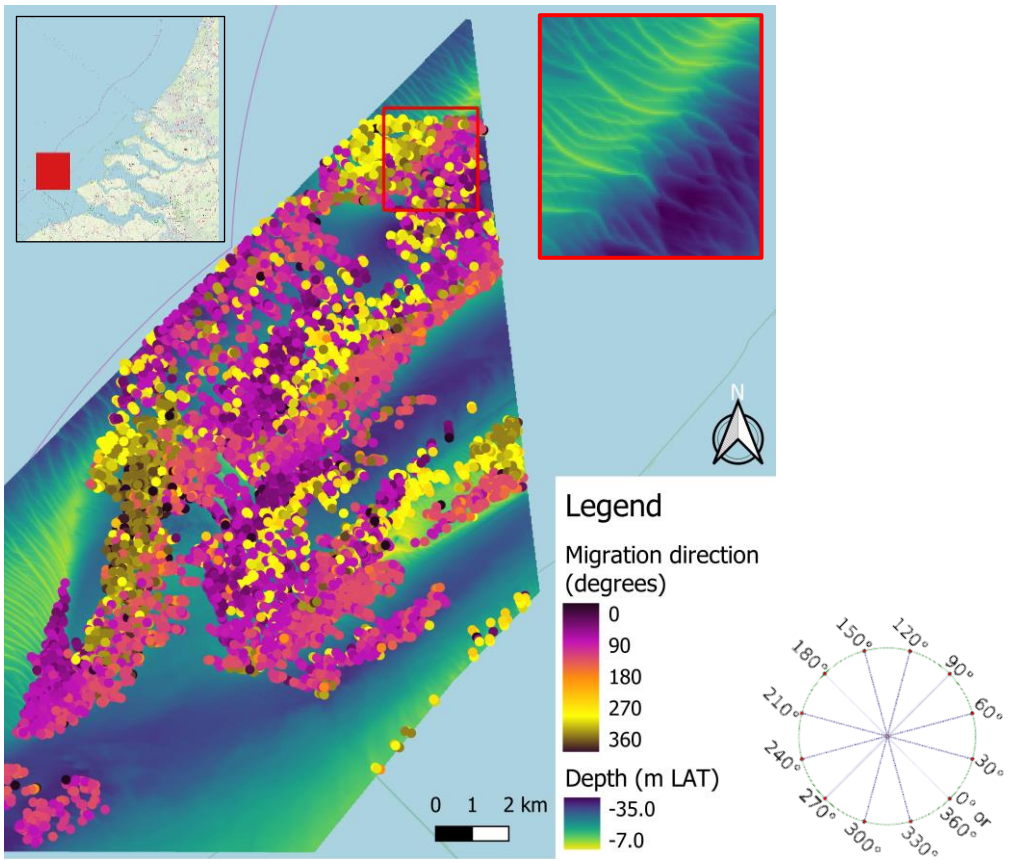

Figure 80 Migration directions, bathymetry, and sand wave orientation (red square) at Schaar-Rabsbank

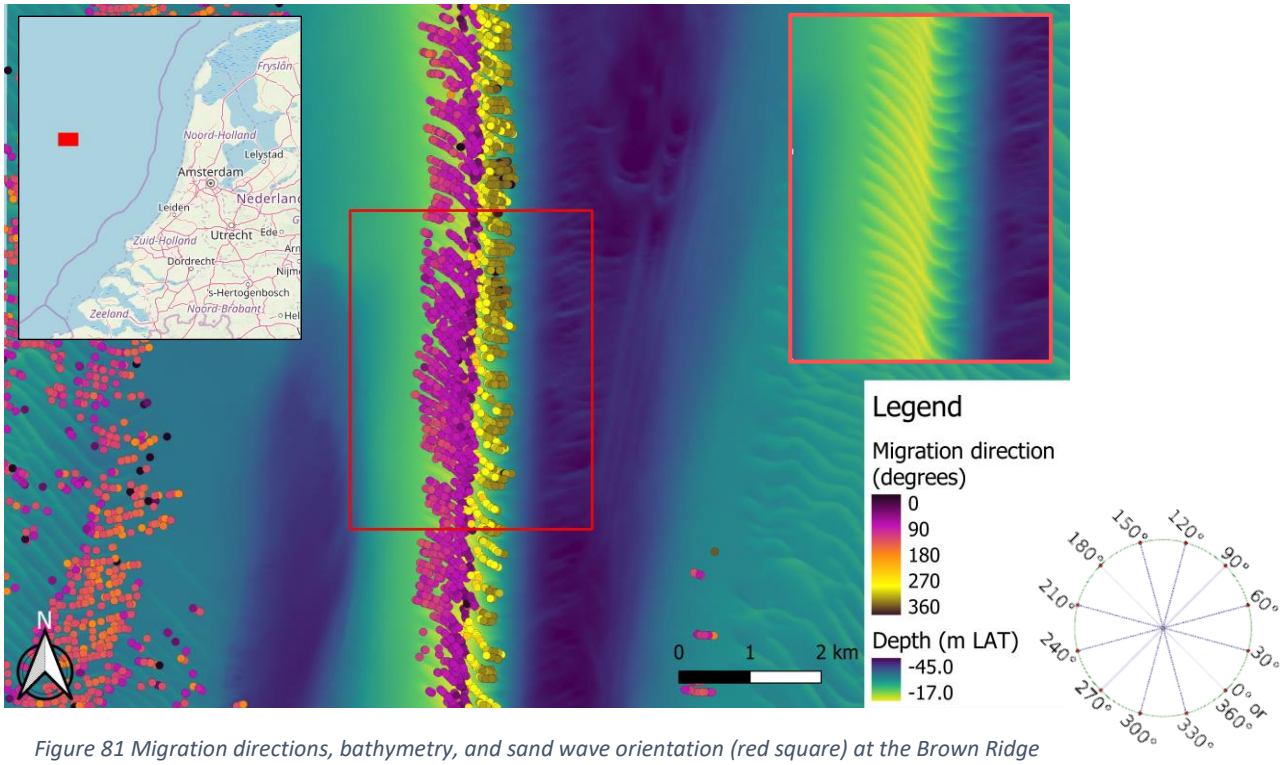

Figure 81 Migration directions, bathymetry, and sand wave orientation (red square) at the Brown Ridge

Providing a physical explanation for the observed contradiction is not straightforward. It might be the case that the occurrence of multiple large sandbanks close together, combined with a strong variability of flood- and ebb-dominated tidal currents, changes the tide-averaged hydrodynamics in such a way that the influence of the Coriolis effect is less dominant. Extensive process-based modelling studies using a comparable underlying bathymetry and comparable hydrodynamic input parameters should provide further clarity on this phenomenon.

In general, the estimated migration rates per square kilometre agree quite well with literature. The observed spatial patterns, which include the upward trend from North Hinder towards the Wadden Islands and increased migration rates near the coast and on top of sandbanks, are also confirmed by literature. Hence, in a qualitative sense, no notable differences are identified. The discussion that follows is therefore limited to some quantitative differences.

In literature, the sand waves at North Hinder and in the approach route to the Maasvlakte are reported as relatively static, with migration rates ranging between 0-0.5 m/year (Knaapen, 2005; Van Dijk, et al., 2011; Dorst et al., 2011). The estimated migration rates per square kilometre fall within this range. However, since the dynamics are low relative to the data resolution of 25 m, the amount of noise in the raw data points is significant. On a local scale, the uncertainty of the results is relatively high, as is indicated by the higher variation coefficients for this region (see section 8.4). Therefore, it is unlikely that the measured migration rates at a certain location are the same as those reported in other studies for that same location.

Further to the north, net migration rates for survey sites offshore of IJmuiden and Egmond are mostly estimated around 2 m/year (Van Dijk & Kleinhans, 2005; Van Dijk et al., 2008; Van Dijk et al., 2011; Dorst et al., 2011), which is comparable to the estimated migration rates per square kilometre in the current research. However, differences between estimated values and those reported in literature arise near the coast. Several kilometres of the coast of Zandvoort, Van Dijk & Kleinhans (2005) report migration rates of 6.5-20 m/year, whereas the average estimates in section 8.4 do not exceed 9 m/year. This difference is mainly explained by the fact that, for the large-scale analysis in chapter 8, only long-term timeseries with several years in between are used as opposed to the shorter timeseries (which comprise four surveys that are collected over the course of one year) as used by Van Dijk & Kleinhans (2005). For these short timeseries, seasonally increased waves or wind effects can have a significant (local) impact on migration rates. Another explanation for the quantitative difference is the fact that Van Dijk & Kleinhans (2005) only measure the migration of a single sand wave along a crest-perpendicular profile. This way, the measurement are based on only a few data points, which increases the impact of these seasonally changing wind and wave effects. In the current research, the measured migration rates are averaged per square kilometre, which smooths out the highest observations and gives a more robust estimate for the sand wave field as a whole.

At parts of the Brown Ridge and at the Breeveertien Banks, observed migration rates on the seaward flank (up to 6 m/year) are significantly higher than on the landward flank (0.2-0.8 m/year). An explanation for this phenomenon was given by Leenders et al. (2020). In modelling the migration direction of tidal sand waves around sandbanks, Leenders et al. (2020) included a residual current in the flood direction, which resulted in significantly higher migration rates on the western (seaward) flank than on the eastern (landward) flank. A similar explanation applies to the Brown Ridge and the Breeveertien Banks, as the residual tidal currents are in the (north-eastern) flood direction and become stronger further to the north (Sündermann & Pohlmann, 2011; Damen et al., 2018). Comparable observations for the Breeveertien Banks were done by Van Dijk et al. (2011), who reported the western flanks as more dynamic than the eastern flanks. However, they did not observe any difference between both flanks at the Brown Ridge. Moreover, Van Dijk et al. (2011) measured migration rates between

0.4-0.8 m/year, whereas the seaward flank shows much higher migration rates in the current research. A possible explanation for this difference is the fact that Van Dijk et al. (2011) only analysed eight sand waves in total, which were divided over two horizontal transects. Using only two transects on a sandbank of several tens of kilometres in length does not provide a comprehensive insight in the sand wave dynamics. Moreover, the transects were placed perpendicular to the crest of the Brown Ridge. This way, migration is only measured along these transects in eastern and western direction, whereas sand wave migration occurs to the north-east and south-west, oblique to the crest of the Brown Ridge. Hence, this leads to a significant underestimation of the actual migration rates.

Finally, Van Dijk et al. (2011) report the sand wave fields at the Wadden Islands are reported as highly dynamic, with average migration rates of 16-19 m/year for Texel and 12 m/year for Vlieland. The obtained results in section 8.4 of the current research confirm the qualitative difference between the Wadden Islands and the rest of the NCS, but the estimated quantities are lower. Average migration rates typically range between 2-8 m/year and the highest values of 10-21 m/year are only observed close to the shoreline. This difference might be partly explained by the fact that no datasets older than the year 2000 are used in the current analysis. Van Dijk et al. (2011) report that migration rates at Vlieland between 1990-2003 are three times higher than those between 2003-2009, possibly caused by different methods of horizontal positioning.

The second part of this research is scientifically relevant due to the unprecedented spatial coverage of the obtained results. Besides the practical applicability of the insights (see Chapter 11), the results can be valuable for the verification and validation of future process-based models, for correlation to physical parameters to assess the contribution of the processes that drive sand wave migration and for the correlation to morphological sand wave characteristics such that dynamics can possibly be predicted when timeseries are absent.

9.1.3. Physical explanation for observed dynamics

The dataset of average migration rates per square kilometre comprises 11,596 data points. The significant coverage of the NCS, which comes with the large-scale spatial differences that are revealed, allows for extensive correlation analyses to gain insight in the contribution of the physical parameters that drive and affect sand wave migration. To provide a starting point for future research, the migration rates per square kilometre are plotted against four physical parameters: water depth, the D50 grain size, tidal peak velocity difference and the 99th percentile of significant surface wave height. See Figure 82 to Figure 85. The environmental parameters are extracted from the public repository that was provided by Damen et al. (2018).

The plots indicate that the migration rate is proportional to the tidal peak velocity difference and the surface wave height and inversely proportional to the water depth and grain size. The relationship with the tidal peak velocity difference and water depth seems to be the strongest, which makes sense because sand wave migration is driven by residual currents and increases in shallow water, where the influence of wave stirring and longshore currents is stronger (Besio et al., 2003; Van Dijk & Kleinhans, 2005). The relation with grain size and wave height is less pronounced, but its character is in line with existing knowledge (Van Dijk & Kleinhans, 2005; Sterlini, 2009; Li et al., 2011; Campmans, 2018).

More extensive analyses should reveal the exact correlation between the sand wave migration rate and these (and more) physical parameters.

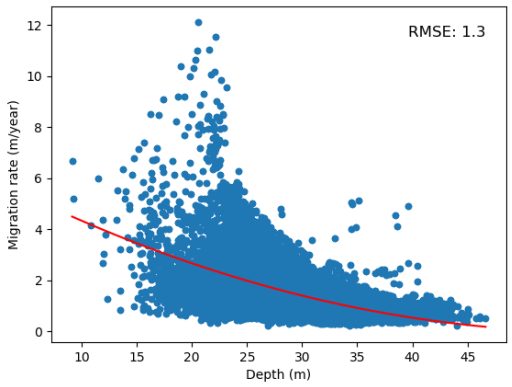

Figure 82 Migration rate per km² (m/year) plotted against depth per km² (m)

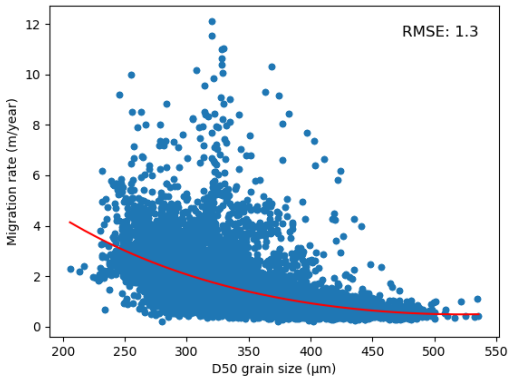

Figure 83 Migration rate per km² (m/year) plotted against D50 grain size per km² (µm)

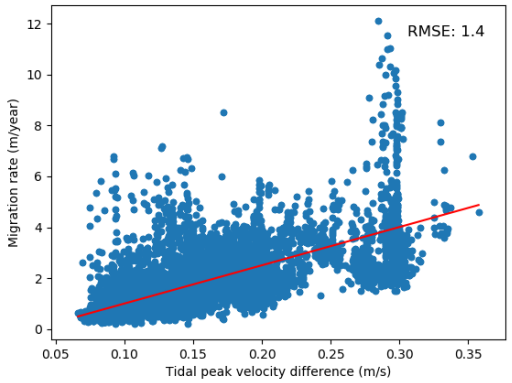

Figure 84 Migration rate per km² (m/year) plotted against tidal peak velocity difference per km² (m/s)

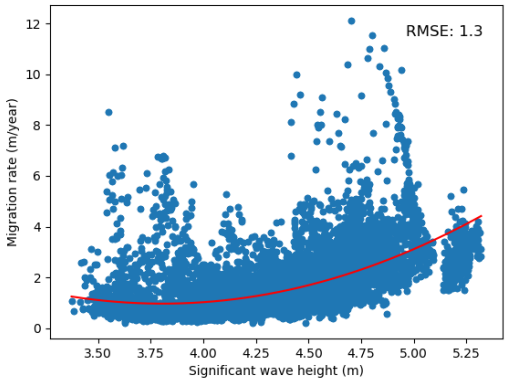

Figure 85 Migration rate per km² (m/year) plotted against significant wave height per km² (m)

9.2. Limitations of the research

9.2.1. Developing and testing the migration detection methods

The main factor hampering the accuracy of both PSTP and SCC is the relatively low resolution of the bathymetric data. For a large-scale analysis in which migration data is aggregated, the current resolution is sufficient as there is no need to filter out small-scale bed features and the computation times are manageable. However, in case a higher accuracy is desired, high-resolution bathymetric data is required.

In chapter 5, a limited number of scenarios is considered with a strongly simplified artificial sand wave field. These are mainly meant as a way of verifying if the detection methods perform as they should. However, limited insight is obtained in the accuracy of PSTP and SCC when *morphometry* is more complex and migration rates and directions are variable.

Besides accuracy and flexibility, a factor that can keep PSTP and SCC from being used as a management tool in the field, is the limited degree of automation. Both methods are semi-automated and still require manual input, pre- and post-processing of (bathymetric) data.

9.2.2. Quantification of sand wave migration at the NCS

Due to the limited time that is available for the research, not all estimated migration rates and directions are based on multiple timeseries. It is attempted to create at least two or three timeseries (hence, two or three unique survey combinations) for each square kilometre of seafloor by using the surveys that are collected after the year 2000. Older data is used for locations where no timeseries could be created from the more recent data. However, no additional timeseries are prepared for regions where at least one timeseries is available comprising the most recent data.

By using only one timeseries, which sometimes comprise surveys that are collected with only a few years in between, limited insight is obtained in the net, long-term migration rates. This might also explain the presence of contrasting spots in the non-linearly coloured migration map, which are visible in the coastal region between IJmuiden and Hoek van Holland for instance. Uncertainty, indicated by a higher coefficient of variation in Figure 79, for these locations is increased by the fact that only limited time is available for data cleaning. Besides line *vectors* that do not correspond to a crest or trough line, outliers in the plotted target points are removed as good as possible, but noisy points are still present in the data that is used for aggregation.

For simplicity reasons, the arithmetic mean is used as a typical value for migration rate and migration direction per square kilometre. In doing so, all data points are equally weighted and the distance of each point to the centre of the raster cell is not considered. The use of Kriging as a spatial interpolation technique might have led to different, more accurate, results. Also, the minimum requirement of 10 data points per square kilometre is somewhat arbitrary. For a few locations where this requirement is just satisfied, estimated migration rates are still a bit uncertain. Increasing this limit or requiring a minimum sand wave coverage of 80 percent like Damen et al. (2018), improves the robustness of results.

9.2.3. Validity of the obtained results

It is important to note that limitations described in sections 9.2.1 and 9.2.2 do not have significant impact on the outcome of the research. After all, SCC is mainly unfavourable because of limitations of the method itself and the large-scale migration patterns do not change when more data is included, or a different method of aggregation is applied. Hence, the validity of the research is confirmed.

10. Conclusions

The aim of the research is defined as follows:

To gain insight in the spatial variability of tidal sand wave migration rate and direction on the Netherlands Continental Shelf, by developing a 2DH measurement methodology for analysing timeseries of bathymetric data.

The aim is translated into two research questions, which are answered below.

Q1: Which methods can be used, and which method is favourable to quantify sand wave migration based on timeseries of bathymetric data on a large spatial scale?

After a preliminary selection procedure, two migration detection methods were implemented in QGIS: Pairs of Source and Target Points (PSTP) and Spatial Cross Correlation (SCC). PSTP quantifies migration rate and direction by measuring the displacement of vectorised crest and trough lines, which are extracted from consecutive bathymetric datasets in time. SCC locates the two most correlated points in different bathymetric datasets and quantifies migration rate and direction by measuring the distance and angle between these points.

To validate the output of PSTP and SCC, artificial bathymetric datasets were prepared for which migration distance and direction was pre-defined. When the migration distance is between the raster resolution (25 m) and half the wavelength, migration is measured in the correct direction and with sufficient accuracy. It was found that, when analysing field data, the accuracy of both methods is limited for migration distances that are small relative to the raster resolution. To account for this, the time in between two surveys was taken sufficiently long. The performance of PSTP and SCC was tested at four field sites, for which migration rates and directions were quantified. The output of both methods was qualitatively comparable for all locations. Quantitative differences mainly occur because the measurements of PSTP are restricted to integer grid cell positions whereas SCC can provide measurements in between these grid cell positions. Furthermore, using a single set of input parameters for SCC is not optimal at locations where the sand wave morphodynamics strongly vary.

It is concluded that PSTP is more suitable for a large-scale analysis of sand wave migration at the NCS. Its preferability is mainly based on the fact that, compared to SCC, the optimal input parameters are quickly found and need less changing in between different analyses. In addition, sources of errors and anomalies can be readily identified.

Q2: What is the spatial variability of sand wave migration rate and direction on the Netherlands Continental Shelf?

Using PSTP, over 300 timeseries were analysed. To gain insight in the spatial variability of migration rate and direction, the resulting 1,900,000 data points were aggregated to an average value per square kilometre.

Regarding migration direction, three distinct types of patterns are revealed. First, virtually all sand waves north of Rotterdam migrate towards the north or the north-east. Strong deflection to the east is seen on the seaward flanks of the Brown Ridge and the Breeveertien banks, which are located offshore of Noord-Holland. Furthermore, bilateral reverse migration to the north-east or south-west occurs on the flanks of the Zeeland Banks and the Brown Ridge. Finally, the sand waves at North Hinder in the south-western corner of the NCS migrate to the north-east and south-west.

Average migration rates at the main sand wave field typically range between 0-3 m/year, although migration rates of up to 12 m/year are observed at the Zeeland Banks. The fields at the Wadden Island are more dynamic, with average migration rates typically ranging between 2-8 m/year. The highest migration rates of 10-21 m/year occur near the coast of Texel and Vlieland. Three spatial patterns are revealed. First, migration rates increase non-linearly from North Hinder in the south-western corner of the NCS in north-eastern direction towards the Wadden Islands. Furthermore, migration rates are highest near the coast and decrease in the offshore direction. Finally, migration rates are higher on top of a shoreface connected ridge or a sandbank. For the Brown Ridge and the Breeveertien Banks, the migration rates on the seaward flank are higher than on the landward flank.

Finally, it is concluded that GIS are highly applicable for analysing the spatial variability of bedform or landform migration worldwide. Present-day GIS packages come with a vast amount of ready-to-use data manipulation and visualisation tools, which gives them an edge over programming packages such as Python or MATLAB. Even more so because GIS packages such as QGIS and ArcGIS have an integrated Python environment in which procedures can be automated. With PSTP and SCC, two methods have been developed that can be used for future analyses on bedform or landform migration at different spatial scales. The results from the NCS-wide analysis, which was conducted using PSTP, provide insight in the spatial variability of sand wave migration rate and direction at an unprecedented coverage.

11. Recommendations

11.1. Suggestions for future work

11.1.1. Improving PSTP and SCC

Research directions that are aimed at further improving PSTP and SCC are summarized below.

High-resolution DEMs. The accuracy of the obtained measurements in this research are hampered by the resolution of the DEMs, which is relatively low at 25 m. However, when using high-resolution DEMs, they might prove valuable for engineering applications where high accuracy is desired. Further tests with high-resolution DEMs should give insight in how these methods perform in term of accuracy and computation time. Higher resolution data can either be obtained by regridding the 25 m resolution DEMs using interpolation techniques or by creating entirely new DEMs from the raw SBES and MBES data in the BAS-database (see section 2.2.3. and 3.3).

Artificial sand wave fields. In Chapter 5, a limited number of test scenarios on a strongly simplified bathymetry are considered. Additional scenarios in which a variety of migration rates in different directions are applied to a more complex, three-dimensional sand wave pattern can be set up to gain more insight in the accuracy and limitations of PSTP and SCC.

Variable window size and vector type for SCC. The general applicability of SCC is currently limited by the fact that a single optimal window size and vector cannot be found when *morphometry* and dynamics vary strongly. Allowing these input parameters to be variable during the analysis might significantly improve the applicability of SCC for large-scale analyses. An extensive pre-analysis on (heterogeneity of) the present *morphometry* might help in applying the optimal window size for different sections of the seafloor.

Automation of PSTP. For PSTP, the steps that can still be automated are the filtering of crest and trough cells from the maximum curvature and convergence index *raster*, the plotting of a certain number of data points on the vectorised crest and trough lines, entering a *buffer* distance and a maximum migration distance. The values that are entered in the former two are relatively constant over large areas of seafloor and need to be determined only once. The *buffer* distance and maximum distance depend on the expected dynamics in the time between the two surveys. Some knowledge of migration rates in the past is therefore sufficient to automate these steps.

Automation of SCC. For SCC, the steps that can still be automated are the selection of a window size, search zone and a threshold value. Machine learning might be helpful, since automation can for example be achieved by initiating a certain combination of input parameters and allowing the algorithm to try and evaluate different (random) combinations. Performance criteria to evaluate the outcome might be the standard deviation of obtained migration rates or migration directions.

11.1.2. Tidal sand wave migration

Research directions on tidal sand wave migration are summarized below.

Timeseries analyses for the NCS. When timeseries become available for areas where these were absent before, the gaps in the migration maps can be filled in. In addition, the contrasting spot that are still visible in the migration maps can be smoothed out when better timeseries become available.

Aggregation of migration data. Aggregating the raw migration data to a higher resolution than 1 km^2, using more complex spatial interpolation techniques such as Kriging, results in more detailed migration maps in which migration aggregation artefacts (see Appendix VI) reduced.

Correlation to environmental parameters. Extensive analyses on the correlation between the migration rates per square kilometre and a variety of environmental parameters can give insight in the contribution of the mechanisms governing sand wave migration. The four parameters that are briefly considered in section 9.1.3 provide a starting point for future analyses. The conducted analysis indicated that water depth and tidal peak velocity difference have a strong relationship with the sand wave migration rate. Since the tidal peak velocity difference can be seen as a proxy for the residual current strength, the parameters that should at least be included in future analyses are tide-driven, pressure-driven, or wind-driven residual currents and sediment transport.

Correlation to morphological parameters. When a strong correlation between migration rate and morphological characteristics such as sand wave length, height, asymmetry and steepness is found, it might be possible to predict the migration rate based on only one survey, which is practical when timeseries are absent. This was already attempted by Knaapen (2005), who calibrated an empirical migration predictor with data from a dozen survey sites. The vast amount of data that is obtained in the current research means that future migration predictors can be much better calibrated.

Tidal circulation and sand wave migration around sandbanks. Both clockwise and anti-clockwise sand wave migration are observed on the flanks of the Zeeland Banks, whereas theory states that clockwise migration should occur due to the influence of the Coriolis effect. Process based modelling of (residual) tidal flows at the full bathymetry of the Zeeland banks should provide an explanation for the contradicting observations here.

11.2. Practical implications

The obtained insights regarding the magnitude and direction of sand wave migration at the NCS are highly relevant for a variety of offshore activities, such as the optimisation of hydrographic re-survey strategies and the planning, design, and execution of offshore infrastructure projects.

The hydrographic re-survey strategy of the NLHO is given in Figure 86. Controlling parameters in the division of the categories are the water depth and the importance for shipping (Van Dijk et al., 2011). The areas of seafloor that are most frequently surveyed are the main shipping routes, *separation zones* and the approach channels to IJmuiden and Rotterdam. These high-priority areas are added to the migration map in Figure 87.

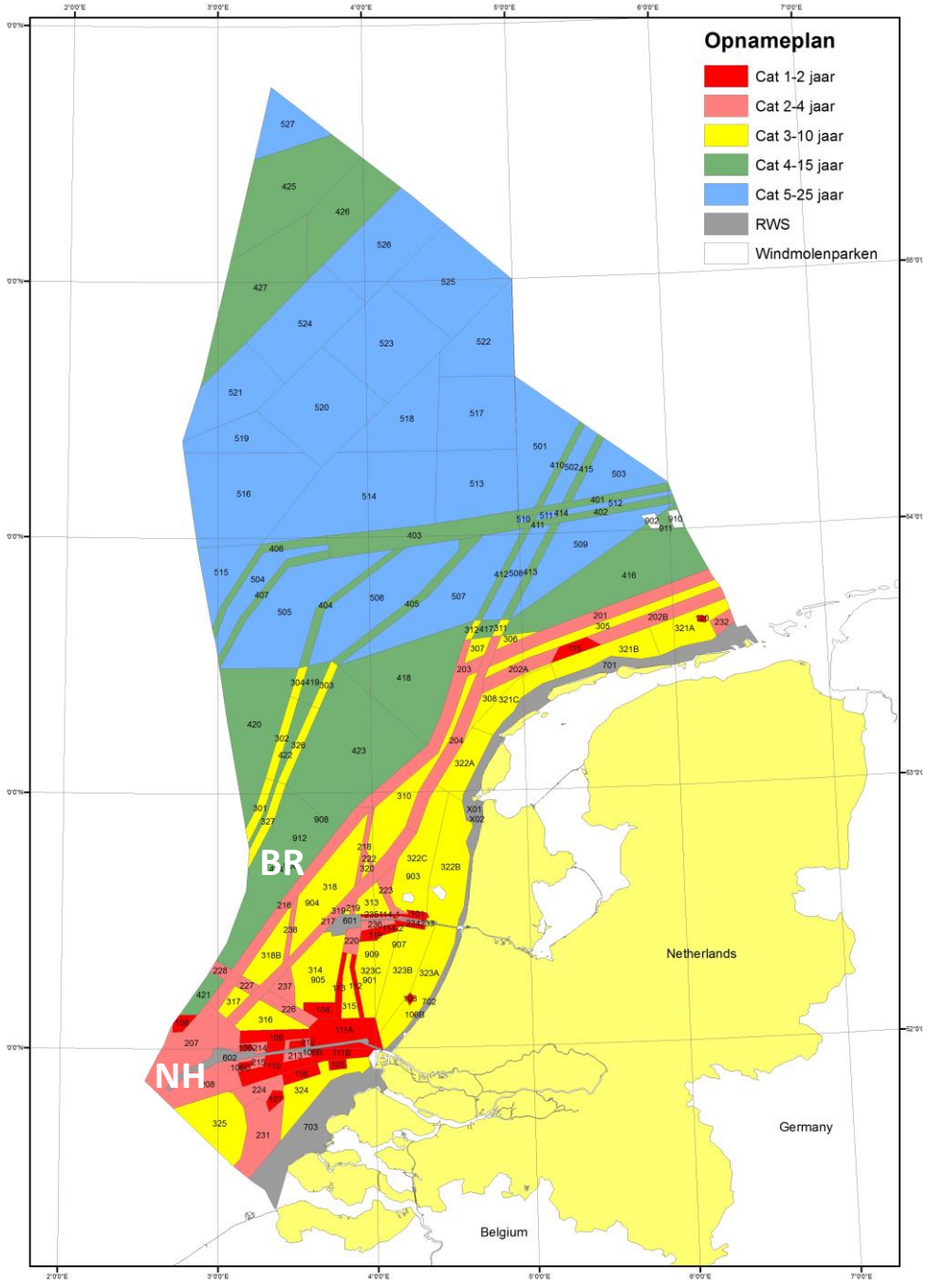

Figure 86 Re-survey strategy of the Netherlands Hydrographic Office. North Hinder and the Brown Ridge are abbreviated with NH and BR, respectively (Netherlands Hydrographic Office, 2021b).

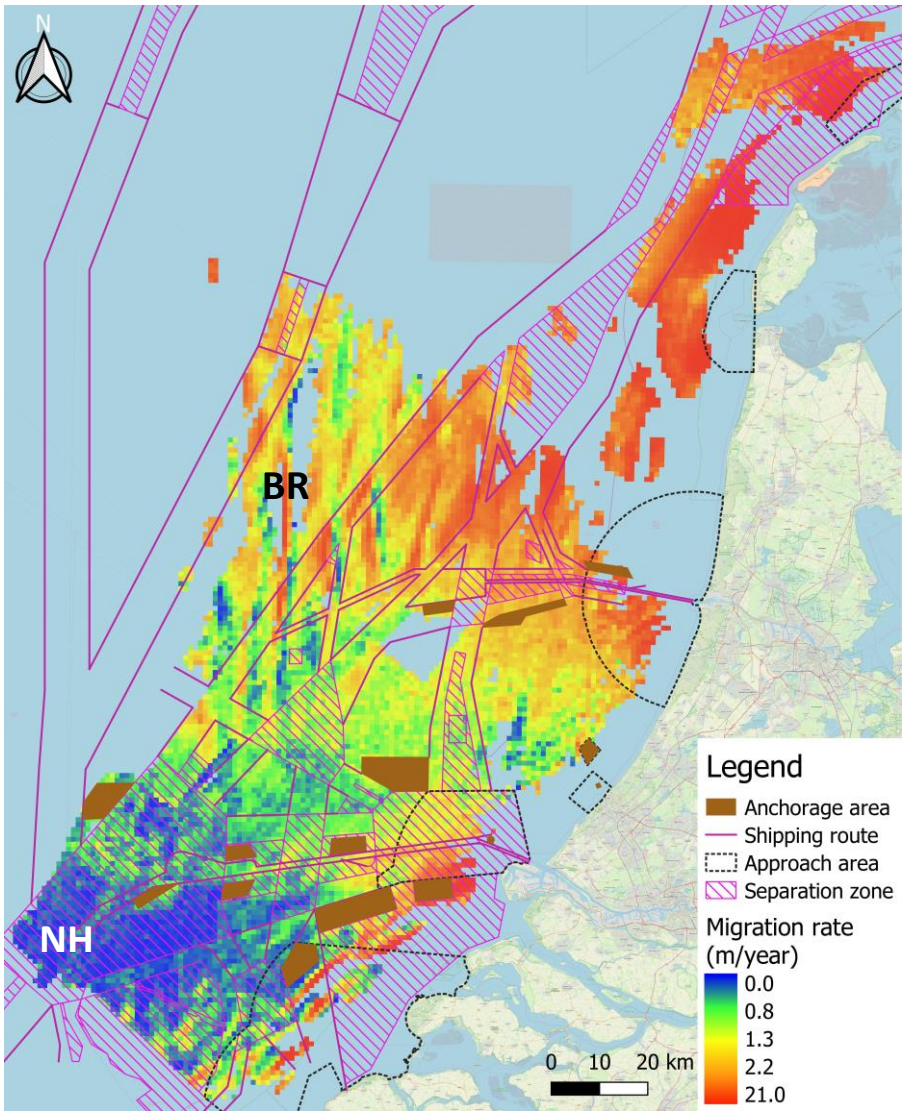

Figure 87 Average sand wave migration rate per km² and shipping routes on the NCS. North Hinder and the Brown Ridge are abbreviated with NH and BR, respectively (Rijkswaterstaat, 2021).

When regarding sand wave dynamics, and hence the degree of change of the seafloor, as an equally important factor (next to water depth and importance for shipping) controlling the division of the categories in Figure 86, two changes to the re-survey policy are suggested.

- **North Hinder**. The North Hinder region (abbreviated with NH in Figure 86 and Figure 87) is of importance for shipping as it is marked as a *separation zone*. Since the measured water depth below *LAT* is larger than the *critical water depth*, the survey frequency is every 2-4 years (Van Dijk et al., 2011). However, the seafloor barely changes due to the low magnitude of sand wave migration. Combined with the large water depth, decreasing the survey frequency to once every 3-10 years can be considered.
- **Brown Ridge**. Due to its large water depth and unimportance for shipping, the region around the Brown Ridge (abbreviated with BR in Figure 86 and Figure 87) is surveyed every 4-15 years. However, the degree of change due to sand wave migration is rather significant with migration rates typically ranging between 1-2 m/year, except for some of the seaward facing flanks, where migration rates can be as high as 5-6 m/year. It can be considered to increase the survey frequency to once every 3-10 years, mainly because the region is marked as a study area for future wind farms (see Figure 90).

The sand waves at the Wadden Islands are highly dynamic with migration rates typically ranging between 2-8 m/year. Based on this, one might argue that the survey frequency for the shipping lanes should be increased from 2-4 years to 1-2 years. However, as is indicated by Figure 88, the sand waves have relatively low heights and long wavelengths, which causes the seafloor not to change significantly in a period of 2-4 years. Even more so because most sand waves do not migrate perpendicular to the shipping route. It is therefore not necessary to increase the survey frequency here.

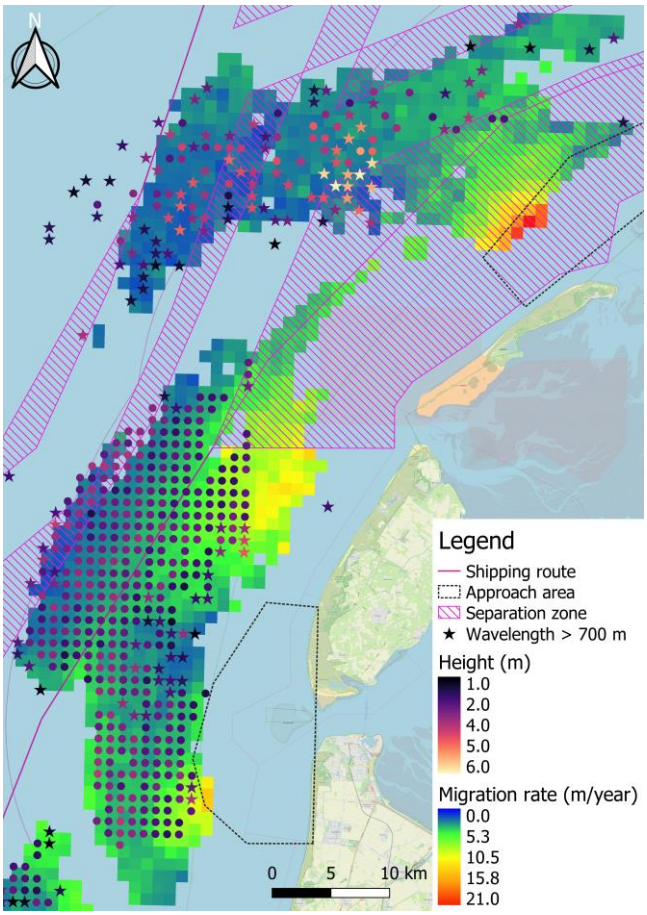

Figure 88 Average sand wave migration rate and height per km² at the Wadden Islands, including shipping routes (Rijkswaterstaat, 2021).

Figure 89, which comprises the average migration rate along with the present pipeline and cable trajectories, indicates that the risk of free spanning is largest for the pipelines on the northern half of the NCS, where the sand wave migration rates are highest. Migration rates of several metres per year can expose a significant section of pipeline or cable over the course of its lifetime, which averages 20-40 years (Chis, 2015). Especially when the route is perpendicular to the crest orientation of the sand waves, it is important to avoid large sand waves or bury the pipeline where sand waves cannot be avoided. Note that the resolution of the migration rates per km² in Figure 89 is too course for future pipeline or cable trajectories to be based on. Surveying the intended trajectory several times before construction is still required. Operators could use the migration map rather as a tool to assess the survey frequency during the life cycle of operational pipelines and cables.

Figure 90, comprising the migration rate and the locations of wind farms and offshore installations, indicates that vertical structures are mostly located in relatively dynamic regions of the NCS. With typical sand wave heights of several metres, the foundations of these structures can become significantly exposed over time. For future wind farms in the designated areas, it is important to properly design the foundation to prevent serious exposure from sand wave migration.

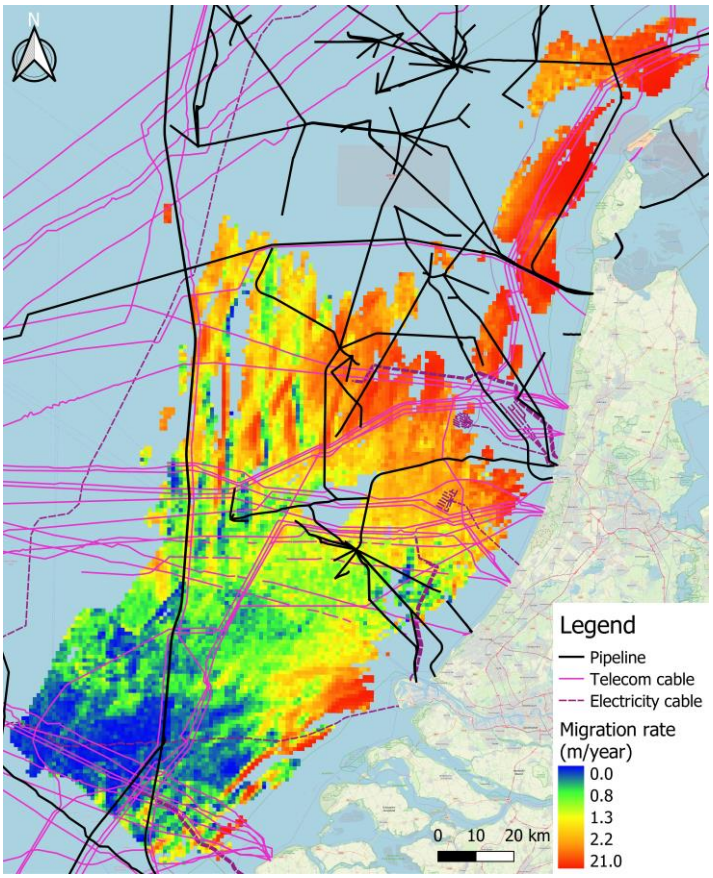

Figure 89 Average sand wave migration rate per km², pipelines and cables

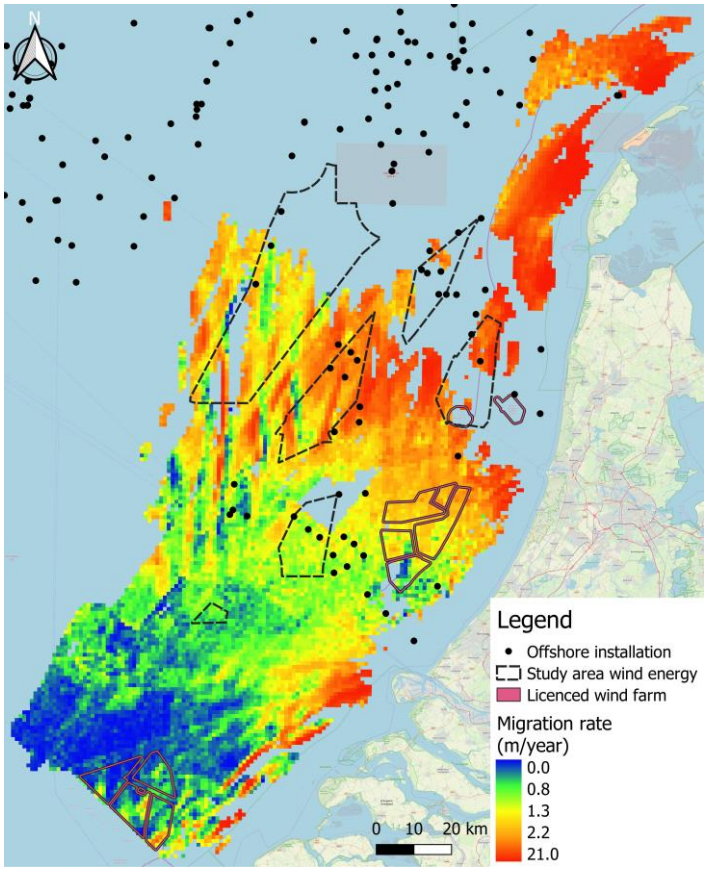

Figure 90 Average sand wave migration rate per km², present and future windfarms and offshore installations

References

Aliotta, S., & Perillo, G. (1987). A sand wave field in the entrance to Bahía Blanca Estuary, Argentina. *Marine Geology, 76*, 1-14. doi:https://doi.org/10.1016/0025-3227(87)90013-2

Ashly, G. (1990). Classification of large-scale subaqueous bedforms: a new look at an old problem. SEPM Bedforms and Bedding Structure Research Symposium. *Journal of Sedimentary Research, 60*, 160-172. doi:10.2110/jsr.60.160

Besio, G., Blondeaux, P., Brocchini, M., & Vittori, G. (2003). Migrating sand waves. *Ocean Dynamics, 53*, 232-238. doi:DOI 10.1007/s10236-003-0043-x

Besio, G., Blondeaux, P., Brocchini, M., & Vittori, G. (2004). On the modelling of sand wave migration. *Journal of Geophysical Research, 109, C04018*. doi:10.1029/2002JC001622

Bolle, A., Mathys, M., & Haerens, P. (2013). How the Belgian wind farm business made us discover the challenging environment of marine sand dunes. *Fourth International Conference on Marine and River Dune Dynamics* (pp. 45-52). Bruges: Royal Belgian Institute of Natural Sciences and SHOM.

Borsje, B., Kranenburg, W., Roos, P., Matthieu, J., & Hulscher, S. (2014). The role of suspended load transport in the occurrence of tidal sand waves. *Journal of Geophysical Research: Earth Surface, 119*, 701-716. doi:10.1002/2013JF002828

Borsje, B., Roos, P., Kranenburg, W., & Hulscher, S. (2013). Modeling tidal sand wave formation in a numerical shallow water model: The role of turbulence formulation. *Continental Shelf Research, 60*, 17-27. doi:https://doi.org/10.1016/j.csr.2013.04.023

Buijsman, M., & Ridderinkhof, H. (2008). Long-term evolution of sand waves in the Marsdiep inlet. I: High-resolution observations. *Continental Shelf Research, 28*(9), 1190-1201. doi:https://doi.org/10.1016/j.csr.2007.10.011

Campmans, G. (2018). *Modeling storm effects on sand wave dynamics.* Enschede: University of Twente. doi:10.3990/1.9789036546003

Campmans, G., Roos, P., Schrijen, E., & Hulscher, S. (2018). Modeling wave and wind climate effects on tidal sand wave dynamics: A North Sea case study. *Estuarine, Coastal and Shelf Science, 213*, 137-147. doi:https://doi.org/10.1016/j.ecss.2018.08.015

Campmans, G., Roos, P., Vriend, H. D., & Hulscher, S. (2018). The Influence of Storms on Sand Wave Evolution: A Nonlinear Idealized Modeling Approach. *Journal of Geophysical Research: Earth Surface*, 2070-2086.

Cheng, C. H., Soetaert, K., & Borsje, B. (2020). Sediment Characteristics over Asymmetrical Tidal Sand Waves in the Dutch North Sea. *Journal of Marine Science and Engineering, 8*(6). doi:https://doi.org/10.3390/jmse8060409

Chis, T. (2015). THE LIFE CYCLE AS AN OFFSHORE PIPELINE. *AFASES 2015.* Brasov.

Damen, J., van Dijk, T., & Hulscher, S. (2018). Spatially Varying Environmental Properties Controlling Observed Sand Wave Morphology. *Journal of Geophysical Research: Earth Surface, 123*, 262-280. doi:10.1002/2017JF004322

Damveld, J. (2020). *The feedbacks among tidal sand waves, benthic organisms and sediment sorting processes.* Enschede: University of Twente. doi:10.3990/1.9789036550000

Damveld, J., Borsje, B., Roos, P., & Hulscher, S. (2020). Horizontal and Vertical Sediment Sorting in Tidal Sand Waves: Modelling the Finite-Amplitude Stage. *Journal of Geophysical Research: Earth Surface, 125*(10). doi:https://doi-org.ezproxy2.utwente.nl/10.1029/2019JF005430

Deltares. (2015). *Morphodynamics of Borssele Wind Farm Zone WFS-I and WFS-II.* Delft: Deltares.

Deltares. (2017a). *Scour and Scour Mitigation for Hollandse Kust (zuid).* Utrecht: Netherlands Enterprice Agency.

Deltares. (2017b). *Dataset documentation bathymetry NLHO*. Retrieved from publikwiki.deltares.nl: https://publicwiki.deltares.nl/display/OET/Dataset+documentation+bathymetry+NLHO

Dong, P. (2015). Automated measurement of sand dune migration using multi-temporal lidar data and GIS. *International Journal of Remote Sensing, 36*(21), 5426–5447. doi:http://dx.doi.org/10.1080/01431161.2015.1093192

Dorst, L. (2009). *Estimating sea floor dynamics in the southern North Sea to improve bathymetric survey planning.* Delft: Netherlands Geodetic Commission.

Dorst, L., Hulscher, S., Roos, P., & Lindenbergh, R. (2009). The estimation of sea floor dynamics from bathymetric surveys of a sand wave area. *Journal of Applied Geodesy, 3*, 97-120. doi:10.1515/JAG.2009.011

Dorst, L., Roos, P., & Hulscher, S. (2006). Estimation of sand wave dynamics in the Southern North Sea. *Proceedings of 30th Conference on Coastal Engineering* (pp. -). San Diego: ICCE.

Dorst, L., Roos, P., & Hulscher, S. (2011). Spatial differences in sand wave dynamics between the Amsterdam and the Rotterdam region in the Southern North Sea. *Continental Shelf Research*, 1096-1105.

Duffy, G., & Hughes-Clarke, J. (2005). Application of spatial cross correlation to detection of migration of submarine sand dunes. *Journal of Geophysical Research: Earth Surface, 110*(F4). doi: https://doi-org.ezproxy2.utwente.nl/10.1029/2004JF000192

EMODnet. (2021). *Exclusive Economic Zone.* Retrieved from emodnet-humanactivities.eu: https://www.emodnet-humanactivities.eu/search-results.php?dataname=Exclusive+Economic+Zone

Environmental Systems Research Institute, Inc. (2016). *How Curvature works*. Retrieved from desktop.arcgis.com: https://desktop.arcgis.com/en/arcmap/10.3/tools/spatial-analyst-toolbox/how-curvature-works.htm

Games, K., & Gordon, D. (2015). Study of sand wave migration over five years as observed in two windfarm development areas, and the implications for building on moving substrates in the North Sea. *Earth and Environmental Science Transactions of the Royal Society of Edinburgh*, 241-249. doi:https://doi.org/10.1017/S1755691015000110

Garlan, T. (2009, January). *GIS and mapping of moving marine sand dunes.* Retrieved from https://www.researchgate.net/publication/228691507

Ghadiry, M., & Koch, B. (2010). Developing a Monitoring System for Sand Dunes Migration in Dakhla Oasis, Western Desert, Egypt. *30th EARSeL Symposium: Remote Sensing for Science, Education and Culture.* Paris: European Association of Remote Sensing Laboratories.

Harris, P. (1989). Sandwave movement under tidal and wind-driven currents in a shallow marine environment: Adolphus Channel, northeastern Australia. *Continental Shelf Research, 9*(11), 981-1002. doi:https://doi.org/10.1016/0278-4343(89)90003-4

Hell, B., Broman, B., Jakobssen, L., Jakobssen, M., Magnussen, Â., & Wiberg, P. (2012). The Use of Bathymetric Data in Society and Science: A Review from the Baltic Sea. *Ambio, 41*(2), 138-150. doi:https://doi.org/10.1007/s13280-011-0192-y

Hounjet, M., Bijlsma, A., Verlaan, M., & Dorst, L. (2012). Accurate water levels using PREMO: Tool for reduction of hydrographic measurements. *Hydro12- Taking care of the sea.* Deinze: Hydrographic Society Benelux. doi:10.3990/2.243

Huang, X., Chen, Z., Zhao, W., Zhang, Z., Zhou, C., Yang, Q., & Tian, J. (2016). An extreme internal solitary wave event observed in the northern South China Sea. *Scientific Reports, 6, 30041*. doi:10.1038/srep30041

Hulscher, S. (1996). Tidal-induced large-scale regular bed form patterns in a three-dimensional shallow water model. *Journal of geophysical research : Oceans*, 20727-20744.

Hulscher, S., & Dohmen-Janssen, C. (2005). Introduction to special section on Marine Sand Wave and River Dune Dynamics. *Journal of Geophysical Research, 110*(F04S01). doi:10.1029/2005JF000404

Hulscher, S., & Van den Brink, G. (2001). Comparison between predicted and observed sand waves and sand banks in the North Sea. *Journal of Geophysical Research, 106*(C5), 9327-9338. doi:https://doi-org.ezproxy2.utwente.nl/10.1029/2001JC900003

Huthnance, J. (1982). On One Mechanism Forming Linear Sand Banks. *Estuarine, Coastal and Shelf Science, 14*(1), 79-99. doi:https://doi.org/10.1016/S0302-3524(82)80068-6

J. Minár, I. E. (2020). A comprehensive system of definitions of land surface (topographic) curvatures, with implications for their application in geoscience modelling and prediction. *Earth-Science Reviews, 211, 103414*. doi:https://doi.org/10.1016/j.earscirev.2020.103414

Jisheng, X., & Dong, P. (2016). A GIS add-in for automated measurement of sand dune migration using LIDAR-derived multitemporal and high-resolution digital elevation models. *Geosphere, 12*(4), 1316-1322. doi:10.1130/GES01329.1

Katoh, K., Kume, H., Kuroki, K., & Hasegawa, J. (1998). The development of sand waves and the maintenance of navigation channels in the Bisanseto Sea. *Coastal Engineering, 26*(1). doi:https://doi.org/10.9753/icce.v26.%25p

Kiss, R. (2004). Determination of drainage network in digital elevation models, utilities and limitations. *Journal of Hungarian Geomathematics, 2*, 16-29. Retrieved from https://www-researchgate-net.ezproxy2.utwente.nl/publication/267714660_Determination_of_drainage_network_in_digital_elevation_models_utilities_and_limitations

Knaapen, M. (2004). Measuring sand wave migration in the field. Comparison of different data sources and an error analysis. *Marine sandwave and river dune dynamics II, 1-2 April 2004, Enschede, The Netherlands* (pp. 152-160). Enschede: University of Twente.

Knaapen, M. (2005). Sandwave migration predictor based on shape information. *Journal of Geophysical Research*(Vol. 110,F04S11). doi:10.1029/2004JF000195

Knaapen, M., Hulscher, S., & Vriend, H. D. (2001). A new type of sea bed waves. *Geophysical Research Letters, 28*(7), 1323-1326. doi:10.1029/2000GL012007

Knaapen, M., Van Bergen Henegouw, C., & Hu, Y. (2005). Quantifying bedform migration using multi-beam sonar. *Geo-Mar Lett, 25*, 306-314. doi:10.1007/s00367-005-0005-z

Leenders, S., Damveld, J., Schouten, J., Hoekstra, R., Roetert, T., & Borsje, B. (2020). Numerical modelling of the migration direction of tidal sand waves over sand banks. *Coastal Engineering, 163*. doi:https://doi.org/10.1016/j.coastaleng.2020.103790

Lewis, J. (1995). Fast Template Matching. *Vision Interface, 95*, 120-123. Retrieved from http://scribblethink.org/Work/nvisionInterface/vi95_lewis.pdf

Li, Y., Lin, M., Jiang, W., & Fan, F. (2011). Process control of the sand wave migration in Beibu Gulf of the South China Sea. *Journal of Hydrodynamics, ser. B, 23*(4), 439-446. doi:10.1016/S1001-6058(10)60134-5

Lin, M., Fan, F.-X., Li, Y., Yan, J., Jiang, W.-B., & Gong, D.-J. (2009). Observations and theoretical analysis for the sand-waves migration in the north gulf of the South China Sea. *Chinese Journal of Geophysics, 52*(2), 451-460.

Mayer, L. (2006). Frontiers in Seafloor Mapping and Visualization. *Marine Geophysical Research*(27), 7-17. doi:10.1007/s11001-005-0267-x

Ministry of Defence. (2021). *Netherlands boundaries in the North Sea*. Retrieved from english.defensie.nl: https://english.defensie.nl/topics/hydrography/maritime-limits-and-boundaries/netherlands-boundaries-in-the-north-sea

Ministry of Defence. (2021). Personal communication.

Morelissen, R., Hulscher, S., Knaapen, M., Németh, A., & Bijker, R. (2003). Mathematical modelling of sand wave migration and the interaction with pipelines. *Coastal Engineering, 48*, 197-209. doi:10.1016/S0378-3839(03)00028-0

National Ocean Service. (2020, April 12). *How is bathymetric data used? Accurate bathymetry is essential for navigation and ocean science.* Retrieved from https://oceanservice.noaa.gov/facts/bathyuses.html

Neary, V., & Gunawan, B. (2011). *Field Measurements at River and Tidal Current Sites for Hydrokinetic Energy Development: Best Practices Manual.* Oak Ridge National Laboratory. doi:10.2172/1034380

Németh, A., & Hulscher, S. (2003). Offshore sand wave dynamics, engineering problems and future solutions. *Pipeline and Gas Journal*, 67-69.

Németh, A., Hulscher, S., & Vriend, H. D. (2002). Modelling sand wave migration in shallow shelf seas. *Continental Shelf Research, 22*(18-19), 2795-2806. doi:https://doi.org/10.1016/S0278-4343(02)00127-9

Netherlands Hydrographic Office. (2021b). Opnameplan NCP.

Passchier, S., & Kleinhans, M. (2005). Observations of sand waves, megaripples, and hummocks in the Dutch coastal area and their relation to currents and combined flow conditions. *Journal of Geophysical Research: Earth Surface, 110*. doi:10.1029/2004JF000215

Perillo, M., Garcia, M., & Best, J. (2014). A New Phase Diagram for Combined-Flow Bedforms. *Journal of Sedimentary Research, 84*, 301-313. doi:10.2110/jsr.2014.25

REASeuro. (2019). *UXO Desk Study - Unexploded Ordnance Site Data Ten noorden van de Waddeneilanden (TNWWFZ).* Netherlands Enterprise Agency.

Righolt, R., Schaap, J., Dorst, L., & Vos, E. (2010). Needle in a haystack. In V. Oosterom, M. Vosselman, T. Van Dijk, & M. Uitentuis, *Management of massive point cloud data; wet and dry* (pp. 1-8). Delft: Netherlands Geodetic Commission.

Rijkswaterstaat. (2021). *Scheepvaart verkeersscheidingsstelsel Noordzee (Nederlands Continentaal Plat).* Retrieved from nationaalgeoregister.nl: https://nationaalgeoregister.nl/geonetwork/srv/dut/catalog.search;jsessionid=5F827FF375328CCFC23886A6B23E2324#/metadata/5996e444-f7f3-40d2-b485-8b9af6e8aa89?tab=contact

Roos, P., & Hulscher, S. (2003). Large-scale seabed dynamics in offshore morphology: Modeling human intervention. *Reviews of Geophysics, 41*(2). doi:doi:10.1029/2002RG000120

Simons, D. (2009, November 26). Recent developments in multi-beam echo-sounder processing at the Delft University of Technology. Delft: Delft University of Technology. Retrieved from https://ncgeo.nl/downloads/PointCloud_04.pdf

Simons, D., Amiri-Simkooei, A., Siemes, K., & Snellen, M. (2010). Recent developments in multi-beam echo-sounder processing - The multi-beam potential for sediment classification and water column sound speed estimation. In P. Van Oosterum, M. Vosselman, T. Van Dijk, & M. Uitentuis, *Management of massive point cloud data: wet and dry* (pp. 33-44). Delft: Netherlands Geodetic Commission.

Sterlini, F. (2009). *Modelling sand wave variation.* Enschede: University of Twente.

Sterlini, F., Van Dijk, T., IJzer, S., & Hulscher, S. (2011). Seasonal changing sand waves and the effect of surface waves. *5th International Short Conference on Applied Coastal Research* (pp. 570-578). Aachen: Aachen University.

Sündermann, J., & Pohlmann, T. (2011). A brief analysis of North Sea physics. *Oceanologia, 53*(3), 663-689. doi:10.5697/oc.53-3.663

Thibaud, R., Mondo, G. D., Garlan, T., Mascet, A., & Carpentier, C. (2013). A Spatio-Temporal Graph Model for Marine Dune Dynamics Analysis and Representation. *Transactions in GIS, 17*(5), 742-762. doi:10.1111/tgis.12006

Thommeret, N., Bailly, J., & Puech, C. (2010). Extraction of thalweg networks from DTMs: application to badlands. *Hydrology and Earth System Sciences, 14*, 1527-1536. doi:10.5194/hess-14-1527-2010

Tonnon, P., Rijn, L. v., & Walstra, D. (2007). The morphodynamic modelling of tidal sand waves on the shoreface. *Coastal Engineering, 54*, 279-296.

Van der Veen, H. (2008). *Natural and human induced seabed evolution: the occurrence of large-scale bad patterns and the effects of human activities on the North Sea seabed.* Enschede: University of Twente.

Van der Veen, H., Hulscher, S., & Knaapen, M. (2006). Grain size dependency in the occurrence of sand waves. *Ocean Dynamics, 56*, 228-234. doi:10.1007/s10236-005-0049-7

Van Dijk, T., & Kleinhans, M. (2005). Processes controlling the dynamics of compound sand waves in the North Sea, Netherlands. *Journal of geophysical research*.

Van Dijk, T., Lindenbergh, R., & Egberts, P. (2008). Separating bathymetric data representing multiscale rhythmic bed forms: A geostatistical and spectral method compared. *Journal of Geophysical Research, 113*, F04017. doi:10.1029/2007JF000950

Van Dijk, T., van der Tak, C., de Boer, W., Kleuskens, M., Doornenbal, P., Noorlandt, R., & Marges, V. (2011). *The scientific validation of the hydrographic survey policy of the Netherlands Hydrographic Offic, Royal Netherlands Navy.* Delft: Deltares.

Van Gerwen, W., Borsje, B., Damveld, J., & Hulscher, S. (2018). Modelling the effect of suspended load transport and tidal asymmetry on the equilibrium tidal sand wave height. *Coastal Engineering, 136*, 56-64. doi:https://doi.org/10.1016/j.coastaleng.2018.01.006

Van Oyen, T., Blondeaux, P., & Van den Eynde, D. (2013). Sediment sorting along tidal sand waves: A comparison between field observations and theoretical predictions. *Continental Shelf Research*, 23-33.

Van Santen, R., De Swart, H., & Van Dijk, T. (2011). Sensitivity of tidal sand wavelength to environmental parameters: A combined data analysis and modelling approach. *Continental Shelf Research, 31*, 966-978. doi:https://doi.org/10.1016/j.csr.2011.03.003

Wang, Z., Jeuken, C., & De Vriend, H. (1999). *Tidal asymmetry and residual sediment transport in estuaries.* Delft: Deltares. Retrieved from http://resolver.tudelft.nl.ezproxy2.utwente.nl/uuid:08911ef5-5ee8-4a8b-9432-5a5a5dfaa142

Whitehouse, R., Damgaard, J., & Langhorne, D. (2000). Sandwaves and seabed engineering; the application to submarine cables. *Proceedings of the Marine Sandwave Dynamics* (pp. 227 - 234). Lille: University of Lille.

Xu, J., Wong, F., Kvitek, R., Smith, D., & Paull, C. (2008). Sandwave migration in Monterey Submarine Canyon, Central California. *Marine Geology, 248*, 193-212. doi:10.1016/j.margeo.2007.11.005

Zhang, F. K., Zhao, C., & Feng, C. (2016). Using robust correlation matching to estimate sand-wave migration in Monterey Submarine Canyon, California. *Marine Geology, 376*, 102-108. doi:http://dx.doi.org/10.1016/j.margeo.2016.04.002

Zhang, H., Ma, X., Zhuang, L., & Yan, J. (2019). Sand waves near the shelf break of the northern South China Sea: morphology and recent mobility. *Geo-Marine Letters, 39*, 19-36. Retrieved from https://doi.org/10.1007/s00367-018-0557-3

Zhou, J., Wu, Z., Jin, X., Zhao, D., Cao, Z., & Guan, W. (2018). Observations and analysis of giant sand wave fields on the Taiwan Banks, northern South China Sea. *Marine Geology, 406*, 132-141. Retrieved from https://doi.org/10.1016/j.margeo.2018.09.015

Zhou, J., Wu, Z., Zhao, D., Guan, W., Zhu, C., & Flemming, B. (2020). Giant sand waves on the Taiwan Banks, southern Taiwan Strait: Distribution, morphometric relationships, and hydrologic influence factors in a tide-dominated environment. *Marine Geology, 427*. doi:https://doi.org/10.1016/j.margeo.2020.106238

Zwolak, K. (2015). Underwater objects' detection system choice for harbor surveillance purposes. *Zeszyty Naukowe Akademii Marynarki Wojennej, 200*(1), 47-58. doi:10.5604/0860889X.1161261

Appendix I: DEM noise and effect of smoothing

The positive effect of smoothing a noisy DEM on the detection of crest and trough lines can be seen in Figure A1.1 to A1.6.

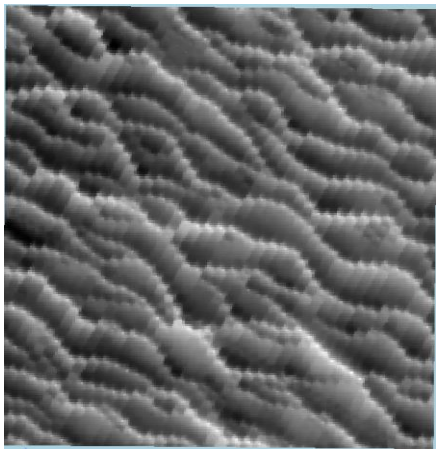

Figure A1.1 noisy DEM

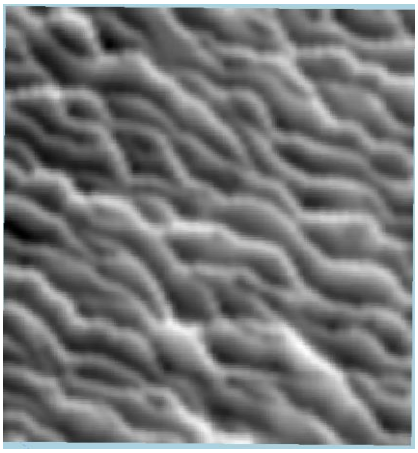

Figure A1.2 smoothed DEM

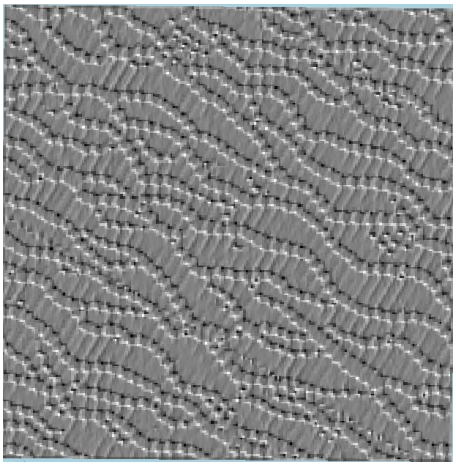

Figure A1.3 crest lines (white) and trough lines (black) determined with convergence index on noisy DEM

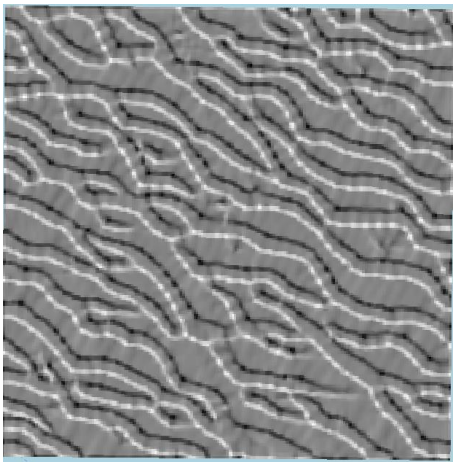

Figure A1.4 crest lines (white) and trough lines (black) determined with convergence index on smoothed DEM

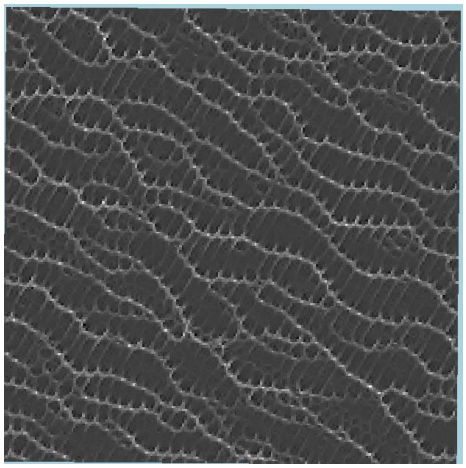

Figure A1.5 crest lines determined with maximum curvature on noisy DEM

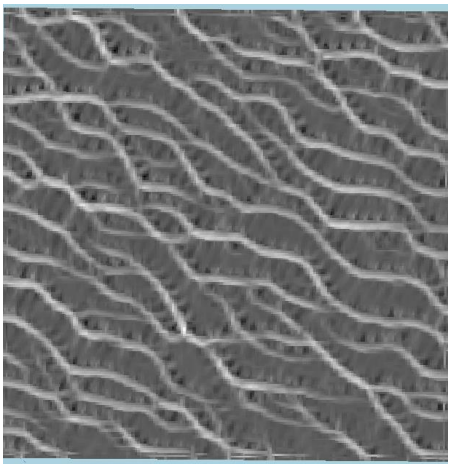

Figure A1.6 crest lines determined with maximum curvature on smoothed DEM

In Figure A1.7 to A1.10, it can be clearly seen that the crests of the smoothed DEM are lowered and shift towards the *stoss* side and the troughs are elevated and shift towards the *stoss* side of the next adjacent sand wave.

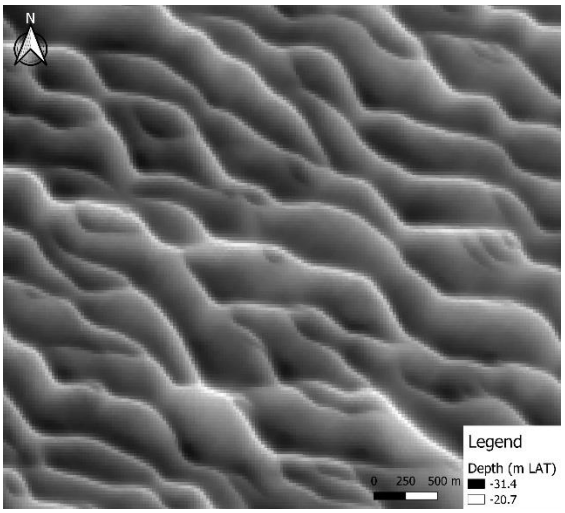

Figure A1.7 raw DEM

-

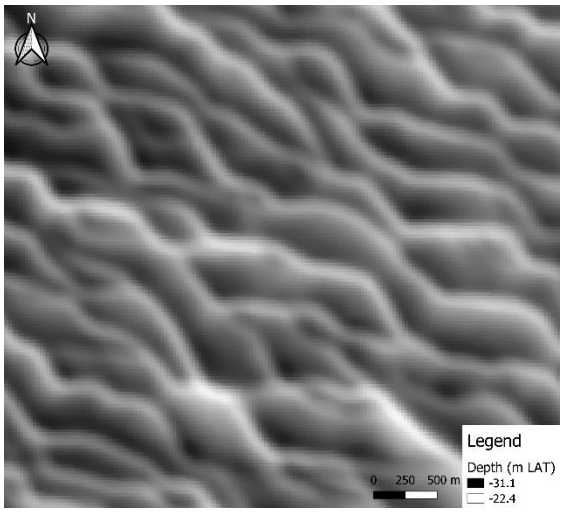

Figure A1.8 smoothed DEM

=

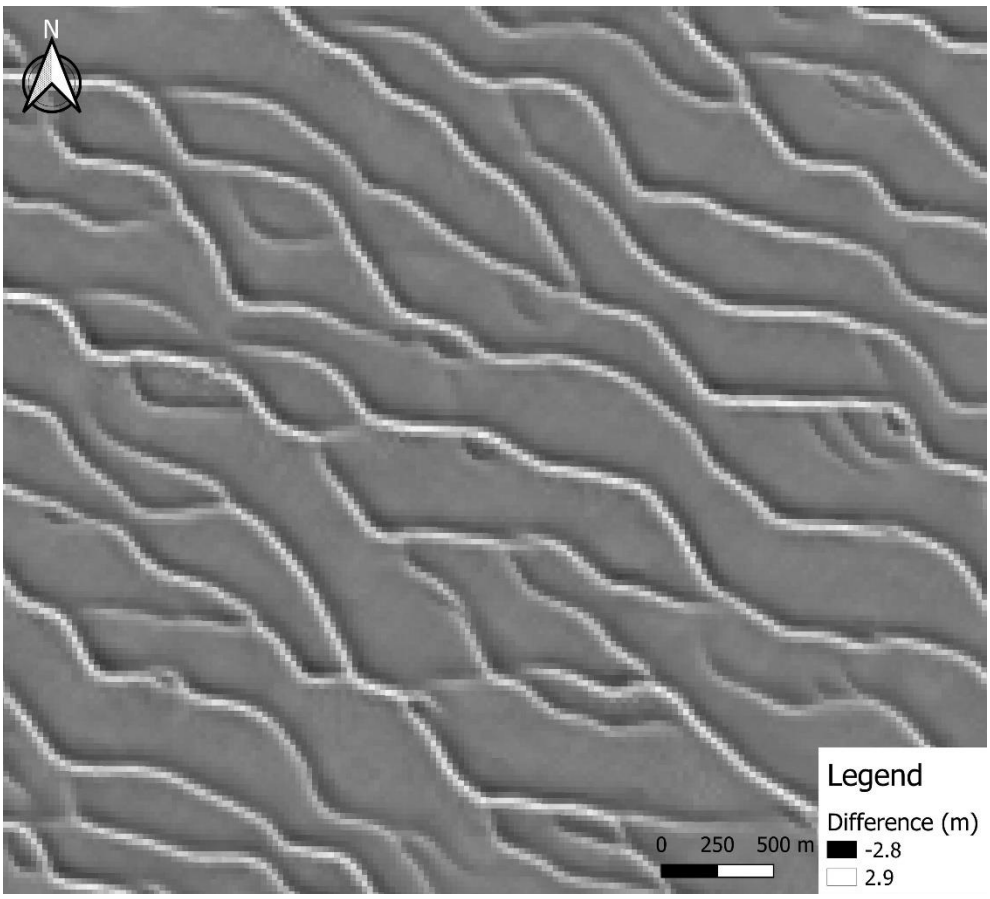

Figure 1.9 difference map after subtracting a smoothed DEM from a raw DEM

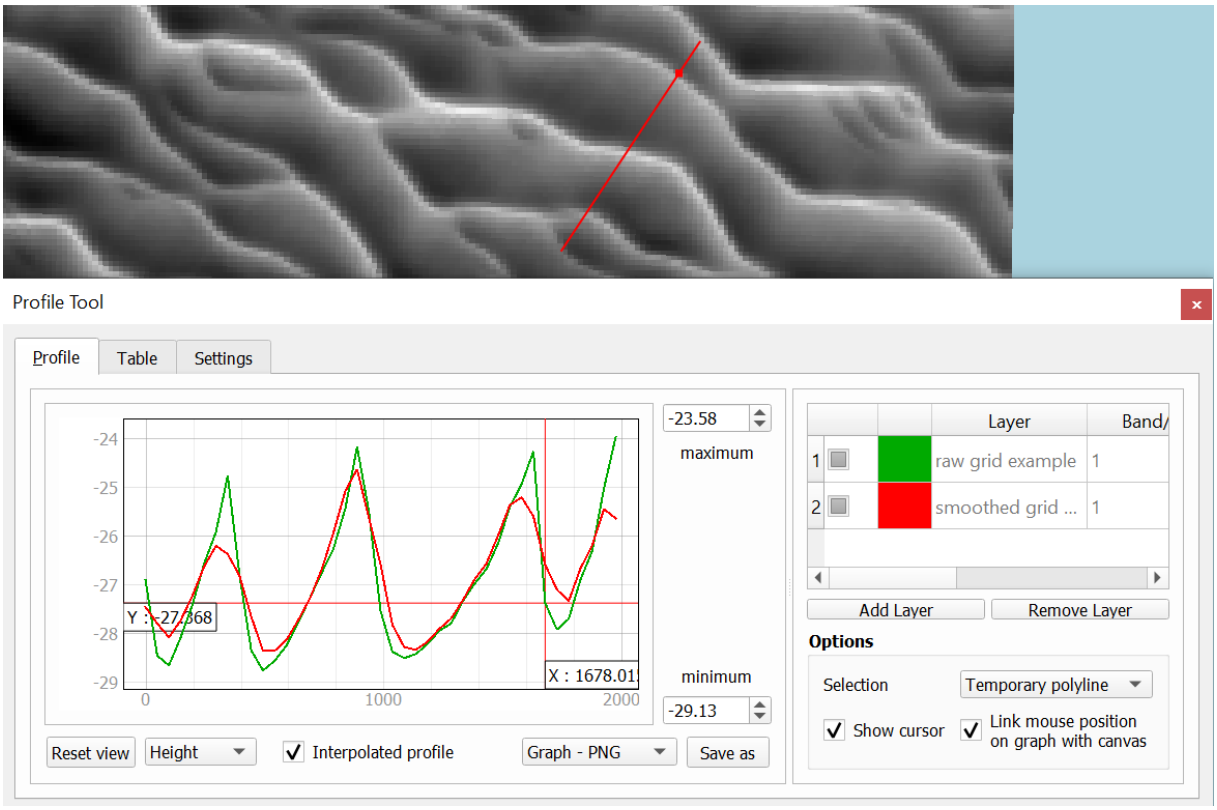

Figure A1.10 2D-profiles of raw and smoothed DEM91

Appendix II: Metadata in NetCDF Deltares

Table A2.1 data layers contained in the netCDF files from the OpenEarth server managed by Deltares

Variable	Type	Dimension	Description	Unit
X	Array of 200 32 bit reals	x	x-coordinate projection in metre resolution 25.0 m	Metre
Y	Array of 200 32 bit reals	y	y-coordinate projection in metre resolution 25.0 m	Metre
Crs	16 bit integer		EPSG 32631 WGS 84 UTM 31	
Lat	grid	Y, x	Degrees positive north	Degree
Lon	Grid	Y, x	Degrees positive east	Degree
Z	Grid	time, y, x	Bed level elevation wrt l*owest astronomical tide* Metre	Metre
Time	Array of 64 bit reals	Time	Average time of begin and end date of survey	Days since 01-01-1970
Isource	Grid	Time, y, x	Zero based index of source file	
Sid	Array of 32 bit reals	Time	Survey ID, unique ID of survey, given by NLHO	
Surveycode	Array of strings	Time	Code of survey starting with HY, given by NLHO	
Areaname	Array of strings	Time	Topographic name of area covered by survey	
Begindate	Array of 64 bit reals	Time	Begin date of survey	Days since 01-01-1970
Enddate	Array of 64 bit reals	Time	End date of survey	Days since 01-01-1970
Organisation	Array of strings	Time	Organisation	
Ship	Array of strings	Time	Name of survey ship	
Positionsystem	Array of strings	Time	Technique used to determine geographic position during survey	
Echosounder	Array of strings	Time	Echo sounder type	Atlas deso 25 = SBES Simrad eo 600 = SBES
Seafloormapping	Array of strings	Time	Sea floor mapping sytem	
Nrpoints	Array of 32 bit integers	Time	Number of points in xyz file of this survey used for interpolation	
Area	Array of 32 bit integers	Time	Surface area obtained from concave hulls around input xyz locations	M2
Density	Array of 64 bit reals	Time	Density of measurement points, equals nrpoints/area	/m2

Appendix III: Preliminary method selection

Table A3.1 explanation of given verdicts in preliminary method selection

Method	Accuracy with available data	Implementable in QGIS	Efficiency and upscaling
Pairs of Source and Target Points (PSTP)	V	V	V
	In order for PSTP to be used for sand wave migration, crest and trough lines are filtered instead of the centreline of the steepest slope. Crest and trough lines can be represented as a line *vector* of one cell width, which is as accurate as one can get.	PSTP is originally developed in ArcGIS. It can therefore easily be implemented in QGIS.	Quantifying migration rate and direction for an area of 2.4 by 9 km takes Dong (2015) two minutes, which is suffciently fast for the method to be used for large-scale analysis on the NCS.
Spatial Cross Correlation (SCC)	V	V	V
	SCC is not bound to the resolution of the bathymetric *raster* as migration distances in between *raster* cells can be detected as well.	The algorithm can be coded in the Python environment that comes standard with QGIS.	The bathymetric *raster* of 5 by 5 km is represented as a Numpy array of 200 by 200 values in Python. Looping a search window over this 2D-array takes seconds.
Deformation Analysis (DA)	X	V	X
	DA describes the seafloor in an idealised way and does therefore not quantify migration directly from the bathymetric data.	(Parts of) the algorithm can be coded in Python, which comes standard with QGIS.	A large number of complicated steps are required. Moreover, input requirements are, among others, the water depth including the measurement uncertainty at equal positions for every survey, a user-defined level of significance and some a priori knowledge of the seafloor morphology. These are not always available.
Raster Change Detection (RCD)	X	V	V
	Subtracting two bathymetric data sets will not always result in a clear difference map as is the case with terrestrial sand dunes since a sand wave pattern is more continuous.	RCD is originally developed in ArcGIS. It can therefore easily be implemented in QGIS.	Although exact computation times are not given in literature, the fact that few computation steps are required should make RCD suitable for large-scale analyses.

Appendix IV: PSTP results - Sinusoidal shift

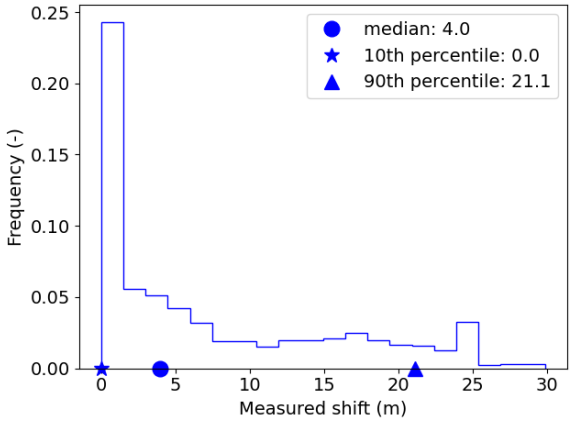

Figure A4.1. Measured distances by PSTP for a pre-defined sinusoidal shift of 5 m

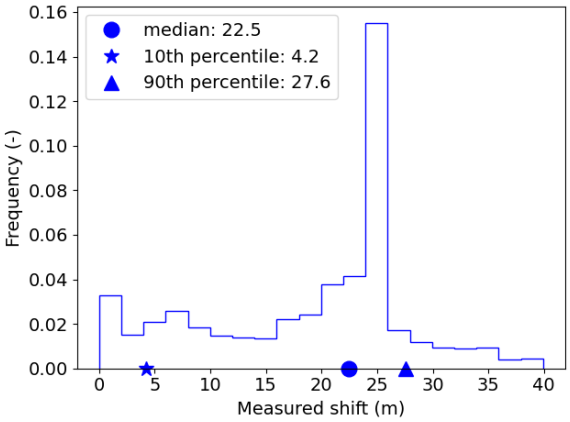

Figure A4.2. Measured migration distances by PSTP for a pre-defined sinusoidal shift of 20 m

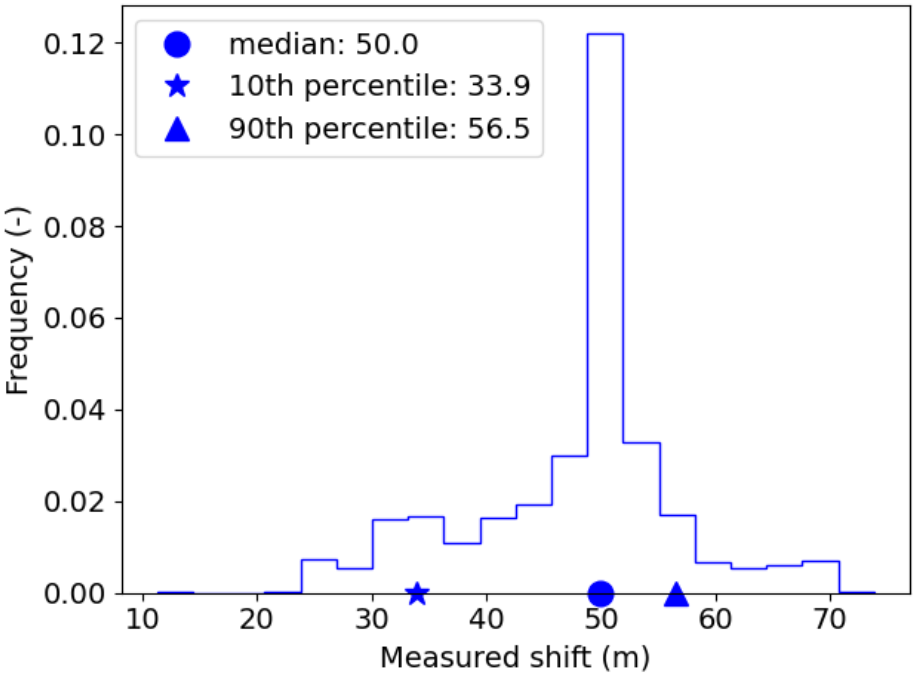

Figure A4.3. Measured migration distances by PSTP for a pre-defined sinusoidal shift of 50 m

Appendix V: Crest and trough migration rate - PSTP North Hinder

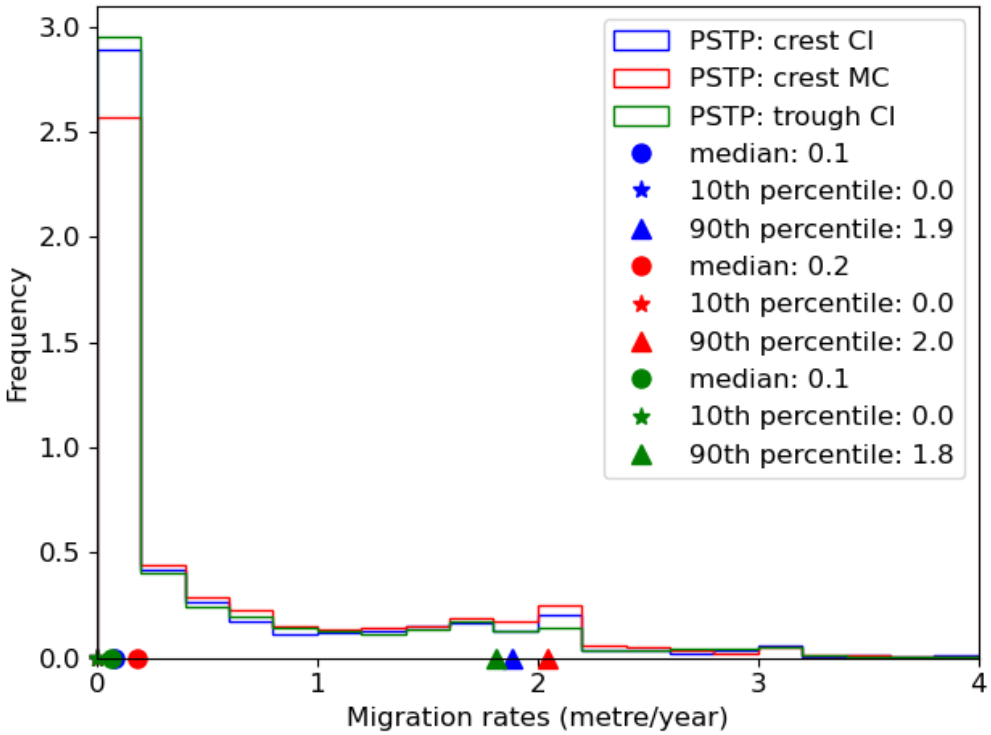

Figure A5.1 Histogram of crest and trough migration rates as measured by PSTP for the field site North Hinder (CI = Convergence Index, MC = Maximal Curvature)

Appendix VI: Migration direction – NCS SW

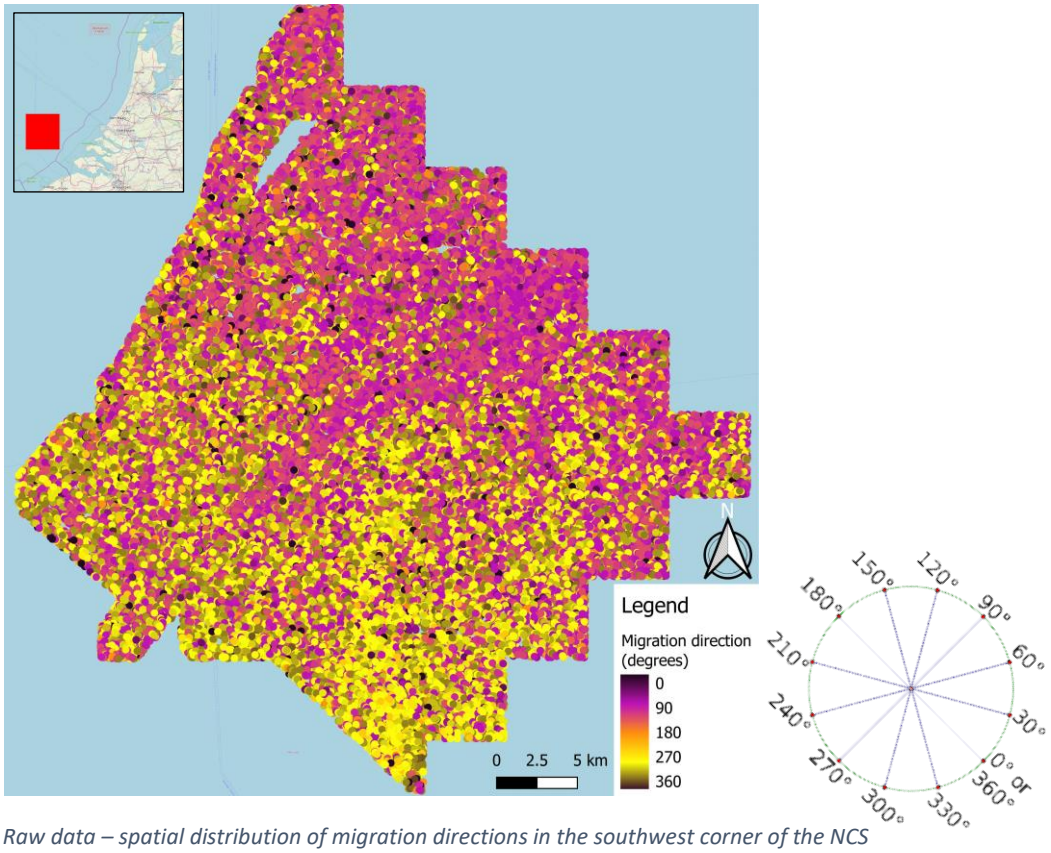

Figure A6.1 Raw data – spatial distribution of migration directions in the southwest corner of the NCS

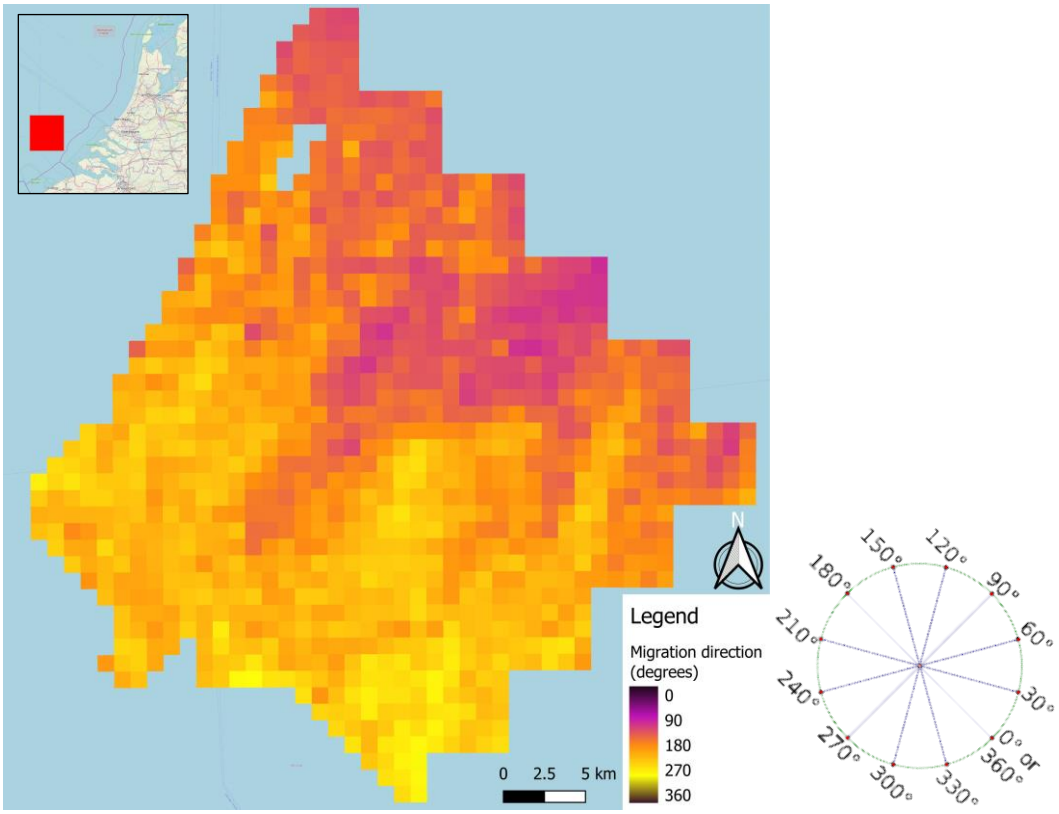

Figure A6.2 Aggregated data – spatial distribution of average migration directions per km² in the southwest corner of the NCS

Appendix VII: Migration rate per km^2 – Standard deviation

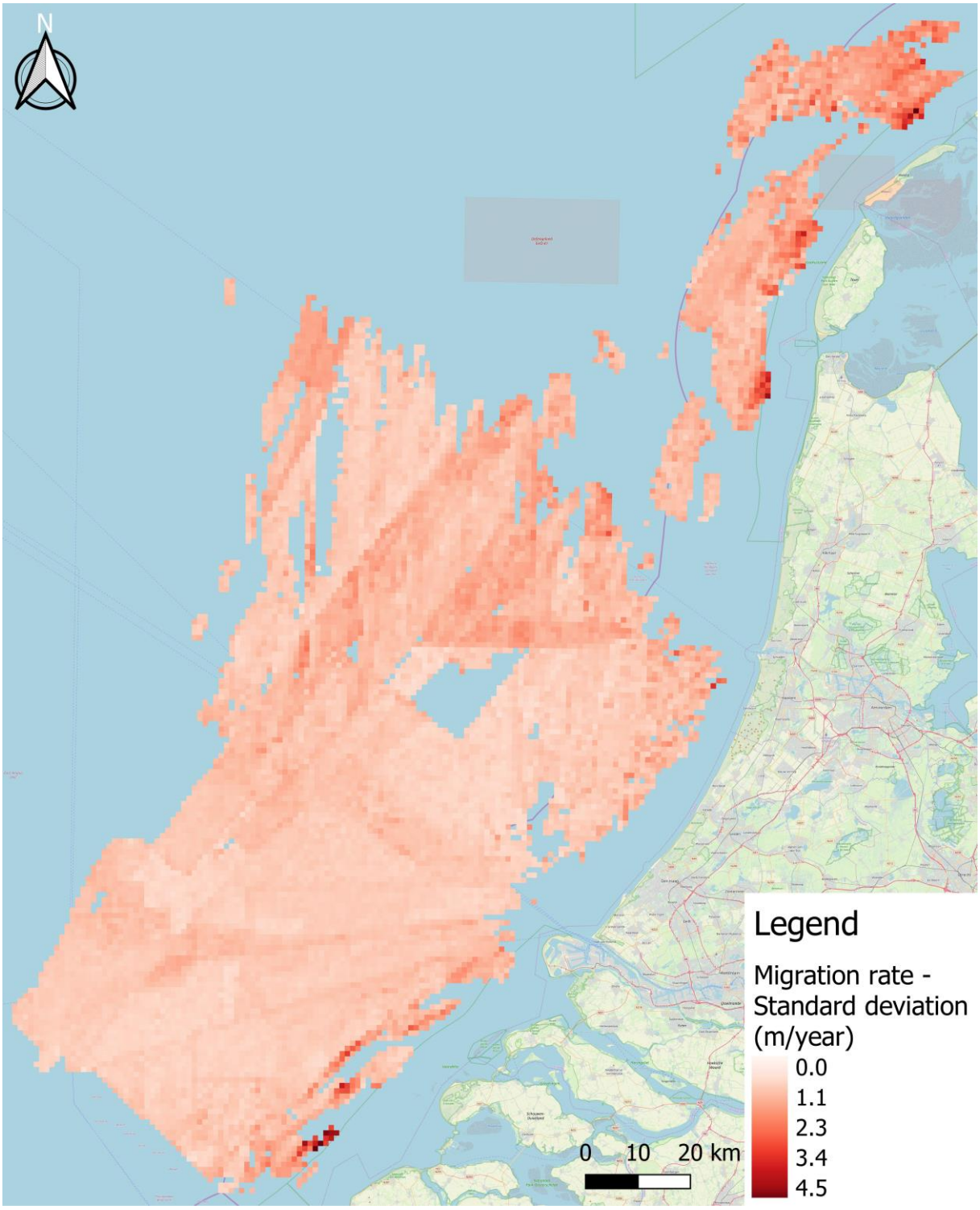

Figure A7.1 Standard deviation of migration rate per km²

Appendix VIII: Migration rate per km^2-histograms

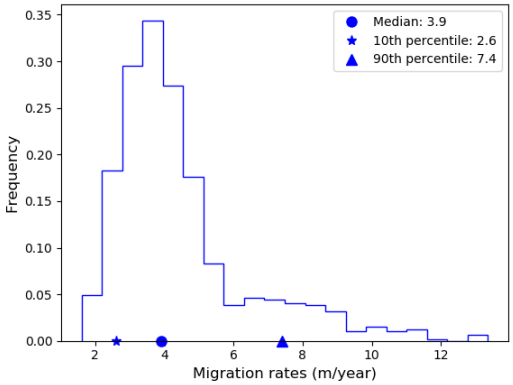

Figure A8.1. Histogram of average migration rates per square kilometre for the sand wave field west of Texel

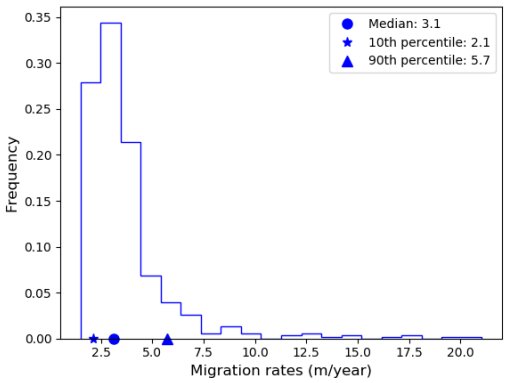

Figure A8.2 Histogram of average migration rates per square kilometre for the sand wave field north of Vlieland

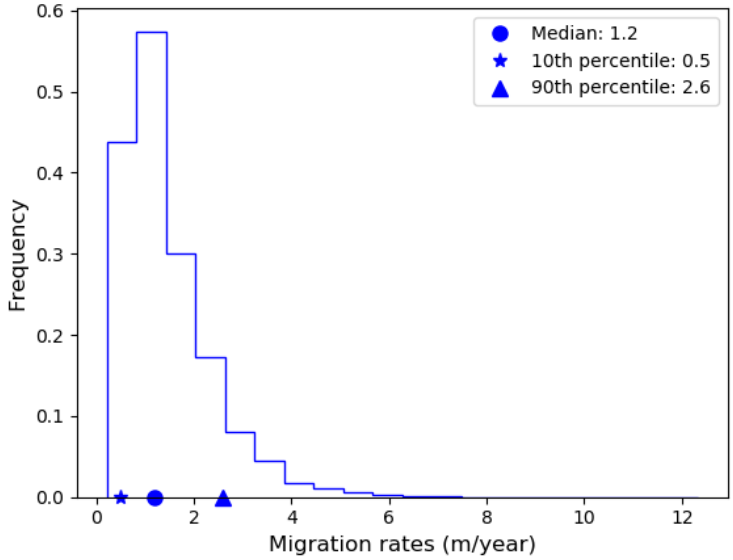

Figure A8.3 Histogram of average migration rates per square kilometre for the main sand wave field between IJmuiden and Zeeland